ISSN 2587-1366

TUJE

TURKISH JOURNAL OF ENGINEERING

VOLUME 3 ISSUE 1 JANUARY 2019

TURKISH JOURNAL OF ENGINEERING (TUJE)

Turkish Journal of Engineering (TUJE) is a multi-disciplinary journal. The Turkish Journal of Engineering (TUJE) publishes the articles in English and is being published 4 times (January, April, July and October) a year. The Journal is a multidisciplinary journal and covers all fields of basic science and engineering. It is the main purpose of the Journal that to convey the latest development on the science and technology towards the related scientists and to the readers. The Journal is also involved in both experimental and theoretical studies on the subject area of basic science and engineering. Submission of an article implies that the work described has not been published previously and it is not under consideration for publication elsewhere. The copyright release form must be signed by the corresponding author on behalf of all authors. All the responsibilities for the article belongs to the authors. The publications of papers are selected through double peer reviewed to ensure originality, relevance and readability.

AIM AND SCOPE

The Journal publishes both experimental and theoretical studies which are reviewed by at least two scientists and researchers for the subject area of basic science and engineering in the fields listed below:

Aerospace Engineering
Environmental Engineering
Civil Engineering
Geomatic Engineering
Mechanical Engineering
Geology Science and Engineering
Mining Engineering
Chemical Engineering
Metallurgical and Materials Engineering
Electrical and Electronics Engineering
Mathematical Applications in Engineering
Computer Engineering
Food Engineering

PEER REVIEW PROCESS

All submissions will be scanned by iThenticate® to prevent plagiarism. Author(s) of the present study and the article about the ethical responsibilities that fit PUBLICATION ETHICS agree. Each author is responsible for the content of the article. Articles submitted for publication are priorly controlled via iThenticate ® (Professional Plagiarism Prevention) program. If articles that are controlled by iThenticate® program identified as plagiarism or self-plagiarism with more than 25% manuscript will return to the author for appropriate citation and correction. All submitted manuscripts are read by the editorial staff. To save time for authors and peer-reviewers, only those papers that seem most likely to meet our editorial criteria are sent for formal review. Reviewer selection is critical to the publication process, and we base our choice on many factors, including expertise, reputation, specific recommendations and our own previous experience of a reviewer's characteristics. For instance, we avoid using people who are slow, careless or do not provide reasoning for their views, whether harsh or lenient. All submissions will be double blind peer reviewed. All papers are expected to have original content. They should not have been previously published and it should not be under review. Prior to the sending out to referees, editors check that the paper aim and scope of the journal. The journal seeks minimum three independent referees. All submissions are subject to a double blind peer review; if two of referees gives a negative feedback on a paper, the paper is being rejected. If two of referees gives a positive feedback on a paper and one referee negative, the editor can decide whether accept or reject. All submitted papers and referee reports are archived by journal Submissions whether they are published or not are not returned. Authors who want to give up publishing their paper in TUJE after the submission have to apply to the editorial board in written. Authors are responsible from the writing quality of their papers. TUJE journal will not pay any copyright fee to authors. A signed Copyright Assignment Form has to be submitted together with the paper.

PUBLICATION ETHICS

Our publication ethics and publication malpractice statement is mainly based on the Code of Conduct and Best-Practice Guidelines for Journal Editors. Committee on Publication Ethics (COPE). (2011, March 7). Code of Conduct and Best-Practice Guidelines for Journal Editors. Retrieved from http://publicationethics.org/files/Code%20of%20Conduct_2.pdf

PUBLICATION FREQUENCY

The TUJE accepts the articles in English and is being published 4 times (January, April, July and October) a year.

CORRESPONDENCE ADDRESS

Journal Contact: tuje@mersin.edu.tr

CONTENTS

Volume 3 – Issue 1

ARTICLES

Turkish Journal of Engineering

Turkish Journal of Engineering (TUJE)
Vol. 3, Issue 1, pp. 1-8, January 2019
ISSN 2587-1366, Turkey
DOI: 10.31127/tuje.416678
Research Article

A COMPARATIVE STUDY TO EVALUATE OF SAP AND LOGO ERP SOFTWARE'S FOR SMES AND BIG BUSINESSES

Emel Yontar *[1]

Mersin University, Tarsus Vocational High School, Mersin, Turkey
ORCID ID 0000-0001-7800-2960
eyontar@mersin.edu.tr

* Corresponding Author
Received: 18/04/2018 Accepted: 25/05/2018

ABSTRACT
Considering that there are hundreds of Enterprise Resource Planning (ERP) software on the market, it is of utmost importance that businesses choose the ERP system for which they will be most profitable. Existing business areas are similar in many respects, but each job has its own special qualities. If perfect harmonization is expected from a system, all details should be analysed from the point of view of the operator. In this study; to select the most suitable ERP software for businesses, ERP software from SAP is a global brand, with the LOGO of the leading software in Turkey, was intended to make a comparison for SMEs and big businesses. Using the Analytical Hierarchy Process (AHP) method, which is one of the Multi Criteria Decision Making Methods, an evaluation for the SMEs was first made in the Expert Choice program; followed by the same evaluation taking into account big businesses. It is analysed and the results are displayed, which is a better choice among the two ERP programs for SMEs and big businesses. Differences and similarities between evaluation criteria are presented. According to the results obtained from Expert Choice program, LOGO ERP software is the most suitable choice for the SMEs with 56,9% ratio in the selection of SAP and LOGO ERP Software. For big businesses, SAP program with 62.5% is more suitable.

Keywords: *ERP, SAP, LOGO, Expert Choice, AHP*

1. INTRODUCTION

Developments in information technologies and information systems have begun to take place in the forefront. Software for companies and the information they contain are a condition for survival in a competitive environment. One of the biggest developments in the field of information technology is Enterprise Resource Planning (ERP) software which is among the indispensable companies.

ERP, emerging in the 1960s is system that production-oriented Materials Requirement Planning (MRP) and extension of Manufacturing Resource Planning (MRP II) systems to include other production related functions. These systems have a technologically augmented structure that allows all business functions to be integrated through a common database instead of independent business functions appearing in classical enterprises. These commercial software packages promise the seamless integration of all the information flowing through a company-financial and accounting information, human resource information, supply chain information, customer information. For managers who have struggled, at great expense and with great frustration, with incompatible information systems and inconsistent operating practices, the promise of an off-the-shelf solution to the problem of business integration is enticing (Davenport, 1998).

Offering a comprehensive information management system for organizations, ERP's work integrates the different processes of the business by eliminating redundant elements while allowing data sharing between business functions. The coordination of an organization's global and geographically distributed planning and audit activities and the integration of top-level information can be achieved through ERP. ERP is a system that uses the most sophisticated information technologies that respond to all of these needs (Beşkese, 2004).

A successful ERP system benefits process rationalization, standardization, error reduction and cost reduction (Su and Yang, 2010). In the opposite case, the inability to create an effective ERP system will not only lead to cost and time loss, in addition, ERP can lead to serious loss by causing damage to company cultures, minimizing production, introducing excessive training needs, and misleading customer requests. The researches revealed that the main reason for the emergence of these problems is that the enterprises regard this system as a technology investment and they cannot be harmonized with their aims, objectives, business processes, they are more interested in purchasing costs. Therefore, when ERP projects are structured, firstly the objectives and future goals of the business should be clearly defined, the general operation and business processes should be examined and then the ERP software should be targeted for the enterprise's organizational structures (Görener, 2011).

In addition, in the increasingly competitive and globalizing markets, SMEs are forced to take advantage of ERP systems, which enable them to live their lives, organize in-house processes and provide integrated solutions in coordination between departments. The first step in doing this is to ensure that the appropriate ERP program is selected to be compatible with the operation.

At the same time, it is very important to select the appropriate ERP software because the installation of the ERP system is very costly, the installation and recycling takes a long time, and the wrong operation of the process leads to serious loss in the short and long term, because each ERP system has its own unique structure.

In this study; to select the most suitable ERP software for businesses, ERP software from SAP is a global brand, with the LOGO of the leading software in Turkey, was intended to make a comparison for SMEs and big businesses. Using the Analytical Hierarchy Process (AHP) method, which is one of the Multi Criteria Decision Making Methods, an evaluation for the SMEs was first made in the Expert Choise program; followed by the same evaluation taking into account big businesses. It is analysed and the results are displayed, which is a better choice among the two ERP programs for SMEs and big businesses.

2. LITERATURE REVIEW

The academic study on ERP, a short history, has gained momentum in the last few years. In our country, ERP software is becoming increasingly popular especially in large-scale enterprises and becoming popular in many sectors.

Many studies have been done in the literature about determining the criteria and choosing the appropriate software. Evaluation methods between SMEs and big businesses, installation process analysis and selection criteria have been evaluated by different authors. Wei *et al*. (2005) present a comprehensive ERP selection method using AHP by presenting a seven stages procedure of ERP system selection framework. Özbir (2006) examined the approaches that Turkish firms have shown in the selection and installation processes of ERP systems. Köktener (2009), has announced key decisions taken at the initial stage of the ERP project carried out in SMEs in Turkey. Köstence (2009) tried to determine the distinction between ERP software system selection and installation points, and differences between ERP packages and institutional preference. Özdemir (2009) analyzed SMEs implementing ERP systems operating in the manufacturing sector in Kayseri and perceived performance changes after ERP implementation. Yeşildağ (2010) conducted a survey on the selection and implementation of correct software for selected SMEs in the province of Muğla in Turkey. Turan (2011) examined the adaptability of ERP software to SMEs. Kılıç *et al*. (2015), applied ANP and PROMETHEE method for SME selection of ERP.

In addition to these studies, ERP selection has been emphasized by drawing attention to different sectors. Gül (2010) analysed the problems encountered during the selection and implementation of ERP software in the textile sector. Tanrıverdi (2010) examined the implementation of ERP systems in the retail sector. Hidalgo *et al*. (2011) studied about ERP selection in Metal transformation sector. They used AHP as the decision-making approach for a firm in Spain using ERP success factors. Çolakoğlu (2012) investigated the stock management process of a company operating in the automotive subsidiary industry in Aksaray and using the SAP R/3 ERP system. Yontar (2014) has been working on the company that manufactures harvester spare parts in the agricultural machinery sector. Kasay (2016), studied the ERP selection for the railway sector in Turkey.

Authors who refer to SMEs and big businesses and

different sectors often want to incorporate innovation into their literature by using different methods in their work. These studies have improved day by day, but ERP selection studies seem to use approaches based on the Analytical Hierarchy Process (AHP) method, which was developed mostly by Saaty (1980). Of them; Alanbay (2005) and Rouyendegh *et al*. (2011) reached the resolution using Expert Choice software for AHP. Başlıgil (2005), Lien and Liang (2005), Ayağ and Özdemir (2007) and Razmi *et al*. (2009), evaluated the application by combining the fuzzy logic theory and the AHP method. Büyüközkan *et al*. (2004), used the extended fuzzy AHP method. Kahraman *et al*. (2010), combines blur theory with AHP. Onut and Efendigil (2010) used the fuzzy AHP method under cost and quality constraints. Hamidi (2015) used Fuzzy AHP in order to select the most suitable ERP system because the chosen selection criteria were numerous and fuzzy. Lesani (2016) performed its work using the AHP and the Fuzzy Analytic Hierarchy Process (FAHP). Kasay (2016) conducted a study combining AHP and TOPSIS methods. After examining these studies with AHP method, it is aimed to solve the method applied in this study more complexly in Expert Choice program. At the same time, no comparison has been made between SMEs and large enterprises regarding the ERP program, emphasizing the originality of the article.

3. SAP AND LOGO SOFTWARE

SAP and LOGO ERP software are programs that are open to evaluation to choose between different criteria and different types of businesses. The SAP firm is a software company with world-wide recognition; LOGO firm is a software company with the highest revenue and awareness in Turkey.

Founded in 1972, SAP (System Analyse und Programmentwicklung) is a global company headquartered in Walldorf, Germany. The legal corporate name is SAP SE. SAP is the market leader in enterprise application software. The company is also the fastest-growing major database company. Globally, more than 76% of all business transactions worldwide touch an SAP software system. With more than 345,000 customers in more than 180 countries, the SAP Group includes subsidiaries in all major countries and employs more than 84,100 people.

The SAP firm has carried out its first major product, R/1, which made instant accounting transactions in 1973. The SAP firm introduced R/2 for 6 years, and R/3 (R: Real-time data processing) ERP system in 1992 (Farhoomand, 2007).

With strong business partners, strong research and development capabilities, strong financial position, ability to reach different geographies and markets, big data, cloud computing and mobile application needs continue to make the SAP company strong in this market (Saylam *et al.*, 2016).

Logo Software is very advantageous with its wide, experienced and knowledgeable distribution network, simple and easy to use products and low prices according to international competitors. In this regard, Logo, and it focuses on SMEs in Turkey's market.

Having entered the industry in 1984 by developing application software for personal computers, Logo is one of the largest software companies in Turkey. It is the innovative leader in the Turkish software industry with various solutions, services and innovations. As one of the fastest growing companies in the industry with more than 800 dealers and an extensive network of distribution channel, more than 85,000 companies are actively using Logo products.

Having invested in new business models and technologies throughout its 30 years of software industry experience, Logo has strengthened its position in the market with strategic acquisitions since 2010. Market share, which is 14.4% in 2012 as shown in Fig.1, has expanded both its product range and its geographical presence by adding Netsis to its portfolio in 2013 and followed by a market share of 23.3%. Logo, which operates with the goal of becoming a global brand, operates in 41 countries.

4. AHP METHOD-EXPERT CHOICE

The enterprise that will select ERP software should first decide whether an ERP solution will give positive results in terms of business. Deciding whether the implementation of the ERP system is necessary is as important as choosing the right system. Although there are no strict rules for implementing an effective electoral method, there are certain criteria that the business operator should particularly consider and some steps that must be taken to successfully complete the electoral action. At this point, selection can be concluded by adopting Multi Criteria Decision Making Methods.

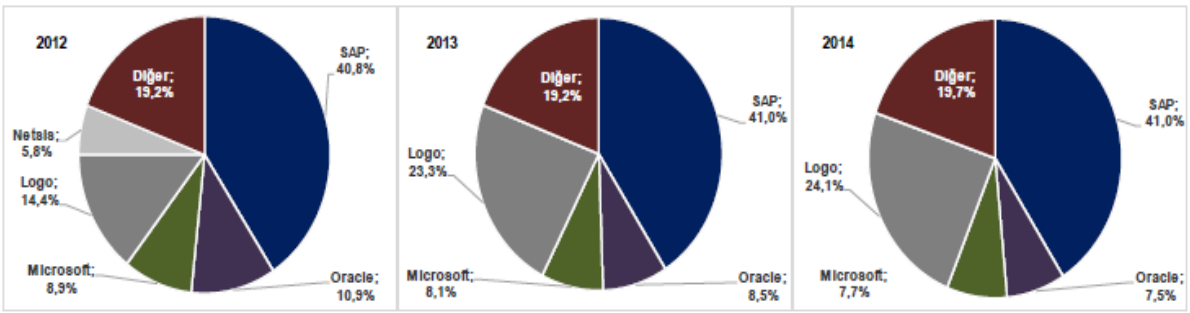

Fig. 1. LOGO Software market share by years

The Analytic Hierarchy Process (AHP) used in this study is one of Multi Criteria Decision Making Method that was originally developed by Prof. Thomas L. Saaty. Also, in 1983, Dr. Saaty joined Dr. Ernest Forman, a professor of management science at George Washington University, to co-found Expert Choice.

The Analytic Hierarchy Process (AHP) is a powerful and flexible decision-making process to help people set priorities and make the best decision when both qualitative and quantitative aspects of a decision need to be considered. By reducing complex decisions to a series of one-on-one comparisons, then synthesizing the results, AHP not only helps decision makers arrive at the best decision, but also provides a clear rationale that it is the best.

The AHP is based on three basic principles used in problem solving. These principles are decomposition, comparative judgments and synthesis of priorities (Başkaya and Akar, 2005). Decomposition principle consists of structuring the hierarchy to determine the basic elements of the problem. An effective way of doing this is by going from the upper level criterion to the lower level criterion connected to it. After that, go to the third level subcriteria and then alternatives (Saat, 2000). This leads to a more general and sometimes vague, more specific and distinctive one.

Comparative judgments principle is used in the construction of a matrix to make binary comparisons of the relative importance of the elements of a level of the hierarchy in terms of common criteria at a higher level (Saaty, 1988). The eigenvector of this matrix gives the priority of the criteria (Yetim, 2004).

Synthesis of priorities principle is to set priorities for the whole of the problem, or for the target at the top of the hierarchy, moving from the priorities derived from the lowest level of the hierarchy (Saaty, 1988).

The AHP identifies the set of criteria that will affect multipurpose decisions in real life, and the relative importance of these criteria to the relative importance of their actions, based on the evaluations of experts. Thus, a quantitative performance measurement with a systematic approach is combined with subjective evaluations to obtain healthy results (Tektaş and Hortaçsu, 2003).

The Analytical Hierarchy Process decision stages are generally given as follows (Saaty, 1988):

- Defining the Decision Problem
- Establishing Hierarchical Structure
- Creating Binary Comparison Matrices
- Transformation to Priorities Vectors
- Calculation of Compliance (Consistency) Ratio
- Sorting of Options

The Expert Choice program, which is based on the AHP methodology, helps us to export through the correct computer without dealing with calculations. Each step used in the AHP method gives us convenience in the Expert Choice program.

The AHP and Expert Choice software engage decision makers in structuring a decision into smaller parts, proceeding from the goal to objectives to sub-objectives down to the alternative courses of action. Decision makers then make simple pairwise comparison judgments throughout the hierarchy to arrive at overall priorities for the alternatives. The decision problem may involve social, political, technical, and economic factors.

4.1. ERP Selection Application for SMEs and Big Businesses

The success of the information system projects in the enterprises is ensured by choosing the right software. A properly selected software will support the business processes of the business, and the decision maker will provide accurate and up-to-date information.

The problem created in this study is to identify the best SAP and LOGO ERP Software for SMEs and big businesses. A hierarchical structure (Fig.2) was created in order to select the most suitable ERP software system for these two business groups and this hierarchical structure has been used for both SMEs and big businesses. With the same evaluation criteria, SAP and LOGO ERP Software were selected.

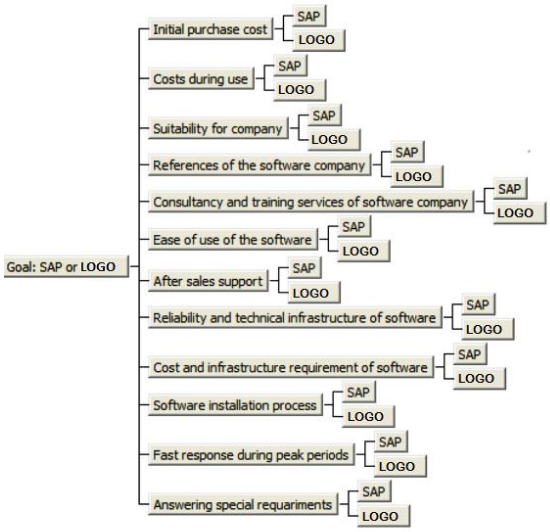

Fig. 2. Hierarchical structure for ERP selection

The hierarchy consists of the following components:

I. Goal: SAP or LOGO
II. 12 Criteria (Initial purchase cost, costs during use, suitability for company, references of the software company, consultancy and training services of software company, ease of use of the software, after sales support, reliability and technical infrastructure of software, cost and infrastructure requirement of software, software installation process, fast response during peak periods, answering special requirements)
III. 2 Alternatives (SAP, LOGO)

Criteria considered in the study were placed in the hierarchy by determining the most important and the common issues that constitute the basis of ERP in the final ERP selection of the literature review. For the solution, the Expert Choice program was used, following the steps of the AHP method. Expert Choice is a program developed for the AHP technique and used effectively.

	Initial purcl	Costs durir	Suitability	Reference:	Consultanc	Ease of us	After sales	Reliability	Cost and ir	Software in	Answering	Fast respo
Initial purchase cost		1,3	1,95	5,78	3,94	3,84	5,23	2,51	3,28	3,26	3,44	4,08
Costs during use			1,75	4,02	2,71	2,48	4,02	2,17	1,42	2,65	3,24	4,63
Suitability for company				6,05	1,42	1,22	1,32	4,14	2,12	1,33	3,82	1,71
References of the software company					2,91	3,59	2,93	7,12	5,33	1,77	2,12	1,77
Consultancy and training services of software company						2,36	1,88	2,93	1,92	1,09	2,56	1,54
Ease of use of the software							2,10	1,79	2,37	2,75	3,64	2,88
After sales support								2,55	1,95	1,28	2,04	2,16
Reliability and technical infrastructure of software									3,55	4,9	4,99	5,43
Cost and infrastructure requirement of software										6,01	6,48	7,81
Software installation process											4,66	3,09
Answering special requariments												1,17
Fast response during peak periods	Incon: 0,06											

Fig. 3. ERP criterion comparison matrix

Fig. 4. Weights of criteria

Criteria and alternatives are entered into the program to form a decision application. It allows to enter verbal and numerical data in comparison of criteria and alternatives. Once the decision structure is established within the program, Expert Choice calculations are made. In the study, 12 hierarchical matrices (Fig.3) were created in Expert Choice after the hierarchical structure was established. At this point, the opinions of 5 decision makers who are experts in the field of SMEs (3) and large enterprises (2) were consulted. The evaluation of the criteria was scored by taking the opinions of these experts.

As shown in the matrix created in the Expert Choice program (Fig.3), some of the data are colored red and some are colored black. The comparison matrixes are constructed on the basis of the comparison of row element and column element. The Expert Choice program makes it easier to understand the data in matrixes; the row element is black if it has a higher weight than the column element; the column element is colored in red if it has a higher weight than the row element.

By entering the programme matrixes and the data, the program calculates the weight of each criterion and the alternative, and the consistency ratio, which is the reliability of the matrix. For example, according to the weights of the comparison matrices of the criteria in Fig.4 the first purchase cost criterion was 19.8% more important than the other criteria. The consistency rate was 0.06. Thus, it has been found that the comparisons result in evaluations and the reliability of the result obtained. Because the consistency rate is 0.06 <0.1.

Fig. 5. Initial purchase cost for SAP and LOGO software selection for SMEs

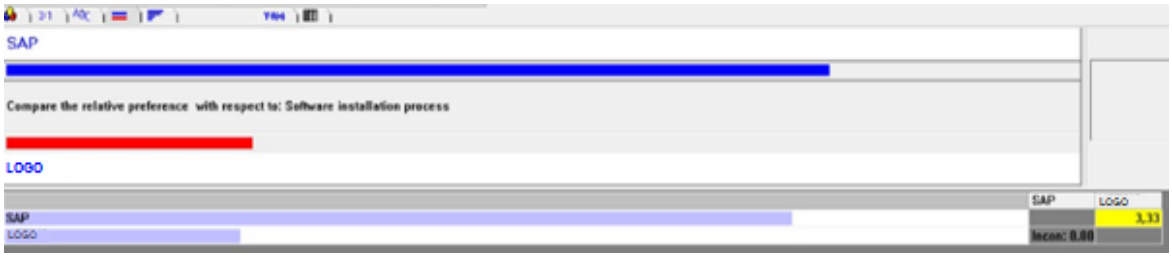

Fig. 6. Software installation process in SAP and LOGO software selection for big business

After the criteria, alternatives (SAP and LOGO) are added at Expert Choice. Then, each matrix of alternatives has been constructed in terms of all sub criteria, the weight of each alternative is calculated. First, a matrix of criteria for alternatives to SAP and LOGO was created, taking into consideration the ERP choice for SMEs. Then the weights of the alternatives are calculated as a result of the matrixes created. Then the same operations were done considering ERP selection for big business. In Fig. 5, the initial purchase cost for SAP and LOGO software selection for SMEs was determined as 8.01 for LOGO. In the same way, LOGO's SAP weight is determined to be 2.25 in comparison to big business.

Again, in Fig. 6, SAP and LOGO software for large enterprises are evaluated in the software installation process criterion comparison matrix, and SAP's LOGO software has a weight of 3.33. When SMEs are considered, SAP's LOGO software has a weight of 1.45. Thus, two separate results emerged from the same evaluation criteria on two separate problems.

In addition to these differences, references of the software company, consultancy and training services of software company, after sales support, reliability and technical infrastructure of software, answering special requirements, fast response during peak periods criteria have the same values in the comparison matrix.

By entering the comparison matrices generated as a result of the programme evaluations and calculating the weight of each alternative, the final result tables given in Fig.7 are used to decide on ERP selection for SMEs, Fig. 8 are used to decide on ERP selection for big business.

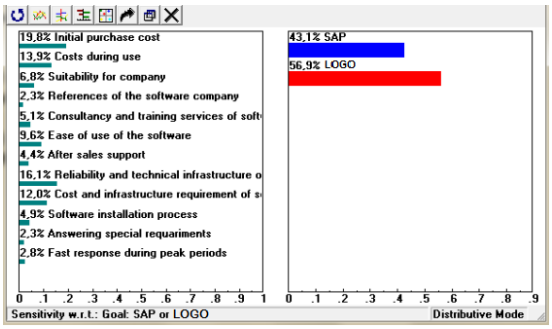

Fig. 7. SME-Results table

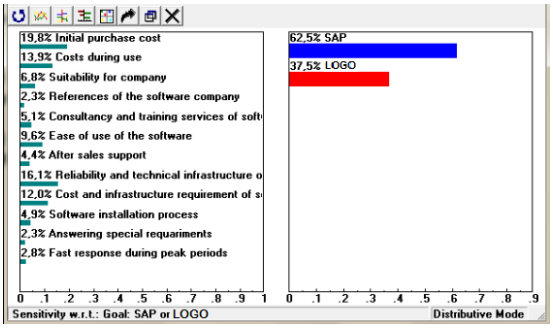

Fig. 8. Big businesses-Result table

According to the results obtained from the Expert Choice program for SMEs in Fig.7 SAP and ERP software selection LOGO with a rate of 56.9% in the first rank, SAP was included in second with 43.1%. In other words, as a result of evaluating the criteria by comparison, it is concluded that the most suitable choice for SMEs is LOGO.

In Fig. 8 SAP and LOGO ERP for big business SAP ranks first with 62.5% and LOGO second with 37.5%. Here again, SAP program is more suitable for big businesses by evaluating the same criteria.

5. CONCLUSION

The choice of ERP software for businesses is a strategic decision that requires a large number of factors to be taken into consideration. The most important feature of successful companies in ERP projects; they choose their solutions in accordance with their own sectors, institutional structures and technological systems. Errors in software selection will not only cause time and cost loss but will also result in problems in terms of effective and efficient use of the system.

In this study, it is desired to make an ERP selection for SMEs and big businesses, taking into consideration the different criteria that play a role in the selection of ERP software. SAP and LOGO ERP Software programs which were compared with the 12 criterias that were created as a result of the literature review were evaluated. For the solution using the AHP method, the Expert Choice program was applied.

According to the results obtained from Expert Choice program, LOGO ERP software is the most suitable choice for the SMEs with 56,9% ratio in the selection of SAP and LOGO ERP Software. For big businesses, SAP program with 62.5% is more suitable. Also, Kasay's (2016) study showed that the best ERP alternative for both Private Sector Company and state-owned company according to selection criteria is SAP. At another study Özdemir (2009), 90% of manufacturing SMEs in Kayseri who participated in the research went to provide ERP systems from domestic firms. Only the global ERP suppliers were able to take part in the SAP Kayseri market. At the same time, Uluköy and Vatansever (2013), the SAP with the highest ranking among the 5 software alternatives in the ERP selection in the big business, and LOGO 3rd place.

The proposed method can enable companies to analyse the problem by taking into consideration the factors that affect ERP software selection decisions (SME or big businesses) and to choose the most suitable ones from among the alternatives. On the other hand, the easy and flexible use of the method makes it possible to adapt it to real life problems. The proposed approach can be applied to all software selection problems, with some changes specific to the firm, by providing the managers with a perspective on how to make software selection decisions.

REFERENCES

Alanbay, O. (2005) "ERP Selection Using Expert Choice Software." *Honolulu, Hawaii, July*: 8-10.

Ayağ, Z., and Özdemir R. G. (2007) "An Intelligent Approach to ERP Software Selection Through Fuzzy ANP." *International Journal of Production Research* 45.10: 2169-2194.

Aydın, G. (2008), Analitik Hiyerarşi Prosesi (AHP) ve Bir Sanayi İşletmesinde Uygulaması, Kocaeli

Üniversitesi, Sosyal Bilimler Enstitüsü, Yüksek Lisans Tezi, Kocaeli.

Başkaya, Z., and Akar, C. (2005), To Select the Best Production Alternative by Using Analytical Hierarchy Process: The Case of Textile Company. *Anadolu University Journal of Social Sciences*, *5*(1), 273-286.

Başlıgil, H. (2005/3) "The Fuzzy Analytic Hierarchy Process for Software Selection Problems", Yıldız Teknik Üniversitesi, Mühendislik ve Fen Bilimleri Dergisi.

Beşkese, B. (2004), Bilişim Teknolojisi Yatırımlarının Değerlendirilmesine Yönelik Uygun Yöntemin Seçilmesi Modeli-ERP Yazılımı Seçimi Uygulaması, Doktora Tezi, İstanbul Teknik Üniversitesi Fen Bilimleri Enstitüsü, İstanbul.

Büyüközkan, G., Kahraman, C., and Ruan, D. (2004), A Fuzzy Multi-Criteria Decision Approach for Software Development Strategy Selection. *International Journal of General Systems*, *33*(2-3), 259-280.

Çolakoğlu, N. (2012), Stok Yönetiminde Yazılım Kullanımı: Otomotiv Yan Sanayi Sektöründe Bir Firma Uygulaması, Yüksek Lisans Tezi, Aksaray Üniversitesi Sosyal Bilimler Enstitüsü, Aksaray.

Davenport, T. H. (1998), Putting the Enterprise into The Enterprise System, Harvard Business Review.

Farhoomand, A. (2007), Opening up of the Software Industry: The Case of SAP. In *Management of eBusiness, 2007. WCMeB 2007. Eighth World Congress on the* (pp. 8-8). IEEE.

Görener, A. (2011), Bütünleşik ANP-VIKOR yaklaşımı ile ERP yazılımı seçimi. *Havacılık ve Uzay Teknolojileri Dergisi*, *5*(1), 97-110.

Hamidi, H. (2015), Selecting Enterprise Resource Planning System Using Fuzzy Analytic Hierarchy Process Method. Information Systems and Telecommunication, 3 (4).

Hidalgo N., A, Jose Albors Garrigos, and Luis Gomez. (2011), "ERP Software Selection Processes: a Case Study in The Metal Transformation Sector." *Intelligent Information Management*. Vol. 3. No. 1. Scientific Research Publishing.

Kahraman, C., Beskese, A., and Kaya, I. (2010), Selection Among ERP Outsourcing Alternatives Using a Fuzzy Multi-Criteria Decision-Making Methodology. *International Journal of Production Research*, *48*(2), 547-566.

Kasay, A. (2016), *Enterprıse Resource Plannıng Selectıon for Raılway Industry*., Phd Thesis. Atılım Unıversıty.

Kilic, H. S., Zaim S, and Dursun D. (2015), Selecting "The Best" ERP System for SMEs Using a Combination of ANP and PROMETHEE Methods. *Expert Systems with Applications* 42.5: 2343-2352.

Köktener B. (2009), *Genişletilmiş Kurumsal Kaynak Planlaması Projelerinin Başlangıç Aşamasında Alınan Kararların Açıklanması: Türkiye'deki Kobilerde Kalitatif Bir Çalışma*, Fen Bilimleri Enstitüsü.

Köstence, N.T. (2009), Kurumsal Kaynak Planlama Yazılım Paketleri ve Kuruma Özel Yazılımların Seçim Aşamasında Karşılaştırılması. Yüksek Lisans Tezi, Bahçeşehir Üniversitesi, Fen Bilimleri Enstitüsü, İstanbul.

Lesani S. H. (2016), Analytıcal Hıerarchy Process Approach For Selectıng Enterprıse Resource Plannıng Software Package In Oıl And Gas Equıpment Manufacturıng Fırms, Master Thesıs, The Department Of Industrıal Engıneerıng, Atilim University, Ankara, Turkey.

Lien, Chi-Tai, and Shing-Ko Liang (2005) "An ERP System Selection Model with Project Management Viewpoint–A Fuzzy Multi-Criteria Decision-Making Approach." *International Journal of the Information Systems for Logistics and Management* 1.1: 39-46.

Onut, S., and Efendigil, T. (2010), A Theorical Model Design for ERP Software Selection Process Under the Constraints of Cost and Quality: A Fuzzy Approach. Journal of Intelligent & Fuzzy Systems, 21(6), 365-378.

Özbir, Ş. (2006) "ERP Sistemlerinin Seçim ve Kurulum Prosesi ve Bir Uygulama." Marmara Üniversitesi, Sosyal Bilimler Enstitüsü, Yüksek Lisans Tezi, İstanbul.

Özdemir, A. İ. (2009) "ERP Kullanımının Kobilerin Algılanan Performansı Üzerine Etkisi: Kayseri İmalat Sektörü Örneği." *Erciyes Üniversitesi İktisadi ve İdari Bilimler Fakültesi Dergisi* 33: 173-187.

Razmi, J., Sangari, M. S., and Ghodsi, R. (2009), Developing a Practical Framework for ERP Readiness Assessment Using Fuzzy Analytic Network Process. *Advances in Engineering Software*, *40*(11), 1168-1178.

Rouyendegh, B. D., and Turan E. E. (2011) "ERP System Selection by AHP Method: Case Study From Turkey." Int. J. Bus. Manag. Stud 3.1.

Saat, M. (2000), Çok Amaçlı Karar Vermede Bir Yaklaşım: Analitik Hiyerarşi Yöntemi, Gazi Üniversitesi İktisadi İdari Bilimler Fakültesi Dergisi, (2).

Saaty, T. L. (1980), The Analytic Hierarchy Process, McGraw-Hill, USA.

Saaty, T. L (1988)., Mathematical Methods of Operations Research, Dover Publications, New York.

Saylam, R., Keskinkılıç M., and Timuroğlu K. (2016). "SAP Uygulamalarının SWOT Analizi İle İncelenmesi." *Yönetim Bilişim Sistemleri Dergisi* 1.3: 78-86.

Su Y., and Yang, C. (2010), A Structural Equation Model for Analyzing The Impact of ERP on SCM. Expert Systems with Applications 37: 456-469.

Tanrıverdi, S. (2010), Perakende Sektöründe Kurumsal Kaynak Planlama Uygulaması, Yüksek Lisans Tezi, Marmara Üniversitesi Sosyal Bilimler Enstitüsü, İstanbul.

Tektaş, A., Hortaçsu, A. (2003), Karar Vermede Etkinliği Artıran Bir Yöntem: Analitik Hiyerarşi Süreci Ve Mağaza Seçimine Uygulanması, İktisat, İşletme ve Finans Dergisi,18: 209.

Turan, S. (2011), Kobi'lerin Kurumsal Kaynak Planlama Yazılımlarından Beklentileri ve Sektörel Bazda Yazılım Geliştirilmesi, Yüksek Lisans Tezi, İstanbul Ticaret Üniversitesi, İstanbul.

Uluköy M. and Vatansever K., Determining Enterprise Resource Planning Systems Through Fuzzy Ahp And Fuzzy Moora Methods: An Implementation on Manufacturing Sector, Celal Bayar University Journal of Social Sciences, issue: 11-2 / 2013, pages: 274-293, 2013.

Wei, Chun-Chin, Chen-Fu Chien, and Mao-Jiun J. W. (2005) "An AHP-Based Approach to ERP System Selection." *International journal of production economics* 96.1: 47-62.

Yeşildağ, B. (2010), Muğla İlinde Küçük ve Orta Büyüklükteki İşletmelerde Kurumsal Kaynak Planlama (ERP) Yazılımları Kullanım Düzeyi ve Verimliliğinin Araştırılması, Yüksek Lisans Tezi, Muğla Üniversitesi, Sosyal Bilimler Enstitüsü, Muğla.

Yetim, S. (2004), Analitik Hiyerarşi Sürecine Ait Bazı Matematiksel Kavramlar, Kastamonu Eğitim Dergisi, 12(2), 457-468.

Yontar E. (2014), ERP Kurulum Sürecinin Modellenmesi ve Tarım Makine Sanayinde Uygulanması, Kırıkkale Üniversitesi, Fen Bilimleri Enstitüsü, Endüstri Mühendisliği Anabilim Dalı, Yüksek Lisans Tezi, Kırıkkale.

Turkish Journal of Engineering

Turkish Journal of Engineering (TUJE)
Vol. 3, Issue 1, pp. 9-13, January 2019
ISSN 2587-1366, Turkey
DOI: 10.31127/tuje.421135
Research Article

BALL BURNISHING PROCESS EFFECTS ON SURFACE ROUHGNESS FOR Al 6013 ALLOY

İskender Özkul *[1]

[1] Mersin University, Engineering Faculty, Department of Mechanical Engineering, Mersin, Turkey
ORCID ID 0000-0003-4255-0564
iskender@mersin.edu.tr

* Corresponding Author
Received: 04/05/2018 Accepted: 09/07/2018

ABSTRACT
Ball burnishing process rapidly developing and applied in many applications. The process's advantageous aspects on the material increase the quality of the product surface. In this study, a surface quality research was made on 6013 series of aluminum alloys which are used frequently in the industry. As a result of the experiments, it was seen that the ball burnishing process increased the surface qualities extremely. At the same time, the results obtained were mathematically analyzed.

Keywords: *Al 6013, Surface Roughness, Taguchi Method, Ball Burnishing*

1. INTRODUCTION

Aluminum's production availability and usage area is increasing day by day. The high strength stiffness to weight ratio and high corrosion resistance make aluminum popular in material selection (Miller *et al.*, 2000). Aluminum is easy to shape and process according to other ferrous materials (Nouari *et al.,* 2003). Even if the machined material is aluminum, the surfaces obtained after the treatment may not always be satisfactory. Because of this, surface finishing is required after machining process. Operations such as grinding, electro polishing, etc., provide only topographic correction on the surface of aluminum. During the surface finishing process, the ball burnishing process causes the surface hardness to increase due to the deformation toughness of the surface as well as the topography of the surface. Ball burnishing is easy to apply and relatively inexpensive (Buldum *et al.,* 2017; Buldum *et al.,* 2017). Once the appropriate parameters have been determined, it is a convenient method of operation in terms of processing time and consumable expenditure. This advantage is a considerable advantage for the manufacturer. There is no standard ball burnishing tool in the market. Its application is simple, and the tool is low cost product.

In this work, the 6013 series aluminum was roughly machined on a lathe and an average *Ra 6.00µ* value surface roughness was obtained. This surface was improved by ball burnishing under different process parameters. The results are also modelled and optimum conditions were defined.

2. EXPERIMENTS AND METHODS

In this study, the Al 6013 alloy was used which dimensions are 150 mm length and 25 mm diameter as shown Fig. 1. Also, the chemical properties of the Al 6013 materials used in the experiments are given in Table 1.

Fig. 1. The machined specimens for ball burnishing process

Table 1. Chemical composition of the 6013 alloy as wt.%.

Al	Mg	Si	Cu	Mn
Balance	0.91	0.67	0.86	0.7

Three samples were used for experiments and surface of the sample was divided to sections for each experiment

In the experiments, a universal lathe was used. The ball burnishing tool adopted tool post sections and a loadcell application was used to measure the applied force on specimen. The ball burnishing tool shown in Fig. 2. Medium cleanliness provided to prevent the chip or dust contact between part and tool during the operation (Ugurlu *et al.,* 2017).

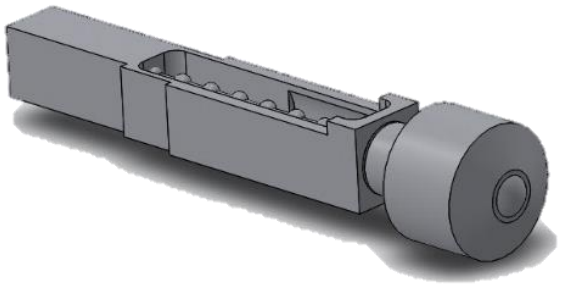

Fig. 2 The ball burnishing equipment (Buldum and Cagan, 2017)

The all specimens were coarse turned in lathe and 6.0µ Ra was obtained. The groves are machined to separate the experimental regions. In the experiments three different input variables were used and experimental scenario designed with Taguchi L9. In this study, three input parameters (levels) were selected as force, feed rate, passes. Three levels and three levels' factors were used. These factors and levels presented in Table 2. The Taguchi L9 experimental design also was given in Table 3.

Table 2. Ball burnishing parameters

	Levels		
Factors	1	2	3
Force (N)	100	200	300
Feed (mm/min)	0.05	0.1	0.2
Number of passes	1	2	3

Table 3. Experimental layout using an L9 orthogonal array

Experiment Number	Force	Feed	Number of Passes
1	1	1	1
2	1	2	2
3	1	3	3
4	2	1	2
5	2	2	3
6	2	3	1
7	3	1	3
8	3	2	1
9	3	3	2

The Taguchi method is generally used for to define the select the optimal parameters used in experiments. The method systematic and effective usage area. It provide low cost technical information for qualified systems (Pavani *et al.* 2015; Gaitonde *et al.,* 2016). The experimental design also provide to reach shortly to results with time and cost (Pavani *et al.,* 2015). The system let the user to choose results evaluation approach like 'Nominal is better', 'Smaller is better' and 'Larger is better' (Pedersen *et al.,* 2016). In this study, surface roughness values are getting importance when they have lower roughness values. So, in the options "Smaller is

better" was selected. Those options computed with following equations.

$$S/N = -10\log\left(\frac{1}{N}\left(\sum_{i=1}^{n} Y_i^2\right)\right) \quad (1)$$

Where Yi is the surface roughness value, n is the number of tests and N is the total number of data points for equation (1).

2.1. Experimental Tests and Analysis

Surface roughness is commonly use to define the characterization materials. The topographical shift on surface the parts measured and the surface roughness average "*R*a" was taken accordance for ISO 4287 norm and the Ra value can be expressed by the following equations (Arbizu *et al.* 2003):

$$R_a = \frac{1}{L}\int_0^L |y|\,dx = \frac{1}{L}\left(\sum S_{ui} + \sum S_{lj}\right) = \frac{S}{L} \quad (2)$$

Therefore**,**

$$R_a = R_t(S_u + S_l) \quad (3)$$

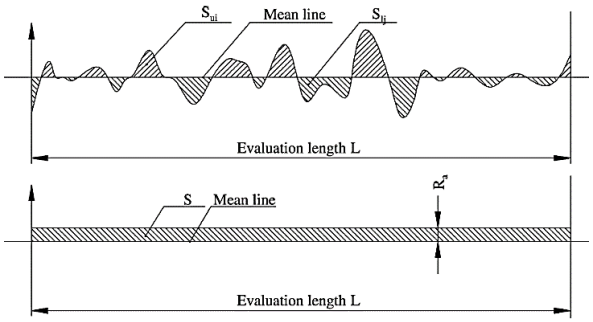

Fig. 3 Scheme of surface roughness (Aldas *et al.* 2014)

After experiments, the surface roughness values were measured performed using a Mitutoyo portable roughness meter model Surftest SJ 201and in different points and arithmetic means are noted.

3. RESULTS AND DISCUSSION

In this experiments, different process conditions such as the effect of the force, feed rate and number of passes effects on Al6013 surface roughness were investigated. The obtained surface roughness values were also mathematically modelled and S/N ratios calculated. That values are presented in Table 4.

Table 4. Parameters and results after burnishing process

Experiments	Parameters			Results	
	Force	Feed rate	Number of Passes	Ra (µm)	S/N Ra (µm)
1	100	0.05	1	0.2615	11.6506
2	100	0.1	2	0.1830	14.7510
3	100	0.2	3	0.7680	2.2928
4	200	0.05	2	0.3960	8.0461
5	200	0.1	3	0.8900	1.0122
6	200	0.2	1	1.4070	-2.9659
7	300	0.05	3	0.5330	5.4655
8	300	0.1	1	1.3450	-2.5744
9	300	0.2	2	1.1050	-0.8672

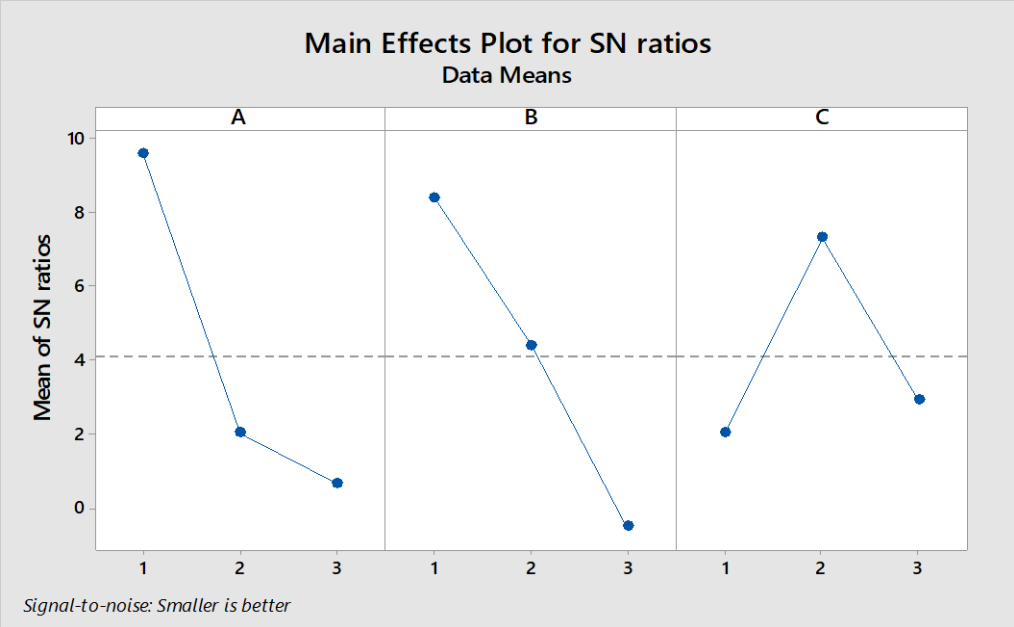

Fig. 4 S/N ratios effects on surface roughness value

In S/N ratios shows the effects of the input parameters. In Fig. 5, a section shows the force inputs and that trend of the plots show lowering tendency similarly with B section which is feed rate. On the other hand, C section Number of Passes exhibit irregular behaviors. The high points in S/N graphs show the optimum values considering the others. In this regards, A1, B1 and C2 parameters can be chosen optimum values.

The relative of the importance parameters can be defined by ANOVA technique. In this study ANOVA modelling was conducted and the results are presented as pie graphs in Fig. 5. As seen in the graphs Force input values is the most effective parameters between others with 43%. However, feed rate has also significant values with the 37% ratio. Number of passes values show the lower impact values considering feed rate and force input values. Error rate is 5% and that proves the reliability of the study.

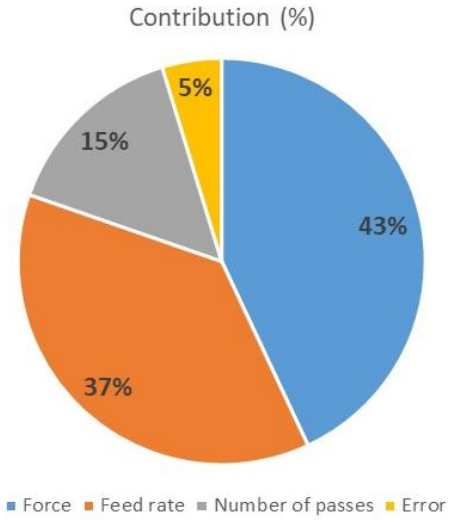

Fig. 5 Contribution of the input parameters on surface roughness

Table 5. The analysis of analysis of variance for surface roughness

Source	DF	Adj SS	Adj MS	F-Value	P-Value
A	2	137.64	68.818	9.11	0.099
B	2	119.26	59.629	7.89	0.112
C	2	47.83	23.917	3.17	0.240
Error	2	15.11	7.555		
Total	8	319.84			

In ANOVA modelling the R^2 is found as 95.28%. The high score of the high R^2 make reliable the equation for this modelling. The mathematical regression equation presented in Table 6 with coefficients.

Table 6. Coefficients of the regression equation

Term	Coef	SE Coef	T-Value	P-Value	VIF
Constant	4.090	0.916	4.46	0.047	
A					
1	5.47	1.30	4.23	0.052	1.33
2	-2.06	1.30	-1.59	0.253	1.33
B					
1	4.30	1.30	3.32	0.080	1.33
2	0.31	1.30	0.24	0.835	1.33
C					
1	-2.05	1.30	-1.58	0.254	1.33
2	3.22	1.30	2.48	0.131	1.33

5. CONCLUSION

In this study, the effect of the force, feed and number of passes were investigated on surface roughness. The results are given below:

- The optimum parameter combination for the

lowest surface roughness was calculated using an analysis of the signal-to-noise ratio. The parameters for optimum surface roughness are obtained as A1B1C2.

- According to the results of ANOVA, force and feed the most effective parameters on the surface roughness with a contribution ratio of 43% and 37%, respectively. Also, it is observed that number of passes 15% play roles in minimizing the surface roughness.
- While as force and feed ratio increasing the surface roughness decreasing. However, that is not validated for number of passes.

REFERENCES

Aldas, K., I. Ozkul and A. Akkurt (2014). "Modelling surface roughness in WEDM process using ANFIS method." *Journal of the Balkan Tribological Association Vol*, Vol. 20, No. 4, pp. 548-558.

Arbizu, I. P. and C. L. Perez (2003). "Surface roughness prediction by factorial design of experiments in turning processes." *Journal of Materials Processing Technology*, Vol. 143, No., pp. 390-396.

Buldum, B. and S. Cagan (2017). "Study of Ball Burnishing Process on the Surface Roughness and Microhardness of AZ91D Alloy." *Experimental Techniques*, Vol., No., pp. 1-9.

Buldum, B. B. and S. C. Cagan (2017). "The optimization of surface roughness of AZ91D magnesium alloy using ANOVA in ball burnishing process." *Turkish Journal of Engineering*, Vol. 1, No. 1, pp. 25.

Gaitonde, V., S. Karnik and J. P. Davim (2016). *Multiple performance optimization in drilling using Taguchi method with utility and modified utility concepts*. Elsevier, USA.

Miller, W., L. Zhuang, J. Bottema, A. J. Wittebrood, P. De Smet, A. Haszler and A. Vieregge (2000). "Recent development in aluminium alloys for the automotive industry." *Materials Science and Engineering: A*, Vol. 280, No. 1, pp. 37-49.

Nouari, M., G. List, F. Girot and D. Coupard (2003). "Experimental analysis and optimisation of tool wear in dry machining of aluminium alloys." *Wear*, Vol. 255, No. 7-12, pp. 1359-1368.

Pavani, P., R. P. Rao and S. Srikiran (2015). "Performance evaluation and optimization of nano boric acid powder weight percentage mixed with vegetable oil using the Taguchi approach." *Journal of Mechanical Science and Technology*, Vol. 29, No. 11, pp. 4877-4883.

Pedersen, S. N., M. E. Christensen and T. J. Howard (2016). "Robust design requirements specification: a quantitative method for requirements development using quality loss functions." *Journal of Engineering Design*, Vol. 27, No. 8, pp. 544-567.

Ugurlu, M., S. C. Cagan and B. B. Buldum (2017). "Improvement of surface roughness using ANOVA for AZ31B magnesium alloy with ball burnishing process." *Int J Engine Res Technol*, Vol. 6, No. 9, pp. 216-221.

Turkish Journal of Engineering

Turkish Journal of Engineering (TUJE)
Vol. 3, Issue 1, pp. 14-24, January 2019
ISSN 2587-1366, Turkey
DOI: 10.31127/tuje.435028
Research Article

DYNAMIC MATHEMATICAL MODELING AND CONTROL ALGORITHMS DESIGN OF AN INVERTED PENDULUM SYSTEM

Ayodeji Akinsoji Okubanjo *[1] and Oluwadamilola Kehinde Oyetola [2]

[1] Olabisi Onabanjo University, Engineering, Electrical Electronics and Computer Engineering, Ago-Iwoye, Nigeria
ORCID ID 0000 – 0003 – 1908 – 0365
okubanjo.ayodeji@oouagoiwoye.edu.ng

[2] Olabisi Onabanjo University, Engineering, Electrical Electronics and Computer Engineering, Ago-Iwoye, Nigeria
ORCID ID 0000 – 0001 – 7169 – 6381
oyetola.oluwadamilola@oouagoiwoye.edu.ng

* Corresponding Author
Received: 20/06/2018 Accepted: 10/07/2018

ABSTRACT
The inimitable features of multivariable, instability, non-minimum phase and non-linearity has established an inverted pendulum system as benchmark to investigate and test new emerging control schemes. In this paper, the objectives are to explicitly model the system dynamics of an inverted pendulum and implement different control algorithms that will stabilize the pendulum in the upright vertical position by controlling the input force applied to the cart in the horizontal position. The mathematical model is derived based on the energy property of Lagrange approach and the control algorithms are expanded on the derived mathematical model in MATLAB-SIMULINK environment. Hence, we proposed four different controls algorithms proportional-integral-derivative controller (PID), pole placement feedback controller (PPFC), linear quadratic regulator controller (LQR) and linear quadratic regulator with estimator (LQR+Estimator) for the control of the linearized inverted pendulum system. The study compares the proposed control algorithms in terms of system response and performance.

Keywords: *Mathematical modeling, Control algorithms, Inverted pendulum, Euler-Lagrange, Simulink*

1. INTRODUCTION

Inverted Pendulum system (IPS) is a classic example of practical model to demonstrate system dynamics and control theory due to its unique features such as multivariable, instability, non-minimum phase and , non-minimum phase and non-linearity. (IRFAN et al., 2013; Ilyas et al., 2017; Krishna et al., 2016; Kumar et al., 2013,). IPS is gaining tremendous attention among the researchers and scholars as a result of its dynamics dominant features that emulates many factual systems in the field of control systems. Also, these dynamics characteristics of inverted pendulum has been established as a baseline to investigate and test new emerging control algorithms. Inverted Pendulum are widely used in balance control of robot manipulator, model flight of rockets and missiles, Segway, unicycle, stabilization of satellite fighting and earthquake resistant of building (Guo and Unversity, n.d.; Kafetzis et al., 2017; Siradjuddin et al., 2017). Recently, IPS are on increasing demand for flying drone especially for balance control of a quadcopter. Inherently, inverted pendulum systems are underactuated mechanical system with complex dynamics which are nonlinear. Instinctively, inverted pendulum possess two equilibrium states i.e. stable state and unstable state (Eizadiyan & Naseriyan, 2015). However, stabilization of the inverted pendulum in an unstable state is a fundamental problem for engineers and scientists. So, several control algorithms have been proposed, implemented and adopted over the past few decades and the quest for new development of inverted pendulum control still continues. Adam and Matlab software based simulation of inverted pendulum is proposed in İlgen *et al.* (2016), a model reference adaptive controller in Krishna *et al*. (2016), Fuzzy control and Genetic Algorithms in Dastranj et al.(2012), PID and LQR in Eizadiyan and Naseriyan, (2015); Jose et al.(2015), fuzzy controller in Sangfeel et al.(2015),state feedback control in Nithya and Vivekanandan,(2014), linear quadratic regulator control, LQR in Chandan et al.(2012), performance comparison model of optimal linear model and Jacobian linearization is proposed in Ababneh et al., 2011, Lagrangian differential transformation approach is proposed in Agarana and Ajayi, (2017), fuzzy and adaptive neuro-fuzzy inference system (ANFIS) in Goswami,(2013),fractional order PID controller in Mishra and Chandra, (2014), Neural network and PID controller in Lee et al.(2009). In the work of Přemysl, Strakoš, Jiří, (2017), a mathematical model of linear inverted pendulum in both state space and transfer function model are derived and pole placement feedback method and a full state observer are implemented. The simulation results justify the superiority of state observer over pole-placement approach. Prayitno et al.(2017), presented a linearized model of an inverted pendulum with three control algorithms, PID, LQR and MPC to stimulate the dynamics of the IPS.

In the research work, the model was analyzed for cases with disturbance and without disturbance and initially controlled with PID controller and later the combined action of PID and LQR, MPC were implemented to compare performances. Hence, it was concluded in the study that the combined action of PID and LQR show better performance over PID alone. Singh and Ph (2015) presented a robust controller to augment the inverted pendulum performance. In their study, a novel H-infinity fuzzy PID controller was proposed and the performance was compared with the conventional PID controller. Simulation results revealed that the new scheme has the affinity to enhance the robustness, transient and steady performance than the PID controller. The use of output feedback controller for inverted pendulum stabilization is addressed in Lee et al.(2015) while pole-placement PI-state feedback controller is designed to stabilize the inverted pendulum cart system in Bettayeb et al. (2014) . Chen et al.(2018) proposed a novel control algorithm to address the repeatability associated with the inverted pendulum when driven by a rotary motion and transmission system. However, Prado et al (2017) analytically and numerically examined the stability of the inverted pendulum based on parametric excitation and large random frequencies. Wang (2011 employed PID controller to address stabilization and tracking problem of three type inverted pendulum and the same problems was addressed via combined action of PD controller and fuzzy PD controllers for a rotational inverted pendulum in Oltean (2014).

In this paper the main objectives are to explicitly model the system dynamics of an inverted pendulum and implement different control algorithms that will stabilize the pendulum in the upright vertical position by controlling the input force applied to the cart in the horizontal position.

Nomenclatures

m_1, m_2	Mass of the cart and the pendulum respectively
k	Spring stiffness coefficients of the cart
b	Friction of the cart
L	Lagrange's function
T	Kinetic energy
V	Potential energy
D	Rayleigh's dissipative function
x	Cart position coordinate
θ	Pendulum angle from vertical
Q_i	Generalized forces
$\boldsymbol{g}$	Center of gravity

Abbreviations

IPS	Degree of freedom
PID	Proportional Integral Derivative Controller
LQR	Linear Quadratic Regulator
PPFC	Pole-Placement Feedback Controller

2. MATHEMATICAL MODELING OF IPS

We derived the dynamics equation of the inverted pendulum using a set of non-linear, second-order, ordinary differential equations and to simulate the dynamics accurately the Lagrangian and Euler-Lagrange was adopted. The motivation for chosen Euler's Lagrange approach over Newton approach is a result of its simplicity, robustness and energy based property. The mathematical model is formulated based on the energy property of Lagrange method and the control algorithms are expounded on the derived mathematical model. However, the Lagrange's equation does not account for dissipative force in the mechanical system, hence,

Rayleigh's dissipation function is integrated into Lagrange's equation to form augmented Lagrange's equation. In order to describe the physical motion of the inverted pendulum system, we choose the cart position and pendulum angle as the generalized coordinates. The inverted pendulum shown in fig.1 consists of a cart of mass m_1 and position x, acted upon by a parallel spring-damper configuration with spring stiffness coefficient k and viscous damping coefficient b and the cart suspended a pendulum consisting of a uniform rod of length l, and mass m_2, pivoting about point A. The force U (t) acts on mass of the cart in the direction of x. Subsequently, we derive the differential equations that describes the dynamics of the inverted pendulum using augmented Lagrange's equation in this form:

$$\frac{d}{dt}\left(\frac{\partial L}{\dot{q}_i}\right)-\left(\frac{\partial L}{\partial q_i}\right)+\left(\frac{\partial D}{\partial \dot{q}_i}\right)=\delta_i \tag{1}$$

$$q_i=(x,\theta) \tag{2}$$

The Lagrange function L is defined as the difference of the system's kinetic and potential energy. So, kinetic energy of the IPS as a function of cart and pendulum position and velocity is expressed as:

$$T\left(\theta,\dot{\theta}\right)=\frac{1}{2}\dot{\theta}^{T}M\left(\theta,\dot{\theta}\right)=\frac{m_i v_i^2}{2} \tag{3}$$

Where, $M\left(\theta,\dot{\theta}\right)$ is the nxn inverted pendulum mass matrix and the subscript I denote 1 and 2. Hence, the total kinetic energy of the IPS is the sum of the cart and the pendulum kinetic energies (T_1 and T_2).

$$T\left(\theta,\dot{\theta}\right)=\frac{m_1 v_1^2}{2}+\frac{m_2 v_2^2}{2} \tag{4}$$

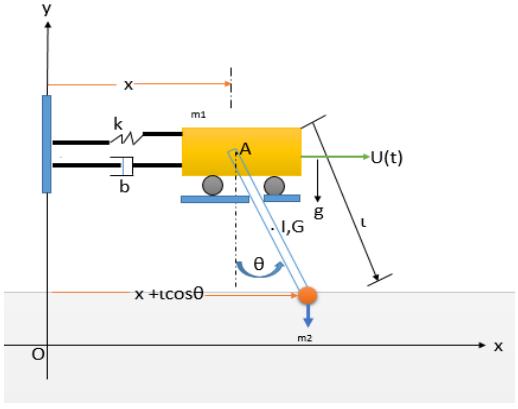

Fig. 1. Inverted Pendulum System (IPS)

To evaluate T_1 and T_2, we need to write the position equations for m_1 and m_2 at point A and subsequently differentiate the respective position to obtain the corresponding velocity and using inner product to obtain the square of the velocity for the cart and pendulum respectively.

$$x_1=x \tag{5}$$

$$y_1=0 \tag{6}$$

$$\begin{aligned} x_2&=x+l\sin(\theta)\\ y_2&=l\cos(\theta)\end{aligned} \tag{7}$$

Let define the velocity as:

$$v=\frac{d}{dt}\begin{pmatrix}x\\ y\end{pmatrix}=\begin{pmatrix}\dot{x}\\ \dot{y}\end{pmatrix} \tag{8}$$

$$v^2=\|v\|^2=v^T v \tag{9}$$

$$v_1^2=\begin{bmatrix}\dot{x} & 0\end{bmatrix}\begin{bmatrix}\dot{x}\\ 0\end{bmatrix}=\dot{x}^2 \tag{10}$$

Similarly, v_2^2 is computed in the same view

$$\begin{aligned} v_2^2=&\dot{x}^2+2\dot{x}l\cos(\theta)\dot{\theta}+l^2\cos^2(\theta)\dot{\theta}-\dot{x}l\sin(\theta)\dot{\theta}-\\ &l^2\sin(\theta)\cos(\theta)\dot{\theta}+\dot{x}l\sin(\theta)\dot{\theta}+l^2\sin(\theta)\cos(\theta)\dot{\theta}+\\ &l^2\sin^2(\theta)\dot{\theta}=\dot{x}^2+2\dot{x}l\cos(\theta)\dot{\theta}+l^2\dot{\theta}^2\end{aligned} \tag{11}$$

Substituting v_1^2 and v_2^2 in equation (3), we obtain the kinetic energy of the inverted pendulum as follows:

$$T_1=\frac{1}{2}m_1\dot{x}^2 \tag{12}$$

$$\begin{aligned} T_2=&\frac{1}{2}m_2\left(\dot{x}^2+2\dot{x}l\cos(\theta)\dot{\theta}+l^2\dot{\theta}^2\right)+\\ &\frac{1}{2}I\dot{\theta}^2\end{aligned} \tag{13}$$

So that the total kinetic energy of the inverted pendulum is obtained from equation (12) and (13) and presented as

$$\begin{aligned} T=&\frac{1}{2}m_1\dot{x}^2+\frac{1}{2}m_2\dot{x}^2+\frac{1}{2}l^2\dot{\theta}^2+\frac{1}{2}I\dot{\theta}^2+\\ &m_2\dot{x}\dot{\theta}l\cos(\theta)\end{aligned} \tag{14}$$

Reference to the cart level of the IPS (considered as a zero potential), the potential energy of the system is the sum of the potential energies of the cart and pendulum.

$$V = m_2 gl\cos(\theta) + \frac{1}{2}kx^2 \quad (15)$$

The Rayleigh's dissipative function account for damping force in the cart and it is expressed as:

$$D = \frac{1}{2}b\dot{x}^2 \quad (16)$$

Generalized forces:

$$\delta_1 = U(t); \delta_2 = 0$$

The Lagrange formulation defines the behaviour of a dynamic systems in terms of work and energy stored in the system (Urrea & Pascal, 2017). The augmented Lagrange function L is denoted as:

$$L = T - V \quad (17)$$

$$L = \frac{1}{2}m_1\dot{x}^2 + \frac{1}{2}m_2\dot{x}^2 + \frac{1}{2}l^2\dot{\theta}^2 + \frac{1}{2}I\dot{\theta}^2 + m_2\dot{x}\dot{\theta}l\cos(\theta) - \left(m_2 gl\cos(\theta) + \frac{1}{2}kx^2\right) \quad (18)$$

We evaluate the following partial derivatives based on equation (16) and (18) and using chain rule as:

$$\left(\frac{\partial L}{\partial x}\right) = -kx \quad (19)$$

$$\left(\frac{\partial L}{\partial \dot{x}}\right) = (m_1 + m_2)\dot{x} + m_2 l\cos(\theta)\dot{\theta} \quad (20)$$

$$\frac{d}{dt}\left(\frac{\partial L}{\partial \dot{x}}\right) = (m_1 + m_2)\ddot{x} + m_2 l\ddot{\theta}\cos(\theta) - m_2 l\dot{\theta}^2\sin(\theta) \quad (21)$$

$$\left(\frac{\partial L}{\partial \theta}\right) = -m_2 l\dot{x}\sin(\theta)\dot{\theta} - m_2 gl\sin(\theta) \quad (22)$$

$$\frac{d}{dt}\left(\frac{\partial L}{\partial \dot{\theta}}\right) = m_2\ddot{x}l\cos(\theta) - m_2\dot{x}l\sin(\theta)\dot{\theta} + m_2 l^2\ddot{\theta} + I\ddot{\theta} \quad (23)$$

$$\left(\frac{\partial L}{\partial \dot{\theta}}\right) = m_2\ddot{x}l\cos(\theta) - m_2 xl\sin(\dot{\theta})\dot{\theta} + \left[m_2 l^2 + I\right]\ddot{\theta} \quad (24)$$

$$\left(\frac{\partial D}{\partial \dot{x}}\right) = b\dot{x} \quad (25)$$

$$\left(\frac{\partial D}{\partial \dot{\theta}}\right) = 0 \quad (26)$$

For the generalized coordinate x, the Lagrange's equation is:

$$\frac{d}{dt}\left(\frac{\partial L}{\partial \dot{x}}\right) - \left(\frac{\partial L}{\partial x}\right) + \left(\frac{\partial D}{\partial \dot{x}}\right) = u \quad (27)$$

Substituting the partial derivatives of Eq. (19), (20), (21), (25) into Eq. (27) leads to:

$$(m_1 + m_2)\ddot{x} + m_2 l\cos(\theta)\ddot{\theta} - m_2 l\sin(\theta)\ddot{\theta} + b\dot{x} + kx = u(t) \quad (28)$$

Similarly, for the generalized co-ordinate θ , the Lagrange's equation is:

$$\frac{d}{dt}\left(\frac{\partial L}{\partial \dot{\theta}}\right) - \left(\frac{\partial L}{\partial \theta}\right) + \left(\frac{\partial D}{\partial \dot{\theta}}\right) = u \quad (29)$$

Substituting the partial derivatives of Eq. (22), (23), (24), (26) into Eq. (29) leads to:

$$\left(I + m_2 l_2^2\right)\ddot{\theta} + m_2 l\ddot{x}\cos(\theta) + m_2 gl\sin(\theta) = 0$$

Equation (28) and (29) describe the IPS equations of motion. For simplicity, these equations can be written in terms of inertial matrix, centrifugal force, Coriolis force vector and gravity force in compact matrix form using the generalized coordinate as a column vector θ . Thus, (28)-(29) can be equivalently written as

$$M(\theta)\ddot{\theta} + C\left(\theta, \dot{\theta}\right)\dot{\theta} + G(\theta) = \tau(u)$$

Where the matrices $M(\theta), C\left(\theta, \dot{\theta}\right), G(\theta)$ and $\tau(u)$ are time dependent and

$$M(\theta)=\begin{bmatrix} m_1+m_2 & m_2 l\cos(\theta) \\ m_2 l\cos(\theta) & m_2 l_2^2 + I \end{bmatrix},$$

$$C\left(\theta, \dot{\theta}\right)=\begin{bmatrix} 0 & -m_2\theta^2\sin(\theta)-b\dot{x} \\ 0 & 0 \end{bmatrix} \quad (31)$$

$$G(\theta)=\begin{bmatrix} kx \\ m_2 gl\sin(\theta) \end{bmatrix}, \tau(u)=\begin{bmatrix} 1 \\ 0 \end{bmatrix}$$

The moment of inertia I has be proven to equal $\frac{m_2 l^2}{12}$ in (Bogdanov, 2004). Apparently, the IPS is strongly nonlinear as a result of the states that exist as product of trigonometric function, however, this function make the system complex in dynamics and challenging to control. Observe now that the inertial matrix $M(\theta)$ is symmetric and nonsingular for every θ, since it determinant is always positive for all θ. So the determinant is

$$\det(M(\theta))=m_2^2 l^2\left[1-\cos^2(\theta)\right]+ (m_1+m_2)I+m_1 m_2 l^2>0 \quad (32)$$

To reduce the complexity and to simulate the dynamics accurately, the IPS is linearized around the (upright) equilibrium point such that the system is within the neighborhood of the linear system. This is hold for small deviations in the linear region such that the system state $x=\begin{bmatrix} x & \dot{x} & \theta & \dot{\theta} \end{bmatrix}^T=\begin{bmatrix}0 & 0 & 0 & 0\end{bmatrix}^T$ and the angle $\theta=\pi+\phi$ is very small such that we can make the approximations

$$\cos(\theta)\approx -1, \sin(\theta)\approx -\phi, \ddot{\theta}\cos(\theta)\approx -\ddot{\phi},$$

$$\dot{\theta}^2\sin(\theta)\approx 0, \dot{\theta}^2\approx 0$$

.

Under these approximations equation (28) and (29) become

$$(m_1+m_2)\ddot{x}-m_2 l\ddot{\phi}+b\dot{x}+kx=u \quad (33)$$

$$(I+m_2 l^2)\ddot{\phi}-m_2 gl\phi=m_2 l\ddot{x} \quad (34)$$

2.1. State Space Representation of the Model

A state space representation is a time domain approach of modeling complex dynamics of single input multiple output and multiple input multiple output systems. However, complex system with many degree-of-freedom and description of such systems with differential equations are often demanding and exhausting. So, state space representation of the system replaces the higher-order differential equations with a first-order matrix differential equations to reduce the system complexity in compact matrix form. Hence, the state and output equations are given in (Norman S, 2011) as:

$$\begin{aligned} \dot{x}(t)&=A..x(t)+B.u(t) \\ y(t)&=C.x(t)+D.u(t) \end{aligned} \quad (35)$$

Where, x, y, u, A, B, C, D are the state vector, output vector, input vector, system matrix, input matrix, output matrix and feedback matrix respectively. Let define the column vector as the state variables

$$x=\begin{bmatrix} x_1 & x_2 & x_3 & x_4 \end{bmatrix}^T=\begin{bmatrix} x & \dot{x} & \theta & \dot{\theta} \end{bmatrix}^T \quad (36)$$

Such that

$$\left.\begin{aligned} x_1&=x \\ \dot{x}_2&=\dot{x}_1=\dot{x} \\ \dot{x}_3&=\theta \\ \dot{x}_4&=\dot{x}_3=\dot{\theta} \end{aligned}\right\}$$

Hence, equation (33) and (34) can be written in state space representation form as

$$\dot{x}_1=x$$

$$\dot{x}_2=\frac{-k\left(I+m_2 l^2\right)}{I(m_1+m_2)+m_1 m_2 l^2}x_1-\frac{b\left(I+m_2 l^2\right)}{I(m_1+m_2)+m_1 m_2 l^2}x_2 + \frac{m_2^2 gl^2}{I(m_1+m_2)+m_1 m_2 l^2}x_3+\frac{I+m_2 l^2}{I(m_1+m_2)+m_1 m_2 l^2}u$$

$$\dot{x}_3=\theta$$

$$\dot{x}_4=\frac{-m_2 lk}{I(m_1+m_2)+m_1 m_2 l^2}x_1-\frac{blm_2}{I(m_1+m_2)+m_1 m_2 l^2}x_2 + \frac{m_2 gl(m_1+m_2)}{I(m_1+m_2)+m_1 m_2 l^2}x_3+\frac{m_2 l}{I(m_1+m_2)+m_1 m_2 l^2}u \quad (37)$$

Equivalently, equation (37) is presented in terms of A, B, C and D matrices of equation (35) as

$$A=\begin{bmatrix} 0 & 1 & 0 & 1 \\ \frac{-k\left(I+m_2l^2\right)}{I\left(m_1+m_2\right)+m_1m_2l^2} & \frac{-b\left(I+m_2l^2\right)}{I\left(m_1+m_2\right)+m_1m_2l^2} & \frac{m_2^2gl^2}{I\left(m_1+m_2\right)+m_1m_2l^2} & 0 \\ 0 & 0 & 0 & 1 \\ \frac{-m_2k}{I\left(m_1+m_2\right)+m_1m_2l^2} & \frac{-blm_2}{I\left(m_1+m_2\right)+m_1m_2l^2} & \frac{m_2gl\left(m_1+m_2\right)}{I\left(m_1+m_2\right)+m_1m_2l^2} & 0 \end{bmatrix}, \quad (38)$$

$$B=\begin{bmatrix} 0 \\ \frac{I+m_2l^2}{I\left(m_1+m_2\right)+m_1m_2l^2} \\ 0 \\ \frac{m_2l}{I\left(m_1+m_2\right)+m_1m_2l^2} \end{bmatrix}, C=\begin{bmatrix} 1 & 0 & 0 & 0 \\ 0 & 0 & 1 & 0 \end{bmatrix}, D=\begin{bmatrix} 0 \\ 0 \end{bmatrix}$$

3. CONTROL ALGORITHMS FOR IPS

Four different control algorithms are implemented on the IPS to effectively control and compare of the model dynamics performances after linearization around equilibrium point. This includes the proportional-integral-derivative controller (PID), Pole –placement approach, Linear Quadratic regulator (LQR) and LQR with Estimator. Since the last three controllers are designed via state space analysis, the model controllability and observability are the key control requirements for arbitrarily closed loop poles placement and state measurements respectively. However, the stability criteria ensures that all eigenvalues of IPS state matrix have a negative real part.

3.1 PID Controllers for IPS

PID controller is widely used in control and mechatronics applications because of its robustness, simplicity in control configuration and suitability for linear system. Hence, Two PID controllers are implemented to control the system such that when the cart reaches a desired position, the inverted pendulum stabilizes in the upright position. The PID controller algorithm combines the P-action, I-action and D-action to adjust the model error. The time domain description of the PID controller is given as:

$$u(t)=k_pe(t)+k_i\int_0^t e(\tau)d\tau+k_D\frac{de(t)}{dt} \quad (39)$$

Where u (t) is the control signal, the error signal e (t) is defined as e (t) =r (t)-y (t), and r (t) is the reference input signal. Fig.1 shows the PID controller Simulation model of an IPS and the parameters value are presented in Table 1.

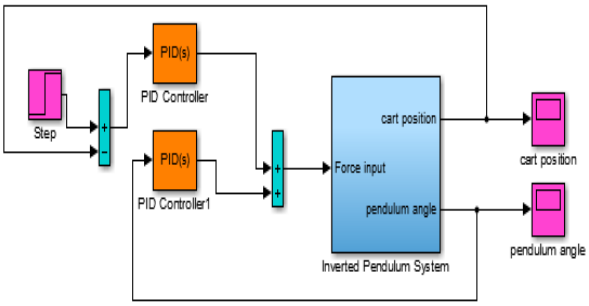

Fig. 2. Simulink implementation of PID controller for IPS

Table 1. parameter of the IPS

Parameter of the IPS	Value	Unit
Mass of the cart m_1	0.5	kg
Mass of the pendulum m_2	0.2	kg
Friction of the cart b	0.1	Ns/m
Spring coefficient of the cart k	0.4	N/m
Length to pendulum center of mass l	0.3	m
Inertial of the pendulum I	0.006	kg-m^2
External force applied to the cart u Cart position coordinate x		
Pendulum angle from vertical θ		
Centre of gravity g	9.8	m/s^2

3.2. Pole-Placement Feedback controller (PPFC) for IPS

The dynamics behaviour of the IPS is determined by its closed loop poles position and it is desirable to ensure that the system is fully controllable such that the rank of

the controllability matrix $Q_c = \begin{bmatrix} A & AB & A^2B \ldots A^{n-1}B \end{bmatrix}$ is non-zero. Hence, closed loop poles can then be arbitrarily assigned through a static state feedback to the pre-specified position. The control signal u is chosen such that $u = r - kx$ and the closed loop state space model can be written as

$$\dot{x} = Ax + Bu = (A - Bk)x + Br), y = Cx \quad (40)$$

This method depends on the performance criteria such as settling time, steady state error, peak time, maximum overshoot etc. In this design, we want to ensure that the system fulfill less than 5s settling time and overshoot of theta less than 20%. Invariably, the desired characteristic equation of the IPS is formulated from the performance criteria and compared with the IPS closed-loop system's characteristic equation using Ackerman's approach. The dominant close-loop poles of $s^2 + 2\xi\omega_n s + \omega_n^2 = 0$ is evaluated from the complex domain specification using the following formulas

$$\xi = \frac{-In\left(\%OS/100\right)}{\sqrt{\pi^2 + In^2\left(\%OS/100\right)}}, T_s < \frac{4}{\xi\omega_n}$$
$$\omega_d = \omega_n\sqrt{1-\xi^2}, \sigma = \xi\omega_n \quad (41)$$

The resulting values from equation (41) are

$$\xi = 0.707, \omega_n = 9.89rad, \sigma = 7, \omega_d = 7$$

So, that the complex dominant poles, $-\sigma \pm j\omega_d$ is approximated as $-7 \pm j7$. The matrices A and B after substituting the parameters value in Table1 turn out to be

$$A = \begin{bmatrix} 0 & 1 & 0 & 0 \\ -0.7273 & -0.1818 & 2.6727 & 0 \\ 0 & 0 & 0 & 1 \\ -1.8182 & -0.4545 & 31.1818 & 0 \end{bmatrix}, B = \begin{bmatrix} 0 \\ 1.8182 \\ 0 \\ 4.5455 \end{bmatrix} \quad (42)$$

$$Poles = \begin{Bmatrix} -5.5897 \\ 5.5521 \\ -0.0721 - 0.7543i \\ -0.9721 + 0.7543i \end{Bmatrix} \quad (43)$$

However, the eigenvalues of A which is the dynamics of the system as depicted in equation (43) are not stable since one of the four poles lies on the right hand side of the s-plane. However, the rank of the controllability matrix confirmed that the system is controllable because the determinant is a non-zero. So, the pole placement approach is computed using a MATLAB function acker () which taken the matrices A, B and poles P as an argument. Where (A, B) is the state space model, P is a vector containing the desired pole positions.

3.3. Linear Quadratic Regulator Controller (LQR) for IPS

It is a known fact that all the desired requirement cannot be satisfied as result of the various tradeoffs that must be made and limitations of the design techniques, hence, optimization based technique that requires some measures of performance index to minimize a cost function is incorporated. We define a cost function depending on the position and the input and minimize it with respect to these parameters, so as to minimize the performance index

$$J = \int_0^\infty \left(x^T Qx + u^T Ru\right)dt \quad (44)$$

Where Q and R, are weight matrices for each parameter and the relative weighting chosen for Q and R determine the relative importance of error reduction and control energy saving. Hence, the controller K, that minimize the cost function J is based on finding the positive definite solution of algebraic Riccati equation (ARE)

$$A^T P + PA - PBR^{-1}B^T P + Q = 0 \quad (45)$$

Such that $u(t) = -kx = -R^{-1}B^T Px(t)$ is optimal for any initial x (0) state. The weighting matrices Q and R are chosen as

$$Q = \begin{bmatrix} x & 0 & 0 & 0 \\ 0 & 0 & 0 & 0 \\ 0 & 0 & y & 0 \\ 0 & 0 & 0 & 0 \end{bmatrix}, R = 1 \quad (46)$$

The matrix Q is selected as indicated in Eq. (46) such that the controller can be easily tuned by changing the non-zero x and y elements in the Q matrix of the m-file function to enhance desirable response. Also, x and y have been used to describe the relative weight of the tracking error in the cart's position and pendulum's angle versus the control effort.

3.4. Linear Quadratic Regulator control with Estimator for IPS

To improve the performance of the IPS, the LQR and the state estimator are combined. The full-order estimator estimates all the state that are not measured. Before we design our estimator, we will first verify that our system is observable. The property of observability determines whether or not based on the measured outputs of the system we can estimate the state of the system. For the system to be completely state observable, the observability matrix $Q_o = \begin{bmatrix} C \\ CA \\ :. \\ CA^{n-1} \end{bmatrix}$ must have rank n where n is the number of state variables of the system. In

this case, the system is observable since observability matrix has a maximum of 4. Hence, an m-file function is generated in MATLAB for simulation and the results are discussed extensively.

4. RESULTS AND DISCUSSION

The mathematic dynamics equations of the linearized model is programmed in m-file function of MATLAB and the simulations are run for all the control algorithms. For the PID controller a simulator is built in SIMULINK and the performance of all the control schemes are compared. The control of the inverted pendulum angle is implemented with four different control algorithms namely;

1. Two PID controllers
2. Pole placement feedback controller
3. Linear Quadratic Regulator, LQR and
4. Combination of LQR with Estimator.

Fig 3, 4, 5 and 6 show the graphical step response of the cart's position and the pendulum angle's for all the four control algorithms. In Fig 6 and 7 the cart position and pendulum angle for all the four control schemes are superimposed to facilitate easy performance comparison. In this figure, the responses for the both cart's position and pendulum angles of PID, PPFC, LQR and LQR +Estimator are in cyan, red, blue and magnate respectively. In fig 9 and 10, the cart's position and pendulum angle's step response for all control algorithms are presented for system performance evaluation. Table 2 shows the summary of the performance of the pendulum angle.

Table 2. Pendulum angle simulation results for all control algorithms

Time response specification	PID	PPFC	LQR	LQR+Estimator
Settling Time (Ts)	1.5 s	1.58 s	1.5s	1.48s
Max.Overshoot (%)	10	16	10	9.98
Steady State error	0	0	0	0

It is evident from the Table 2 that the combined action of LQR and Estimator has a settling time of 1.48sec and overshoot of 9.89% which compensate for fast response and stabilize the pendulum angle with minimum overshoot when compared to other algorithms. However, the PID controller and LQR show similar time response characteristics but their overshoot is a lit bit higher when compared with combined action of LQR and Estimator. It can also be deduced that the pole placement feedback controller shows a worst system response. According to the fig 9, it can be deduced that the LQR and Estimator controller exhibit better response and performance. It can be concluded that the combined action of LQR and Estimator is capable of minimizing the error since all the state are available for measurement so as to stabilize the inverted pendulum in the upright position via selecting a weight matrices Q and R that we save control energy and ensure a fair tradeoff between the performance and control effort.

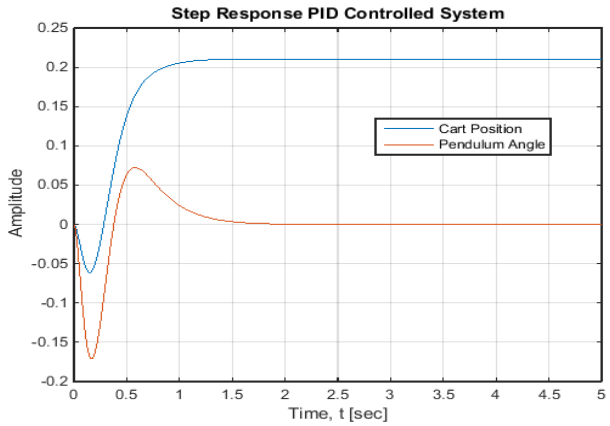

Fig. 3. Step response of PID controller

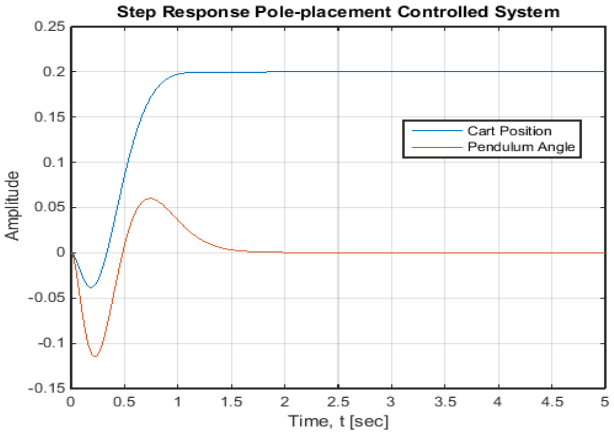

Fig. 4. Step response of PPFC controller

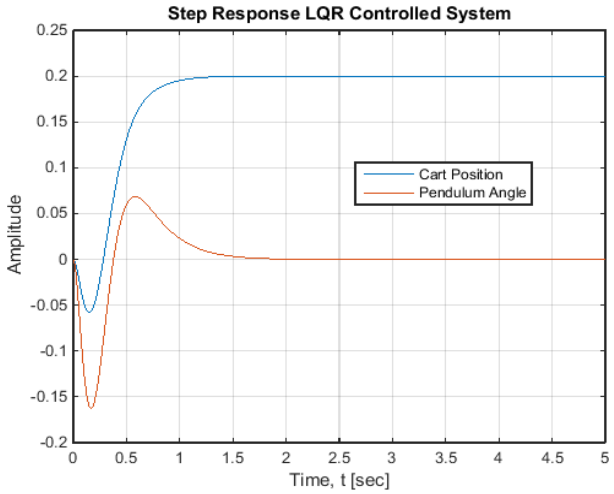

Fig. 5. Step response of LQR controller

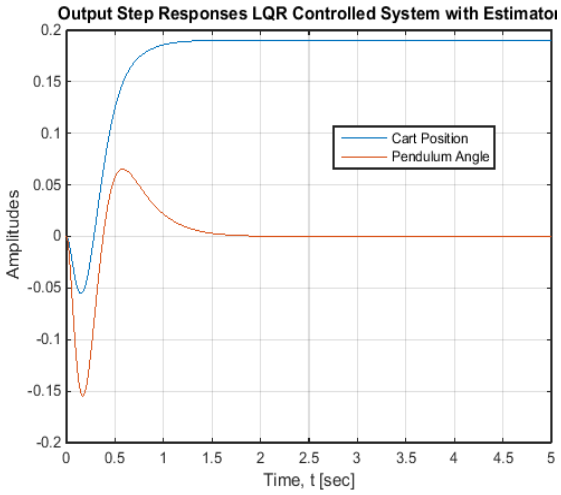

Fig. 6. Step response of LQR + Estimator controller

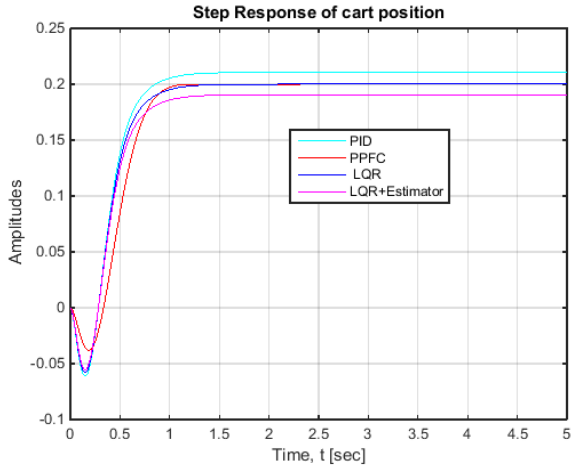

Fig. 9. Step Response for superimposed control algorithms on cart position

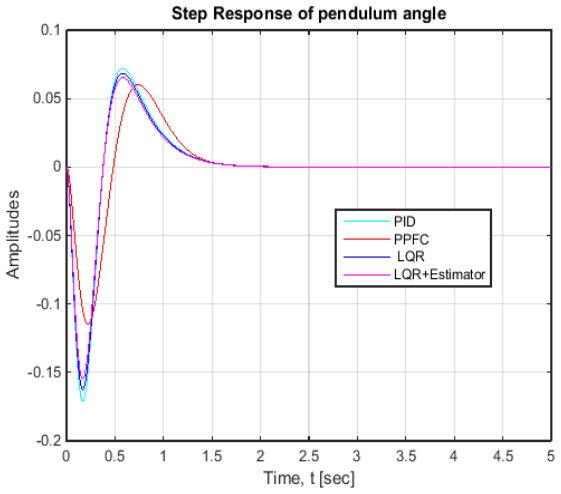

Fig. 10. Step Response for superimposed control algorithms on pendulum angle

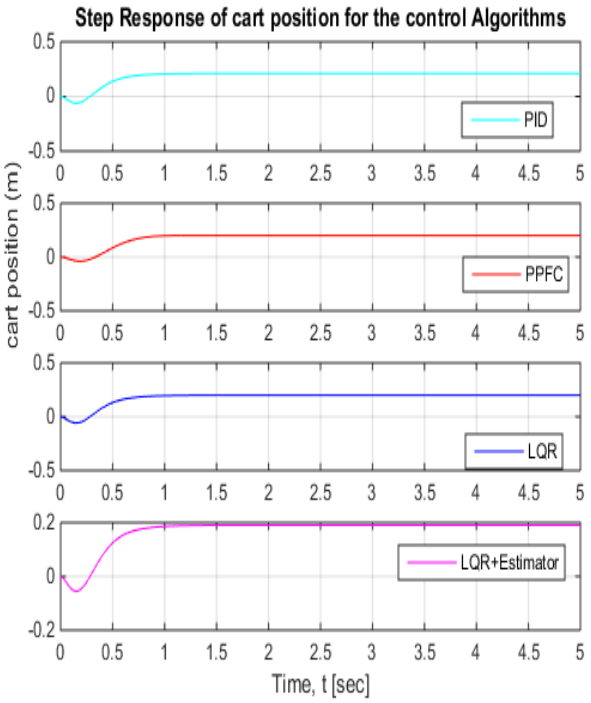

Fig. 7. Step response of cart's position for the control algorithms

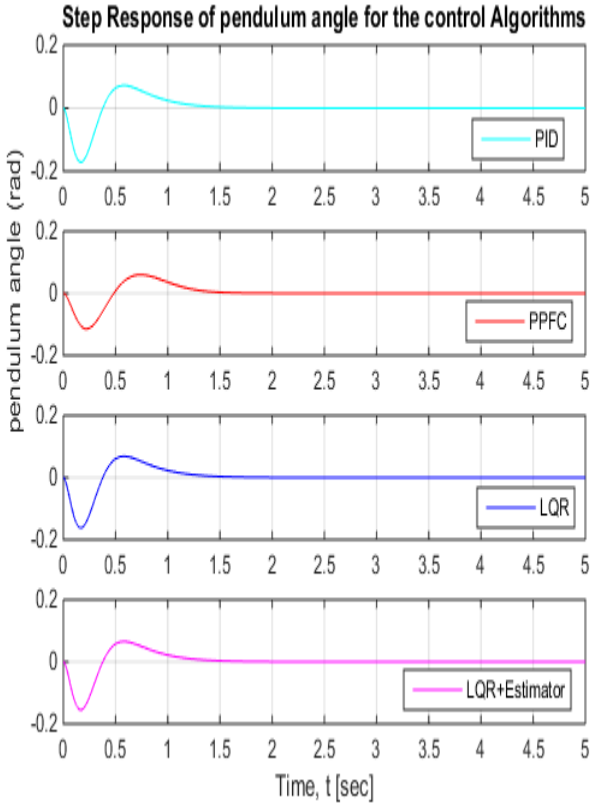

Fig. 8. Step response of pendulum angle's for all the control algorithms

5. CONCLUSION

The dynamic model and control algorithms designed

of an inverted pendulum has been successfully formulated and implemented in this paper. The IPS dynamic model was anatomized based on Lagrangian and Euler-Lagrange approach and to simulate the dynamics accurately, the inverted pendulum system is linearized around the upright point such that the system is within the neighborhood of the linear region. Hence, four different control algorithms are implemented with MATLAB/Simulink environment on the linearized model to investigate the performance characteristics of the IPS.

By relating the responses of all the control algorithms of the Table 2, it is found that there is a tradeoff between the response and overshoot of PID as the gain increases or decreases and this significantly influence the PID controller performance. Although, the performance of the of pole-placement feedback controller is higher than other control algorithms as a result of arbitrarily pole location of the poles that require turning for optimal performance at the expense of performance. The response of LQR and LQR+Estimator are similar but it is obvious that LQR +Estimator controllers is a little improved compared to the LQR as it contains an estimator that estimate all the state that are not measured, which in turn contributes to error minimization. Among all the proposed control algorithms, the combined action of LQR+ estimator control scheme gives a better response and performance. This relative performance investigation for this baseline system substantiates that the proposed LQR+Estimator approach is simple, effective and robust for controlling linearized model of dynamic system.

ACKNOWLEDGEMENTS

The authors are indebted to HAN University of Applied Sciences and Olabisi Onabanjo University for providing facilities and support.

REFERENCES

Ababneh, M., Salah, M., & Alwidyan, K. (2011). Linearization of Nonlinear Dynamical Systems : A Comparative Study. Jordan Journal of Mechanical and Industrial Engineering, 5(6), 567–571.

Agarana, M. C., & Ajayi, O. O. (2017). Dynamic Modeling and Analysis of Inverted Pendulum using Lagrangian-Differential Transform Method. In Proceedings of the World Congress on Engineering 2017 Vol II WCE 2017 (Vol. II, pp. 3–8).

Bettayeb, M., Boussalem, C., Mansouri, R., & Al-saggaf, U. M. (2014). Stabilization of an inverted pendulum-cart system by fractional PI-state feedback. ISA Transactions, 53(2), 508–516.

Bogdanov, A. (2004). Optimal control of a double inverted pendulum on a cart. CSEE, OGI School of Science and Engineering, …. Retrieved from http://speech.bme.ogi.edu/publications/ps/bogdanov04a.pdf%5Cnfile:///C:/Users/Spencer/Documents/Mendeley Desktop/Optimal control of a double inverted pendulum on a cart - 2004 - Bogdanov.pdf

Chandan, Kumar, Santosh, Lal, Nilanjan, Patra, Kaushik, Halder, Motahar, R. et . a. (2012). Optimal Controller Design for Inverted Pendulum System based on LQR method 1,2,3,4. In 2012 IEEE International Conference on Advanced Communication Control and Computing Technologies (ICACCCT) (pp. 259–263).

Chen, X., Yu, R., Huang, K., & Zhen, S. (2018). Simulation Modelling Practice and Theory Linear motor driven double inverted pendulum : A novel mechanical design as a testb e d for control algorithms. Simulation Modelling Practice and Theory, 81, 31–50.

Dastranj, M. R., Moghaddas, M., Ghezi, Y., & Rouhani, M. (2012). Robust Control of Inverted Pendulum Using Fuzzy Sliding Mode Control and Genetic Algorithm. International Journal of Information and Electronics Engineering, 2(5), 773–776.

Eizadiyan, M. A., & Naseriyan, M. (2015). Control Of Inverted Pendulum Cart System by Use of M d F m x F m y d x x, 27(2), 1063–1068.

Goswami, A. (2013). The analysis of inverted pendulum control and its other applications. Journal of Applied Mathematics & Bioinformatics, 3(3), 113–122.

Guo, H., & Unversity, S. L. (n.d.). Modelling and Simulation of a Single Inverted Pendulum System Based on Matlab, 463–464.

İlgen, S., Oflaz, E., Gülbahçe, E., & Çakan, A. (2016). Applied Mathematics , Electronics and Computers Modelling and Control of a Single-Wheel Inverted Pendulum by Using Adams and Matlab. International Journal of Applied Mathematics, Electronics and Computers, 4, 326–328.

Ilyas, A., Yahya, S., & Al-rizzo, H. (2017). Fuzzy-logic control of an inverted pendulum on a cart R. Computers and Electrical Engineering, 61, 31–47.

Irfan, Jamil, Rehan, Jamil, Zhao, Jinquan, Rizwan, Jamil& Abdus, S. (2013). Mathematical Model Analysis And Control Algorithms Design Based On State Feedback Method of Rotary Inverted Pendulum. International Journal of Research In Engineering & Technology, 1(3), 41–50.

Jose, A., Augustine, C., Malola, S. M., & Chacko, K. (2015). Performance Study of PID Controller and LQR Technique for Inverted Pendulum. World Journal of Engineering and Technology, (May), 76–81.

Kafetzis, I., Moysis, L., & Sciences, M. (2017). Inverted Pendulum : A system with innumerable applications 2 . Modeling the Inverted Pendulum Consider the system consisting of a cart with a rod placed on its center as. In IKEECONF-2017 9th International Week Dedicated to MathsAt: Thessaloniki, Greece.

Krishna, N. R., Bindhu, K. R., & Vinod, B. R. (2016). Modeling and controller design of cart inverted pendulum system using MRAC scheme. Frontiers of Current Trends In Engineering And Technology April, 24(April), 21–24.

Kumar, R., Singh, R. B., & Das, J. (2013). Modeling And Simulation of Inverted Pendulum System Using Matlab : Overview. International Journal of Mechanical and

Production Engineering, 1(4), 52–55.

Lee, G. H., Lee, H. J., Choi, H. J., Jeon, H. J., & Jung, S. (2009). Application of Mobile Inverted Pendulum Systems to Boxingbots for a Boxing Game. In 2009 IEEE/ASME International Conference on Advanced Intelligent Mechatronics Suntec Convention and Exhibition Center Singapore (pp. 963–968).

Lee, J., Mukherjee, R., & Khalil, H. K. (2015). Automatica Output feedback stabilization of inverted pendulum on a cart in the presence of uncertainties ☆. Automatica, 54, 146–157.

Mishra, S. K., & Chandra, D. (2014). Stabilization and Tracking Control of Inverted Pendulum Using Fractional Order PID Controllers. Journal of Engineering.

Nithya, R., & Vivekanandan, C. (2014). Stability Analysis and State Feedback Stabilization of Inverted Pendulum. International Journal of Computer Science and Mobile Computing A Monthly Journal of Computer Science and Information Technology ISSN, 3(5), 310–320. Retrieved from www.ijcsmc.com

Norman S, N. (2011). Control Systems Engineering (sixth). River Street Hoboken: Sons, John Wiley & Sons.

Oltean, S.-E. (2014). Swing-up and Stabilization of the Rotational Inverted Pendulum Using PD and Fuzzy-PD Controllers. Procedia Technology, 12, 57–64.

Prado, S. D., & Fernandes, H. A. (2017). Commun Nonlinear Sci Numer Simulat A new look on the stabilization of inverted pendulum with parametric excitation and large random frequencies : Analytical and numerical approaches. Communications in Nonlinear Science and Numerical Simulation, 51, 105–114.

Prayitno, A., Indrawati, V., & Trusulaw, I. I. (2017). Optimal control of inverted pendulum system using PID controller , LQR and MPC Optimal control of inverted pendulum system using PID controller , LQR and MPC. In 14th ICSET-2017 IOP Conf. Series: Materials Science and Engineering.

Přemysl, Strakoš, Jiří, T. (2017). Mathematical Modelling and Controller Design of Inverted Pendulum. In Carpathianian Control Conference (ICCC) 18th International, pp. 388–393.

Sangfeel, K., Eunji, S., Kyungsik, K., & Byungseop, S. (2015). Design of Fuzzy Logic Controller for Inverted Pendulum-type Mobile Robot using Smart In-Wheel Motor. Indian Journal of Science and Technology, 8(April), 493–503.

Singh, A. K., & Ph, D. (2015). Design of a Robust Controller for Inverted Pendulum. International Journal of Computer Applications, 112(16), 23–28.

Siradjuddin, I., Setiawan, B., Fahmi, A., Amalia, Z., & Rohadi, E. (2017). linearised model. International Journal of Mechanical & Mechatronics Engineering IJMME-IJENS, 17(1), 119–126.

Urrea, C., & Pascal, J. (2017). Parameter identification methods for real redundant manipulators. Journal of Applied Research and Technology, 15, 320–331.

Wang, J. (2011). Simulation Modelling Practice and Theory Simulation studies of inverted pendulum based on PID controllers. Simulation Modelling Practice and Theory, 19(1), 440–449.

Turkish Journal of Engineering

Turkish Journal of Engineering (TUJE)
Vol. 3, Issue 1, pp. 25-31, January 2019
ISSN 2587-1366, Turkey
DOI: 10.31127/tuje.419531
Research Article

LASER CLADDING OF HOT WORK TOOL STEEL (H13) WITH TIC NANOPARTICLES

Tuncay Simsek [*1], Mahmut Izciler [2], Sadan Ozcan [3,4] and Adnan Akkurt [5]

[1] Mersin University, Architecture Faculty, Department of Industrial Design, Mersin, Turkey
tuncaysimsek@mersin.edu.tr
ORCID ID 0000-0002-4683-0152

[2] Gazi University, Technology Faculty, Department of Manufacturing Engineering, Ankara, Turkey
ORCID ID /0000-0002-0242-489X
mizciler@gazi.edu.tr

[3] Hacettepe University, Department of Physical Engineering, Ankara, Turkey
[4] Hacettepe University, Division of Nanotechnology and Nanomedicine, Ankara, Turkey
ORCID ID 0000-0001-7966-1845
sadan@hacettepe.edu.tr

[5] Gazi University, Industrial Design Engineering, Ankara, Turkey
ORCID ID 0000-0002-0622-1352
aakurt@gazi.edu.tr

* Corresponding Author
Received: 29/04/2018 Accepted: 06/08/2018

ABSTRACT
In this study, titanium carbide nanoparticles (TiC) were coated on the surface of X40CrMoV51 (H13) hot work tool steel by laser coating method. Two stage laser cladding method was employed for coating processes. In the first stage, TiC powders were mixed in the phonelic resin and precoated at 50 µm thickness on the surface of steel substrate under vacuum. In the second stage, laser was directed to the surface and then hard coating layers were obtained on the steel surfaces. A CO_2 laser with 2000 W power was operated at continuous-wave mode in the experiments. All laser cladding processes were performed under N_2 atmosphere and various laser powers were selected to show the effect of laser power on the quality of coated steel surfaces. The morphology and phase structures were examined by scanning electron microscopy, X-ray spectroscopy and optic microscope, respectively. The hardness of coating layers and bonding strength was defined with micro hardness tests and scratch test. The thickness of the coatings layers were measured in the range of 15-130 µm depending on laser powers. It is seen that crack-free, smooth and homogenous coating layers can be obtained at 237 W laser power. According to the hardness and micro-scratch tests results, hardness was improved significantly, and all coating layers had a good metallurgical strength to the substrate.

Keywords: *Laser Cladding, Nanoparticles, TiC, Tool Steel*

1. INTRODUCTION

With improvements in manufacturing technologies, the usage of tool steels has been increasing in recent years (Barra *et al*., 2003; Dosbaeva *et al*., 2015; Ozkul *et al*., 2017). Especially, H13 tool steel, which is widely used in plastic injection molding, casting, forging and extrusion etc., attracts significant attention due to its high elevated temperature strength, ductility, good annealing resistance and cost (Wei *et al*., 2011) Despite the fact that, H13 hot work tool steels are mostly used as structural material and intensively used in machine manufacturing, it is not preferred in the applications requiring high wear resistance due to its low wear properties. Particularly, under continuous mechanical and thermal loads, severe wears occur in tool steels (Medvedava *et al*., 2009; Luong *et al*., 1981) and these situations limits the usage of these materials (Bailey *et al.*, 2017; Telesang *et al.*, 2014; Mangour *et al.*, 2016). Therefore, in some cases to eliminate these problems whole part or relevant part of the workpieces are coated by various coating methods (Reza *et al.*, 2048; King *et al.*, 2004; Recco *et al.*, 2007). As it is known, while coatings improve the surface properties, it might also affect adversely the properties of the materials such as toughness, hardness etc. so that coating methods should be selected correctly according to substrate and coating materials. Recently, coating studies with nanoparticles showed that tribological and physical properties of materials can be improved significantly with usage of nanomaterials (Li *et al.*, 2006; Lehman *et al.*, 2012). Various methods are used for the coating of nanoparticles. Laser cladding method is one of the important method among them and it is intensively preferred in recent years. By using the superior features of laser beam, hard, homogenous, crackfree and nonporous layers with high wear and corrosion resistance can be obtained on the metal surfaces. A lot of coating studies with different laser sources can be seen in the literature. Most of these studies are conducted with CO_2 and Nd:YAG lasers but it is also seen that usage of fiber and diode laser are increased over time (Campanelli *et al.*, 2017; Yan *et al.*, 2017; Eerfanmanesh *et al.*, 2017; Weng *et al.*, 2017; Zhang *et al.*, 2017; Riverio *et al.*, 2014; Adraider *et al.*, 2012). All these studies specified that bonding between pre-cladding process and substrate before the cladding as well as selected laser parameters such as laser power, laser scanning speed, feed rate, diameter of laser spot, shielding gas and its pressure, play a fundamental role on quality of the cladding (Chew *et al.*, 2017; Cheng *et al.*, 2017; Weng *et al.*, 2017; Shi *et al.*, 2018; Emamian *et al.*, 2011).

In this study, TiC nanoparticles were pre-coated on the surface of H13 hot work tool steel under vacuum without any additive material and then laser clad at different laser powers by using 2 kW CO_2 laser while other parameters were kept constant. Coatings microstructures and bond strength to substrate were investigated.

2. EXPERIMENTAL METHOD

In laser cladding experiments, as coating material TiC nanoparticles with 10 nm crystallite size was used while commercial H13 tool steel was used as substrate. The steel substrate was prepared in the size of 100 (length) X 15 (width) X 1.5 (thickness) mm. The chemical composition of the substrate is given in Table 1 (Simsek, 2010).

Table 1. Chemical composition of DIN 1.2344 X40CrMoV51 (H13) tool steel

	C	Mn	Si	P	S	Cr	V	Mo	Fe
Chemical composition (Wt / %)	0.40	0.40	1.10	0.03	0.03	5.30	1.00	1.40	Bal.

Before the coating, the steel surfaces were sandblasted and cleaned with acetone-ethanol for purification from oil, rust and similar undesired contaminants. Phenolic resin was used in order to bond the nanoparticle to substrate. 5 wt% TiC nanoparticles were mixed with vinyl-phenolic resin (Araldit 71) and pre-coated at 50 µm thickness to metal surfaces carefully. In order to have a strong bond to metal surface, samples were dried in 20 mbar vacuum at 200 ˚C for 4 hours (Yilbas *et al.*, 2013). Prepared samples were exposed to the cladding process under N_2 atmosphere with 2 kW CO_2 laser (Amada, LC-2415 α III) at continuous-wave mode. Fig. 1 shows the schematic view of laser experiments setup.

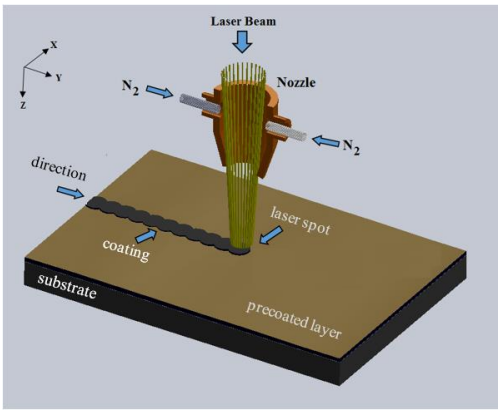

Fig. 1. The schematic view of laser experiments setups

Laser coating parameters are given in Table 2. The laser beam profile was Gaussian type. The laser beam focused on the layers was 300 µm in diameter and the nominal focal length of the lens was held at 127 µm. The overlapping ratio of the laser spot during the scanning was 80%, which formed continuous melting throughout the laser coating process. In the laser cladding experiments, laser energy density were changed while other parameters were kept constant. Table 2 shows the parameters selected during the cladding processes. These parameters were optimized after performing a series of experiments that provided the crack and cavity-free and non-porous coating layers. In the processing of materials, the following (Eq. 1) describes the energy density of a laser beam (also known as beam exposure). At sufficiently high energy densities, lasers can be used to cut through sheet metals, weld materials together, sinter powders together to form solids. Although, the energy density is an important indicator of energy input, there seems to be a strong correlation between energy density and some basic properties of laser coated parts such as porosity, microstructure and phase ratio at the surface

during coating.

$$E_\rho = P / (H.V) \quad (1)$$

where,
E_ρ = laser energy intensity ($J.cm^{-2}$) for single layer deposition
P = laser power (W)
H = Hatch space (μm) calculated as per [Overlap = (Spot size – Hatch space) / Spot size]
V = scan velocity ($cm.s^{-1}$)

Table 2. Laser cladding conditions

Average Laser Power	(W)	13, 73, 160, 237
Energy intensity	(J/cm^{-2})	$4.3x10^3$, $2.43x10^4$, $5.3x10^4$, $7.8x10^4$
Laser Wave Length	(μm)	10.64
Laser Beam Diameter	(mm)	0.3
Focal Length	(mm)	127
Frequency	(Hz)	1500
Scanning Speed	(cm/s)	0.5
Spot Diameter	(μm)	300
Hatch space (80% overlap)	(μm)	60
N_2 Pressure	(kPa)	200

Phase structures of nanoparticles were analysed by using X-Ray diffraction spectrophotometer (XRD, Rigaku, D/MAX-2200) with Cu–Kα radiation generated at 40 kV, 30 mA, in a range of 2θ from 20 to 80°, at 8°/min scanning rate. Scherrer's formula was used to calculate the crystallite size (Equation 2). In Equation 2, $\boldsymbol{\tau}$ represents the crystallite size, K is a constant taken depending on the crystal shape (0.89), λ is the x-ray wavelength (1.54Å), β is the full width at half maximum (FWHM) of the peak and θ is the Bragg angle. The FWHM and the position of (100) peak in the XRD pattern of TiC phase were used for crystallite size calculations. International Center for Diffraction Data (ICDD) powder diffraction files were used in the identification of crystalline phases.

$$\tau = \frac{K \,.\, \lambda}{B \,.\, Cos\,\theta} \quad (2)$$

Coated layers microstructures were characterized via optical microscope (Leica M205 C) and scanning electron microscope (FEI Quanta 200F). Laser coated specimens were cut by using a precise abrasive disc and polished by abrasives. For the microstructure examinations; the specimens were etched in a 5 % nital solution for 10 seconds. Micro hardness was measured by using a hardness tester (CSM instrument) under 200 mN load for 10 seconds with Berkovich B-K32 diamond tip. The measurements were repeated five times carefully in the similar area and the mean values were taken. The bond strengths were examined by scratch tester (CSM Instruments MST). In the scratch test; the load was applied in such a way that it would increase from 0.5 N to 20 N at 3 mm distance with a 100 μm diameter Rockwell diamond tool. Scratched surfaces were also examined by optical microscope (Simsek, 2010).

3. RESULTS AND DISCUSSION

The XRD pattern and SEM images of coating materials are given in Fig. 2. It is noticed that powders are consisted of cubic titanium carbide (ICDD Card No: 2-1179, cubic system, space group Fm-3m) (Sivkov et al., 2016). There were also some WC impurities because of worn of milling vial and balls used during synthesis procedures. It is seen that particles are mostly in irregular shape and morphology and crystallite sizes of the nanoparticles were calculated as approximately 10 nm by Scherrer's equation (Simsek, 2010).

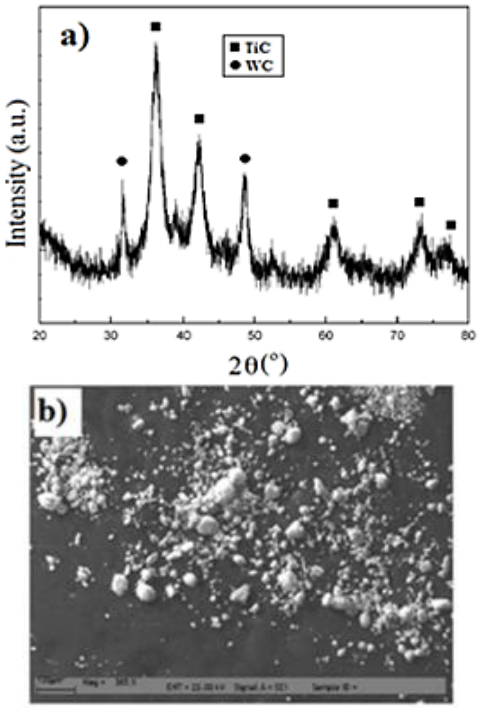

Fig. 2. a) XRD pattern and b) SEM images of the coating materials (Simsek, 2010).

Laser power was chosen in the range of 13-237 W in the experiments for the purpose of preventing any possibility of evaporation during the laser surface treatment. It seen that power below and above this values also caused the intensive crack and pores on the coated layers. The pictures of laser coating during process, precoated and laser treated surfaces are given in Fig. 3a-c, respectively.

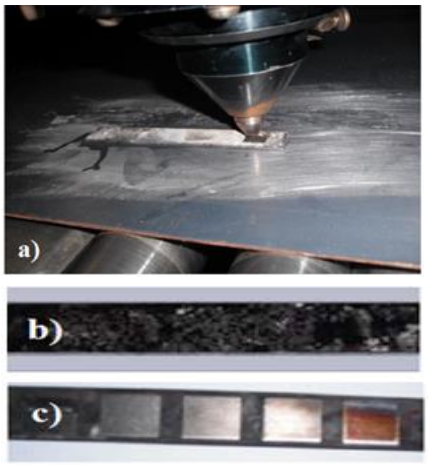

Fig. 3. a) Laser coating process b) Precoated samples c) Laser coated samples

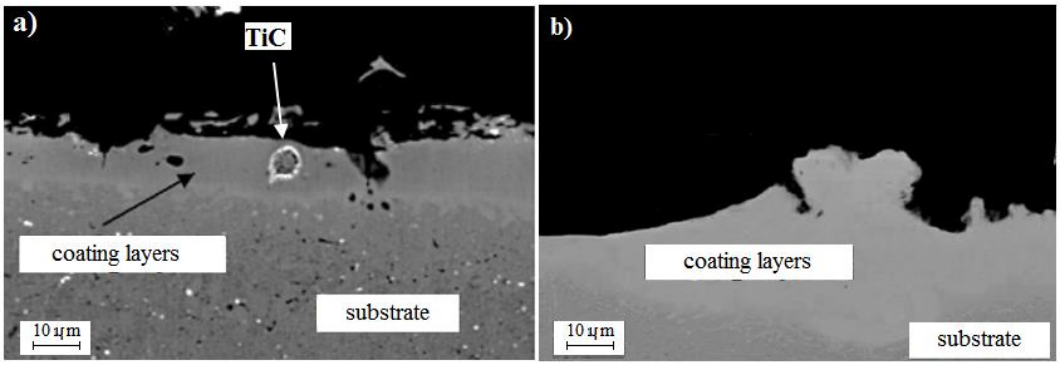

Fig. 4. SEM images of the laser coated layers a) 13 W laser power b) 73 W laser power

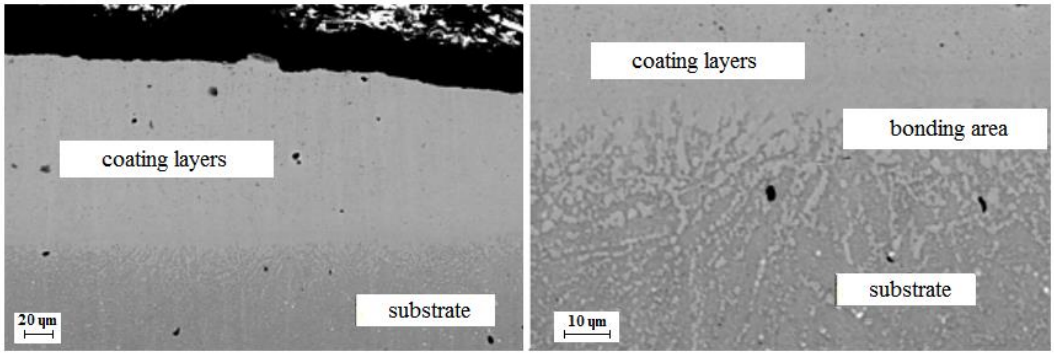

Fig. 5. SEM images of the laser coated layers at 237 W laser power

When the cross-section images in Fig. 4 were examined, it was seen that a thinner cladding layer was obtained at low laser power compared to high laser power (Fig. 5) since surface of base material was less molten. Cracks and cavities were observed on the surfaces of the samples cladded at 13-73 W laser power when compared to the cladding layers obtained at other high powers due to the thermal shocks caused by heat input and immediate cooling (Fig. 5). In the experiments with low laser power, there was no diffusion between the material surface and the coating material. It is also seen that the TiC nanoparticles were not dispersed homogeneously and agglomerated.

Thickness in the sample cladded at 13 W was determined as approximately 15 µm while thickness was not regular at the 73 W laser coated layers. At higher laser powers, transition amount of cladding material increased due to excess of melt amount occurring on the substrate surface. Thus, the thickness of the cladding layer was higher compared to the cladding layers obtained at lower powers (Fig. 5). Cracks and cavities occurring after rapid cooling decreased since there was a sufficient wetting between the ceramic phase and the substrate. It is also observed that the nearly similar problems were occurred with experiments conducted at 160 W laser power. However, no fractures and cavities were seen at layers obtained at 237 W laser power. This was attributed to the self-annealing effect of the layers formed by laser scanning tracks. Each scanned tracks modified the heat conduction and cooling rates in the coating area to be more thermally conductive. Furthermore, it was specified that cladding thickness was within the range of 110-130 µm depending on the increase in the laser power. Cross-sections examinations showed that coating layers with good metallurgical bond to the substrate can be obtained on the surfaces without any porosity and cracks (Fig. 5). Heat affected zone thickness was measured about 30 µm and gradually increased from cladding layer to the substrate. The results showed that the laser power was a very effective factor on the cladding quality (Simsek, 2010).

Comparative variation of the average hardness is given in Fig. 6. The measurements were repeated five times carefully in the similar areas and the mean values were taken into account. It was found that the hardness of substrate which was measured about 480 HV, increased up to approximately 1200 HV on the coated surface. In the experiments performed at low laser powers, the diffusion was very low and the substrate was melted less. Furthermore, due to the problems such as intensive cracks and pores, the hardness values were not taken properly so that the coated layers obtained at 237 W laser power were used in the microhardness and scratch tests. In literature, similar hardness values were also reported in Ignat *et al* studies. They specified that hardness of low carbon steel surface was increased from 200 HV to 1200 HV after cladding processes (Ignat *et al.*, 2003). In another study conducted by Jiang et al with TiC/H13 powder mixtures, they reported that after laser coating processes hardness of the AISI 4140 steel was increased from 200-250 HV to 860 HV (Jiang *et al.*, 2007).

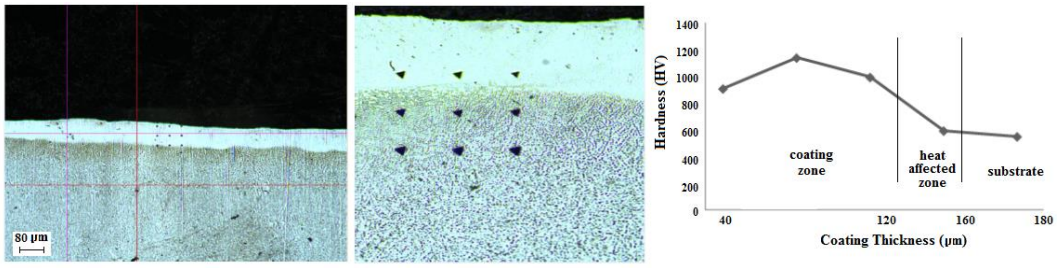

Fig. 6. Optic images and microhardness graphs of coated layers at 237 W (Simsek, 2010).

Normally, smooth surfaces are required for scratch tests otherwise the results can be deceived. Due to the nature of the laser coating process, the roughness of the surfaces after laser processing is not as smooth as the surfaces of the PVD or CVD coating. Scratch test results such as acoustic emission and penetration depth values, depending on the scratch distance were given in Fig. 7. Surface images of coated layers were also examined by optical microscope. It can be seen from acoustic emission graphs that critical load was 8.30 N at the 1.20 mm distance and scratch trace and surrounding small-sized fractures can be seen in the optic microscope images of the samples coated with 237 W laser power (Fig. 7a). Second critic load was observed around 12.20 N (Fig. 7b). Then continuous cracks were observed at 14.15 and continued up to 16.10 N load (Fig. 7c, d). Furthermore, it was seen that the penetration depth of the scratcher showed a regular increasing trend in the all coated layers.

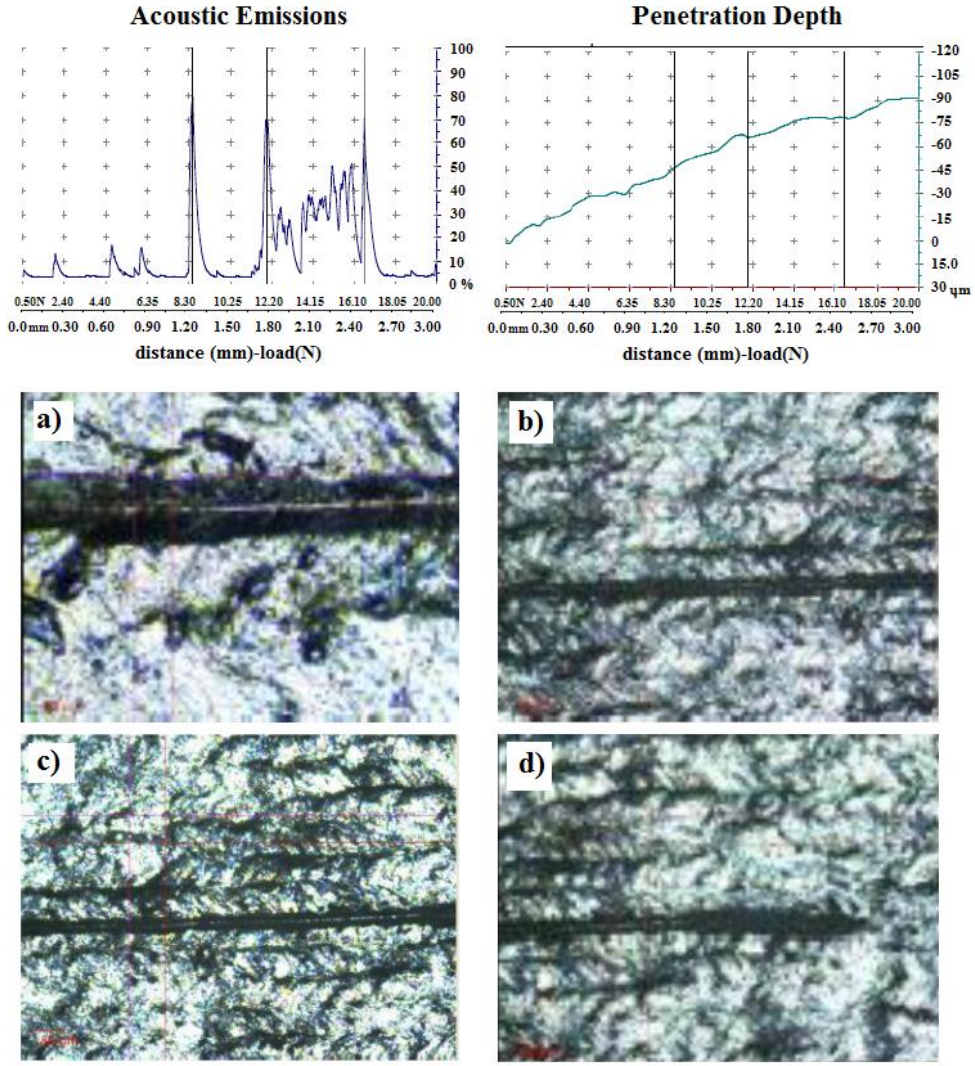

Fig. 7. Acoustic emission, penetration depth and optical microscope (X120) images of the coated layers under progressive load of 0.5-20 N

4. CONCLUSIONS

It is seen that TiC nanoparticles can be successfully coated to surface of H13 hot work tool steel under optimum conditions and careful precoating process. When the microstructures of the resulting coatings were examined, it is found that the laser power is very important factor on the coating quality. In the experiments with low laser power, there was no diffusion between the material surface and the coating materials. It is found that intensive cracks and pores were observed in the coatings and nanoparticles did not disperse homogeneously on the surfaces and get agglomerated. However, the most successful coatings were obtained at a thickness of approximately 130 μm at the surface of the H13 tool steel with the laser power of 237 W under N_2 atmosphere. The hardness was improved nearly 3 times when compared to substrate. It was also determined that hard and wear-resistant phases on the surface increased the resistance of the cladding layer against scratching.

REFERENCES

Adraider, Y., Hodgson S.N.B., Sharp, M.C., Zhang, Z.Y., Nabhani, F., Waidh, A. A., Pang, Y.X. (2012). "Structure characterisation and mechanical properties of crystalline alümina coatings on stainless steel fabricated via sol–gel technology and fibre laser processing." *Journal of the European Ceramic Society*, Vol. 32, pp. 4229–4240.

Bailey, N. S., Katinas, C., Shin Y. C. (2017). "Laser direct deposition of AISI H13 tool steel powder with numerical modeling of solid phase transformation, hardness, and residual stresses*." Journal of Materials Processing Tech,* Vol. 247, pp. 223–233.

Barrau, O., Boher, C., Gras, R., Rezai, A. F. (2003). "Analysis of the friction and wear behaviour of hot work tool steel for forging." *Wear*, Vol. 255, pp. 1444–54.

Campanelli, S. L., Angelastro, A., Signorile, C. G., Casalino, G. (2017). "Investigation on direct laser powder deposition of 18 Ni (300) marage steel using mathematical model and experimental Characterization." *International Journal of Advanced Manufacturing Technology*, Vol. 89, pp. 885–895.

Chew, Y., Pang, J. H., Bia, G, Song, B. (2017). "Effects of laser cladding on fatigue performance of AISI 4340 steel inthe as-clad and machine treated conditions." *Journal of Materials Processing Technology*, Vol. 243, pp. 246–257.

Cheng, Y.H., Cui, R., Wang, H.Z., Han, Z.T, (2017). "Effect of processing parameters of laser on microstructure and properties of cladding 42CrMo steel." *International Journal of Advanced Manufacturing Technology,* pp. 1-10.

Dosbaeva, G.K., El Hakim, M.A., Shalaby, M.A., Krzanowski, J.E., Veldhuis S.C. (2015). "Cutting temperature effect on PCBN and CVD coated carbide tools in hard turning of D2 tool steel." *International Journal of Refractory Metals and Hard Materials,* Vol. 50, pp. 1–8.

Emamian A., Corbin, S. F., Khajepour A. (2011). "The influence of combined laser parameters on in-situ formed TiC morphology during laser cladding." *Surface and Coatings Technology,* Vol. 206, pp. 124–131.

Erfanmanesh, M., Pour, H.A., Semnani, H.M., Razavi, R.S. (2017). "An empirical-statistical model for laser cladding of WC-12Co powder on AISI 321 stainless steel." *Optics and Laser Technology*, Vol. 97, pp. 180–186.

Ignat, S., Sallamand P., Nichici, A., Vannes, B., Grevey, D., Cicala, E. (2003). "$MoSi_2$ laser cladding—A new experimental procedure: double-sided injection of $MoSi_2$ and ZrO_2." *Surface and Coatings Technology*, Vol. 172, pp. 233–241.

Jiang, W.H., Kovacevic, R. (2007). "Laser deposited TiC/H13 tool steel composite coatings and their erosion resistance." *Journal of Materials Processing Technology*, Vol. 186, pp. 331–338.

King, P. C., Reynoldson, R. W., Brownrigg, A., Long, J. M. (2004). "Cr(N,C) diffusion coating formation on pre-nitrocarburised H13 tool steel." *Surface and Coatings Technology*, Vol. 179, pp. 18–26.

Lehman, E.B., Indyka, P., Bigos, A., Kot, M., Tarkowsk, L. (2012). "Electrodeposition of nanocrystalline Ni–W coatings strengthened by ultrafine alumina particles." *Surface and Coatings Technology,* Vol. 211, pp. 62–66.

Li, M., He, Y., Yuan, X., Zhang, S. (2006). "Microstructure of Al2O3 nanocrystalline/cobalt-based alloy composite coatings by laser deposition." *Materials and Design*, Vol. 27, pp. 1114–1119.

Luong, L.H.S., Heijkoop, T. (1981). "The influence of scale on friction in hot metal working." *Wear*, Vol. 71, pp.93–102.

Medvedeva A, Bergstrob, J., Gunnarssona, S., Anderssona, J. (2009). "High-temperature properties and microstructural stability of hot-work tool steels." *Mater Science and Engineering A*, Vol. 523, pp. 39–46.

Mangour, B.A., Grzesiak, D., Yang, J.M. (2016). "Nanocrystalline TiC-reinforced H13 steel matrix nanocomposites fabricated by selective laser melting." *Materials and Design,* Vol. 96, pp. 150–161.

Ozkul, I., Buldum, B.B., Akkurt A. (2017). "Regression Modeling of The Hole Qualities During Cold Work Tool Steels Drilling, With Different Characteristics Drill Bits." *Turkish Journal of Engineering,* Vol. 1, pp. 52-60.

Recco, A.C., Oliveira, I.C., Massi, M., Maciel, H.S., Tschiptschin, A.P. (2007). "Adhesion of reactive magnetron sputtered TINx and TICy coatings to AISI H13 tool steel." *Surface and Coatings Technology*, Vol. 202, pp. 1078–1083.

Reza, M. S., Aqida, S. N., Ismail, I. (2018). "Laser surface modification of Yttria Stabilized Zirconia (YSZ) thermal barrier coating on AISI H13 tool steel substrate."

IOP Conf. Series: Materials Science and Engineering, Vol. 319, pp. 1-4.

Riveiro, A., Mejías, A., Lusquiños, F. , Val J. D , Comesaña, R., Pardo, J., Pou, J. (2014). "Laser cladding of aluminium on AISI 304 stainless steel with high-power diode lasers." *Surface and Coatings Technology,* Vol. 253, pp. 214–220.

Shi Y, Li, Y, Liu, J., Yuan, Z. (2018). "Investigation on the parameter optimization and performance of laser cladding a gradient composite coating by a mixed powder of Co50 and Ni/WC on 20CrMnTi low carbon alloy steel." *Optics and Laser Technology,* Vol. 99, pp. 256–270.

Sivkov, A., Shanenkov, I., Pak, A., Gerasimov, D., Shanenkova, Y. (2016). "Deposition of a TiC/Ti coating with a strong substrate adhesion using a high-speed plasma jet." *Surface and Coatings Technology,* Vol. 291, pp. 1–6.

Şimşek, T. (2010). The laser coating of stainless steel and tool steel with nanotitanium carbide and investigation of the wear behaviour coating layers, Master Thesis, University of Gazi, Ankara, Turkey.

Telasang, G., Majumdar, J. D., Padmanabham, G., Tak, M., Manna, I. (2014). "Effect of laser parameters on microstructure and hardness of laser clad and tempered AISI H13 tool steel." *Surface & Coatings Technology,* Vol. 258, pp. 1108–1118.

Weng, F., Yu, H. , Chen, C. , Liu, J, Zhao, L , Dai, J., Zhao, Z. (2017). "Effect of process parameters on the microstructure evolution and wear property of the laser cladding coatings on Ti-6Al-4V alloy." *Journal of Alloys and Compounds,* Vol. 692, pp. 989-996.

Weng, F., Yu, H., Chen, C., Liu, J., Zhao, L., Dai, J., Zhao, Z. (2017). "Effect of process parameters on the microstructure evolution and wear property of the laser cladding coatings on Ti-6Al-4V alloy." *Journal of Alloys and Compounds,* Vol. 692, pp. 989-996.

Wei, M.X., Wang, S.Q., Wang, L., Cui, X.H., Chen, K.M. (2011). "Effect of tempering conditions on wear resistance in various wear mechanisms of H13 steel." *Tribology International*, Vol. 44, pp. 898–905.

Yan, H., Zhang P., Gao Q., Qin Y., Lic R. (2017). "Laser cladding Ni-based alloy/nano-Ni encapsulated h-BN self-lubricating composite coatings." *Surface and Coatings Technology*, 332, pp. 422–427.

Yilbas, B.S., Patel F., Karatas C. (2013). "Laser controlled melting of HSLA steel surface with presence of B4C particles." *Applied Surface Science*, Vol. 282, pp. 601– 606.

Zhang, P., Liu X., Yan H. (2017). "Phase composition, microstructure evolution and wear behavior of Ni-Mn-Si coatings on copper by laser cladding." *Surface and Coatings Technology,* Vol. 332, pp. 504–510.

Turkish Journal of Engineering

Turkish Journal of Engineering (TUJE)
Vol. 3, Issue 1, pp. 32-38, January 2019
ISSN 2587-1366, Turkey
DOI: 10.31127/tuje.444685
Research Article

LAND USE AND LAND COVER CHANGES USING SPOT 5 PANSHARPEN IMAGES; A CASE STUDY IN AKDENIZ DISTRICT, MERSIN-TURKEY

Çiğdem Göksel *[1] and Filiz Bektaş Balçık [2]

[1] Istanbul Technical University, Geomatics Engineering Department, Istanbul, Turkey
ORCID ID 0000-0001-8480-1435
goksel@itu.edu.tr

[2] Istanbul Technical University, Geomatics Engineering Department, Istanbul, Turkey
ORCID ID 0000-0003-3039-6846
bektasfi@itu.edu.tr

* Corresponding Author
Received: 17/07/2018 Accepted: 06/08/2018

ABSTRACT
The main objective of the study is to quantify main changes in urban area of Akdeniz district of Mersin province using Pan sharpen SPOT 5 MS (with 3 bands) satellite images. In this study, land cover and land use maps of 2006 and, 2014 are produced using Maximum Likelihood supervised classification technique to detect the growth of urban area in the selected area. Preprocessing methods, including geometric and radiometric correction were performed. From to changes method was applied to determine the land cover/land use transformation in the region. An accuracy assessment was conducted using overall accuracy and Kappa statistics. Results show that maps obtained from images for 2006, and 2014 had an overall accuracy of 82.96%, and 84.00%, and a Kappa coefficient of 0.80, and 0.82, respectively. The results showed that between the selected years the district faced a huge transformation from agricultural fields and bare lands to artificial surfaces. Change detection between 2006 and 2014 shows that most of the agricultural fields (6295,1 ha) have been increased; moreover, artificial surfaces and green houses have also increased. The largest decrease has occurred for bare lands area of which approximately 3942,5 ha. According to the results, artificial surfaces was increased by 189 ha from 2006 to 2014 in Akdeniz District of Mersin.

Keywords: *Land Use, Land Cover, Change Detection, SPOT, Remote Sensing*

1. INTRODUCTION AND AIM OF THE STUDY

Acquired Earth Observation data (EO) by remote sensing satellites has greatly provided a temporal broad view of earth surface and remote sensing has improved an important tool to monitor and manage land surfaces. Compared to field-based studies, remote-sensing technology has many advantages for quantitatively measuring and forecasting land-cover changes due to practical data acquisition, effective cost, and application of spatiotemporal data. Change detection is the process of identifying differences in the state of an object or phenomenon by observing it at different times (Coppin *et al*., 2004). Accurate and reliable change detection of land-use/land-cover (LULC) has an important role in order to determine and control local, regional, and global urban sprawl and development around city (Lu *et al*., 2004, Bektas and Goksel, 2005; Bozkaya *et al*., 2014; Bozkaya *et al*., 2015). Management and monitoring of land use features within a time plan is significant for local and regional authorities. Besides, it is highly essential for maintaining life quality of both urban and rural environment and their habitants, and utilizing the existing sources effectively.

Remote sensing allows for determination of land use/land cover statistically and visually based on time and location in a fast and economical way (Banister *et al*., 1997; Goksel, 2016; Hellawell, 1991; Jat *et al*., 2008). A commonly used approach for image analysis is digital image classification. The purpose of image classification is to label the pixels in the image with meaningful information from the real world to produce thematic maps. Subsequently, these thematic maps used to apply change detection. Several studies have stated the crucial necessity to obtain consistent, accurate, and up-to-date spatial information on land cover and the scale of its change for the Earth's resources (Weng, 2002; Dogru *et al*., 2006; Serra *et al*., 2008; Yagoub and Bizreh, 2014)

Traditionally, various pixel-based techniques usually were used to create LULC classifications (Bozkaya *et al*., 2015, Bektas Balcik & Karakacan Kuzucu, 2016). The pixel-based techniques include either a supervised or unsupervised classification or a combination of these (Bektaş Balçık, 2010). In this study, conventional Maximum likelihood supervised classification method conducted to determine main LULC categories in selected district using 3 bands of SPOT 5 MS data.

There are two fundamental methods for temporal change detection established on remotely sensed data; pre-classification and post classification techniques. Though numerous algorithms of pre-classification techniques for instance image rationing, principle components analysis or vegetation indices are applied to define the change or no change maps, post classification techniques compare the classification results of different dated satellite data to produce "from–to" map to map change information (Fung and Siu, 2000; Jensen, 2004).

In this study, change detection of land cover and land use classes were investigated and evaluated for Akdeniz District of Mersin province, Turkey. Selected region has developed rapidly over the last three decades due to emerging industries, urbanization, and tourism. Maximum likelihood of supervised classification was used to extract land use/cover information from the remotely sensed data. The main objectives of this research were: (1) to derive land cover and land use categories of Akdeniz district of Mersin for the years of 2006 and 2014. (2) to apply post processing *from-to* change detection method to explore the LULC transformations and the impacts on surrounded environment in the selected districts that produce; (3) to experience and discuss the potential of 3 bands pan-sharpened SPOT 5 MS data in a heterogeneous study area using conventional supervised classification method and error matrix. The research outcomes showed the transformations and changes in LULC categories of the selected region that has a huge economical and strategic importance in Mediterranean region of Turkey.

2. STUDY AREA AND DATA

Based on the National Strategies on Regional Growth, Mersin is defined as a potential metropolitan city which can be alternative for Istanbul, Ankara and Izmir in Turkey. Based on EU's regional growth systematics NUTS (The Nomenclature of territorial units for statistics), Turkey is divided into three levels, twelve regions, twenty-six sub-regions and eighty-one cities. Mersin is classified as TR62 (Mediterranean region/Adana-Mersin sub-region). Mersin, region, sub-region and country location and administrative structure within the transportation network was evaluated in terms of Turkey's is one of the important city.

Mersin province lies between 36-37° northern latitudes and 33-35° east longitudes. This plain city is located in the mid-south region of Anatolian Peninsula and has a coastal line in Mediterranean Sea and surrounded with Toros mountains. Together with its 13 counties and 304 districts, Mersin is the second biggest city in Cukurova region with a surface area of 16.245 km². The city of Mersin, which is one of the populated urban centers located in the eastern Mediterranean region of Turkey (Alphan and Celik, 2016). This region has developed rapidly over the last three decades due to industries, urbanization, and tourism. Mersin International Port, which is one of the largest ports of Turkey, lies to the east of the city. Geographic locations of the port and the industries have led the city of Mersin to grow on the west coast since the early 1980s.

The selected region, Akdeniz district, has a significant role in Mersin in terms of economic and cultural aspects, with its 1.783 km² surface area, and total population of 276000. Akdeniz District is located in the eastern part of Mersin, Turkey (Fig. 1). The region has Mersin International Port, which is one of the largest ports of Turkey. Subsequently, this part of the city is mostly occupied by industrial and/or commercial units that are associated with the port. The district is an area that experienced a fast increase of urban population in the recent decades in Mersin (Report, 2016). Rapid urbanization and industrialization have important effect on natural resources, agricultural fields and urban environment (Alphan, 2013; Alphan and Sonmez, 2015; Burak *et al*., 2004). The remote sensing technique using satellite imagery has been recognized as an effective and powerful tool in monitoring and detecting land use and land cover changes.

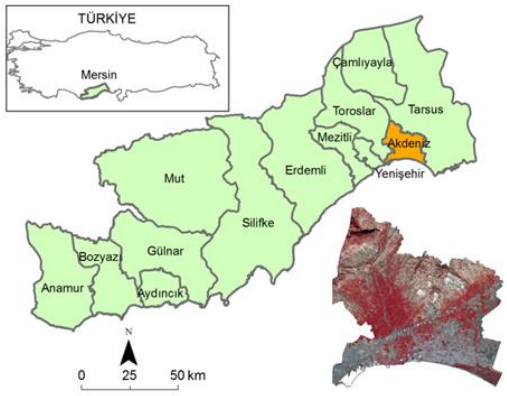

Fig. 1. Study Area

For change detection of land use/land cover, two pan-sharpened SPOT5-MS images, dated 2006 and 2014, were used. The SPOT5-MS images included 3 bands and the spatial resolution of the images was 5m. In addition, 1/25000 scaled standard topographic maps and 1/5000 scaled digital orthophotos were used with these satellite images for rectification and ground truth.

3. METHODOLOGY

In this study, SPOT 5 multispectral data processed using conventional methods and supervised classification. Figure 2 shows the flowchart of the detailed application steps of the study used to derive *from to* changes in Akdeniz district, of Mersin Province.

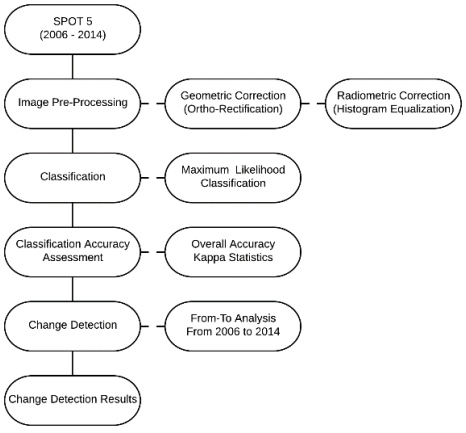

Fig. 2. Flowchart of the study

3.1. Image Preprocessing

In change detection studies, it is inevitable for obtaining accurate results that satellite images should have the same coordinate and projection system (Richards and Jia, 2006). First, geometric correction was applied to eliminate systematic and nonsystematic errors for the dataset consists of more than one frame having different acquisition dates. The SPOT5 images with 5m spatial resolution were processed as ortho (Level 3A) level. The images that are processed in this level are produced by using The Shuttle Radar Topography Mission Digital Terrain Elevation Data 1 (SRTM-DTED1) and satellite orbit parameters and have ±30 m positional accuracy. Then, topographic normalization process was carried out. In ortho-imagery production stage, the ortho-photos belonging to the study area were utilized by means of "map to image" method. 2D geometric correction with 1st degree polynomial transformation was applied in order to increase the positional accuracy of images for accurate change detection analysis. On one hand, geometric correction for 2014 dated SPOT5 MS image was executed with 148 homogenously distributed ground control points. On the other hand, 120 ground control points were used for the geometric correction for 2006 dated SPOT5 MS image. In this context, nearest neighborhood method was chosen for resampling due to its ease of computation and capability of avoiding data loss. Root means square errors (RMSE) were calculated as 7.72 m and 4.98 m for 2006 and 2014 dated images, respectively. The rectification process applied for whole Mersin area and the RMSE values were calculated at acceptable accuracy to produce 1/50 000 scaled Environmental Master Plan of Mersin.

In the second stage, histogram equalization as a radiometric correction technique was applied. As a third step, mosaicking was executed, and then the images that will be classified were prepared based on corresponding province and county borders. As a last step, Maximum Likelihood supervised classification algorithm was applied to determine land cover and land use changes of the Akdeniz region in Mersin.

3.2. Classification of Satellite Images

Classification of a remotely sensed imagery is a process of transforming digital data obtained by satellite images having different spectral resolution to images illustrating land use/land cover. The main goal of classification is to cluster pixels having similar reflectance and assign them to corresponding attribute class in real world (Elachi and van Zyl 2006).

In this study, Maximum Likelihood which is one of the pixel-based supervised classification techniques was applied. In this method, training sites are identified by the analyst (Liu and Mason 2009; Mather 2004). An extensive field survey within the study was conducted for determination of ground truth. Photos of study area were taken at 60 seconds period, with a high resolution camera mounted with 120° on the front window of the survey vehicle. In addition to photographs, GPS coordinates of ground control points were recorded simultaneously. By this way, location information was acquired related to land use/land cover features that lacks of information. Therefore, 1/5000 scaled ortho-photos were used for ground truth. For classification process, 200 training sites were identified. The land use/land cover classes are defined based on Corine Level 1. Figure 3 illustrates the classification results for 2006 and 2014, respectively and Table 1 shows the area of each LULC categories for 2006 and 2014.

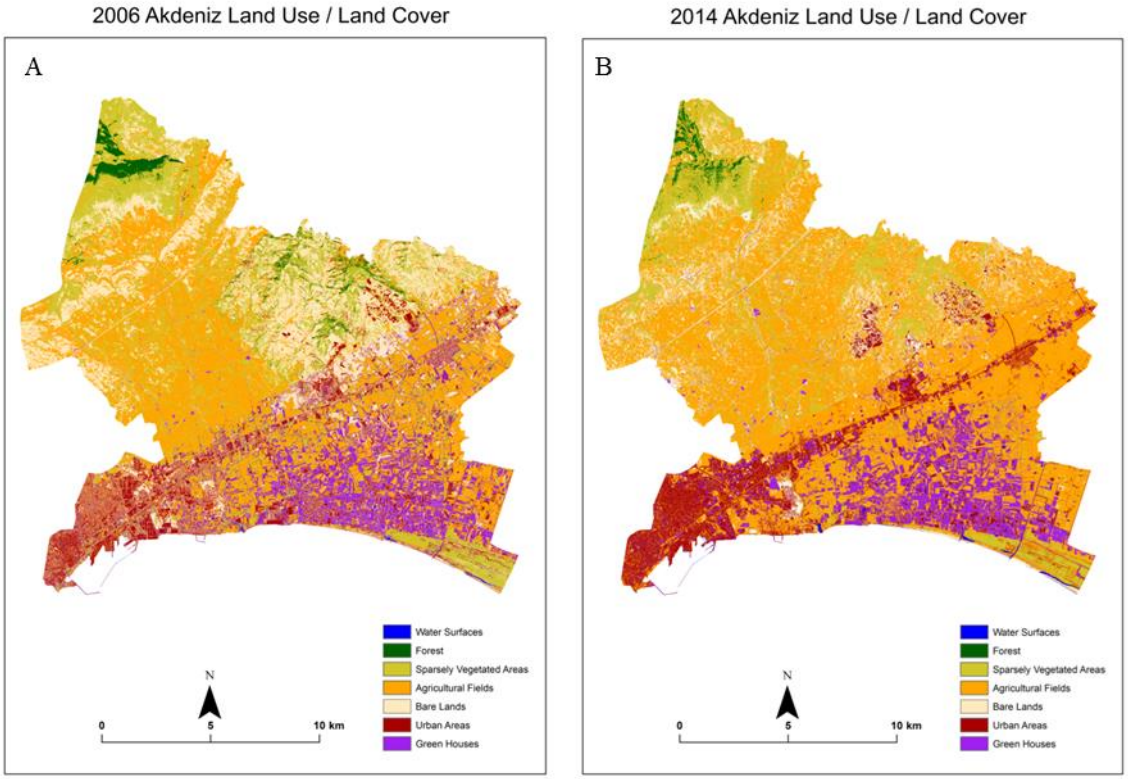

Fig. 3. Akdeniz district LU/LC classification results A) 2006, B) 2014

Table 1. Area of land cover types for 2006 and 2014

Classes	Area (ha) (2006)	Area (ha) (2014)
Water surfaces	66.17	126.38
Forest	573.55	243.53
Sparsely vegetated area	6710.13	4206.95
Agricultural fields	10472.10	16767.20
Bare lands	7296.07	3353.54
Artificial surfaces	2954.72	3144.03
Green houses	2376.27	2607.42

The significant limitations of the classification can be listed as contrasting differences caused by seasonal changes and cloud coverages in the images, mixing greenhouses and bright surfaces (such as quarry and industrial regions, or the type of soil and rock), mixing water features and forests due to SPOT5 imagery consisting of 3 bands. Pixel based traditional supervised classification algorithms are based on spectral information of each pixel of an image and don't take into account the problem of mixed pixels. If a pixel of remote sensing images contains several land cover types, such pixels are known as mixed-pixels (Zhu, 1995). Heterogeneous landscapes of Akdeniz district and selected classification algorithm are the main reasons for mixed pixel problem and the average accuracy assessment results.

3.3. Accuracy Assessment

Accuracy assessment of classification is essential to assure the quality of thematic maps produced using remote sensing data. Additionally, accuracy assessment is very important for understanding the detected change results and employing these results for land management, urban land planning and decision making (Foody, 2002). To evaluate the error ratio in the classified image data, in other words, to determine the consistency of the classified image and the ground truth, accuracy is assessed by comparing the training sites selected in the classified image with the ground truth (Congalton, 1991; Sertel and Akay, 2015). Aerial photos, maps, plans, GPS data and the photos acquired during field survey are used as a reference (ground truth). For assessing accuracy, creating error matrix and computing kappa coefficient (κ) regarding to this matrix is the most widely used method. Kappa statistic (κ) values are between 0 and 1 and 0.8-1 interval indicates the ideal classification results (Cohen, 1960).

Within the study, the accuracy of the classification results was assessed by comparing classified images with the GPS data, the photos acquired during field survey and higher resolution satellite images. In this context, 270 points were selected as field collected training sites. Table 2 shows the accuracy assessment results for 2006 and 2014 dated classified images.

Table 2. Accuracy assessment results

SPOT 5 MS image	Number of control points	Overall Accuracy	Kappa Statistics (κ)
2006	270	% 82.96	0.80
2014	270	% 84.00	0.82

3.4. Change Analysis

The changes in land use/land cover are regarded as driving forces of transformation and modification of earth surface (Turner, 1990). These changes are performed by the decisions of authorities within the social, economic, cultural, political, environmental and ecological procedures (Aspinall and Hill, 2008). To determine the changes accurately, firstly; geometric, atmospheric, and radiometric correction should be carried out and secondly; the images should be classified with high classification accuracy.

For this study, "from-to" analysis for two classified images (2006 and 2014 dated) was employed and the analysis results indicating the differences between two images were presented in detail in Table 3. The change statistics below gives an explanation on the question of where land use/land cover changes are occurring (Table 3). The results include sparsely vegetated areas, agricultural fields, bare lands and greenhouses.

Table 3. From-To change detection results

Classes (ha) 2006 From	Artificial Surfaces Area (ha) 2014 To	Bare Lands Area (ha) (2014) To
Sparsely vegetated area	321.40	640.98
Agricultural fields	593.16	947.207
Bare lands	730.99	-
Green houses	481.723	67.06
Total unchanged area	12541.77	

4. RESULTS

This study has explored the potential of pan-sharpened satellite-remote sensing and geospatial technologies in producing land use/land cover maps and statistical analysis of the selected study area. This research, with the aim to determine the urban development and its effects on Akdeniz district of Mersin province, shows changing land use/land cover dynamics in an objective way by utilizing different dated two SPOT5 MS images with a series of processing procedures and field surveys. Although SPOT 5 pan-sharpened images have high spatial resolution, 3 bands have disadvantages to produce land use/cover maps and statistics because of mixed pixels and similar spectral characteristics of targets in heterogeneous Mediterranean landscape.

General pattern and trajectories of land use and land cover in the Akdeniz district were evaluated through the years, 2006 and 2014. Land use/land cover maps were produced with an overall accuracy of over 82.00% by using Maximum Likelihood supervised classification method. The magnitude of change was calculated and "from–to" change information derived from classified images. The results of change trends in classification showed that the dominancy of artificial surfaces tends to increase at the coastal part of the district in a short period of time (i.e., from 2006 to 2014).

Especially, in the inland areas that includes sparsely vegetated areas and forest a huge transformation were occurred from sparsely vegetated areas to artificial surfaces and bare lands. Therefore, from-to changes results indicated that total unchanged area is 12541.7 ha in the study area. The highest transformation was seen from bare lands to artificial surfaces in the region. Therefore, the agricultural fields were changed to artificial surfaces and bare lands.

Regarding to the temporal change detection results for Akdeniz district which has geographic and strategic importance, following remarks can be expressed:

- Built-up areas were increased, especially in the coastal line (residential tourism areas)
- Rich agricultural areas were transformed into bare land or residential areas.
- In bare lands around Mersin International Port, the built-up areas belonging to logistics industry were increased.
- Based on the general change detection results, green houses were increased in the district.

Akdeniz is crucial not only for industry or service sector, but also for agriculture and undercover greenhouse activities. Agriculture, industry and service sector are actually the fundamental components of sustainable development for both Akdeniz district and whole Mersin.

These results and analyses can be used as a base study for sustainable environmental management of heterogonous Mediterranean region of Turkey. In this context, monitoring using remote sensing technology has a huge importance to keep sustainable management under control.

ACKNOWLEDGEMENTS

This paper was carried out within the scope of "Project of the Province Wide Research and Analytical Works for the Environmental Master Plan of Mersin". We are thankful to Mersin Metropolitan Municipality as the client and contractor PROMER Planning Eng. Inc. of this project. We have to express our appreciation to the project team for sharing their experience and collaboration.

REFERENCES

Alphan, H. (2013). Bi-temporal analysis of landscape changes in the easternmost Mediterranean deltas using binary and clas- sified change information. *Environmental Management*, 51, 541–554.

Alphan, H., & Celik, N. (2016). Monitoring changes in landscape pattern. Use of Ikonos and Quickbird images. *Environmental Monitoring and Assessment*, 188(81).

Alphan, H. and Sonmez, F. (2015). Mapping availability of sea view for potential building development areas. *Environmental Monitoring and Assessment*, 187(7).

Aspinall, R. J., & Hill, M. J. (2008). Land use change: science, policy, and management: CRC Press.

Banister, D., Watson, S., & Wood, C. (1997). Sustainable Cities: Transport, Energy, and Urban Form. *Environment and Planning B: Planning and Design, 24*(1), 125-143, doi:10.1068/b240125.

Bektas, F., & Goksel, C. (2005). Remote sensing and GIS integration for land-cover analysis: a case study:Bozcaada Island.*Water Science and Technology*, 51(11), 239–244.

Bektaş Balçık, F (2010). Mapping And Monitoring Wetland Environment By Analysis of Different Satellite İmages And Field Spectroscopy', PhD Thesis, Istanbul Technical University

Bektas Balcik F., Karakacan Kuzucu A. (2016) "Determination of Land Cover/Land Use Using SPOT 7 Data With Supervised Classification Methods". *GeoAdvances Workshop*, 2016. Istanbul.

Bozkaya, A. G., Bektas Balcik, F., Goksel, C., Dogru, A. O.,Ulugtekin, N. N., & Sozen, S. (2014). Satellite-based multitemporal change detection in Igneada flooded forests. *Romanian Journal of Geography*, 58(2), 161–168.

Bozkaya, A. G., Bektas Balcik, F., Goksel, C., Esbah, H. (2015) Forecasting land-cover growth using remotely sensed data: a case study of the Igneada protection area in Turkey. *Environmental Monitoring Assess*, 187: 59

Burak, S., Doğan, E. and Gazioğlu, C. (2004). Impact of urbanization and tourism on coastal environment. *Ocean and Coastal Management*, 47(9–10): 515–527.

Cohen, J. (1960). A Coefficient of Agreement for Nominal Scales. *Educational and Psychological Measurement, 20*(1), 37-46.

Congalton, R. G. (1991). A review of assessing the accuracy of classifications of remotely sensed data. *Remote Sensing of Environment, 37*(1), 35-46.

Sertel, E., Akay, S.S. (2015). High resolution mapping of urban areas using SPOT-5 images and ancillary data" International Journal of Environment and Geoinformatics (IJEGEO)., 2 (2), 63-76

Coppin, P., Jonckheere, I., Nackaerts, K., Muys, B., Lambin, E. (2004) Digital change detection methods in ecosystem monitoring: A review *International Journal of Remote Sensing*, 25 (9), pp. 1565-1596.

Dogru, A. O., Bektas Balcik, F., Goksel, C., & Ulugtekin, N. N. (2006). Monitoring Coastal Dunes By Using Remote Sensing And GIS Integration In North West Part Of Turkey: A Case Study Of Kilyos Dunes. *Fresenius Environmental Bulletin*, 9b, 15

Elachi, C., & van Zyl, J. J. (2006). *Introduction To The Physics and Techniques of Remote Sensing*: Wiley.

Foody, G. M. (2002). Status of land cover classification accuracy assessment. *Remote Sensing of Environment, 80*(1), 185-201

Fung, T., & Siu, W. (2000). Environmental quality and its changes, an analysis using NDVI. *International Journal of Remote Sensing*, 21(5), 1011–1024.

Goksel, C., Balcik, F. B., Keskin, M., Celik, B., Cihan, C., Yagmur, N. (2016). Evaluation of Classification Methods for Detection of Greenhouses from Spot 5 Satellite Imagery. *6th International Conference on Cartography and GIS*, Albena, Bulgaria, 13-17 June

Hellawell, J. M. (1991). Development of a rationale for monitoring. In B. Goldsmith (Ed.), *Monitoring for Conservation and Ecology* (pp. 1-14). Dordrecht: Springer Netherlands.

Jat, M. K., Garg, P. K., & Khare, D. (2008). Monitoring and modelling of urban sprawl using remote sensing and GIS techniques. *International Journal of Applied Earth Observation and Geoinformation*, 10(1), 26-43.

Jensen, J. R. (2004). *Digital change detection. Introductory digital image processing: A remote sensing perspective* (pp. 467–494). New Jersey: Prentice-Hall

Liu, J. G., & Mason, P. (2009). Essential Image Processing and GIS for Remote Sensing: Wiley.

Lu, D., Mausel, P., Brondízio, E., Moran, E. (2004) Change detection techniques. *International Journal of Remote Sensing*, 25 (12), pp. 2365-2407.

Mather, P. M. (2004). *Computer Processing of Remotely-Sensed Images: An Introduction*: Wiley.

Report, (2016). *Project of the Province Wide Research and Analytical Works for the Environmental Master Plan of Mersin.* Mersin Municipality (Ed.). In Turkish.

Richards, J. A., & Jia, X. (2006). *Remote Sensing Digital Image Analysis: An Introduction*: Springer Berlin Heidelberg.

Sanlı F., Bektaş, F., & Göksel, C. (2008). Defining temporal spatial patterns of mega city Istanbul to see the impacts of increasing population. *Environmental. Monitoring Assess*. 146:267–275

Serra, P., Ponsa, X., & Sauri, D. (2008). Land-cover and land-use change in a Mediterranean landscape: a spatial analysis of driving forces integrating biophysical and human factors. *Applied Geography*, 28, 189–209

Turner, B. L. (1990). *The Earth as Transformed by Human Action: Global and Regional Changes in the Biosphere Over the Past 300 Years*: Cambridge University Press.

Weng, Q. (2002). Land-use change analysis in the Zhujiang Delta of China using satellite remote sensing, GIS and stochastic modelling. *Journal of Environmental Management*, 64, 273–284.

Yagoub, M. M., Bizreh A. Al. (2014) Prediction of Land Cover Change Using Markov and Cellular Automata Models: Case of Al-Ain, UAE, 1992-2030. *Journal of the Indian Society of Remote Sensing*, Volume 42, Issue 3, pp 665–671

Zhu, S. (1995). Based on the mixed-pixel image classification of remote sensing technology. *Journal of the People's Liberation Army Institute of Surveying and Mapping*, 12(4). pp.276-278.

Turkish Journal of Engineering

Turkish Journal of Engineering (TUJE)
Vol. 3, Issue 1, pp. 39-42, January 2019
ISSN 2587-1366, Turkey
DOI: 10.31127/tuje.443482
Research Article

PREVENT THE TRANSMISSION OF USELESS / REPEATED DATA TRANSMISSION IN THE INTERNET OF THINGS NETWORK

Ercüment Öztürk *[1], Ahmet Ulu [2] and Tuğrul Çavdar [3]

[1] Karadeniz Technical University, Engineering Faculty, Department of Computer Engineering, Trabzon, Turkey
ORCID ID 0000-0001-9623-6955
ercumentozturk@ktu.edu.tr

[2] Karadeniz Technical University, Engineering Faculty, Department of Computer Engineering, Trabzon, Turkey
ORCID ID 0000–0002–4618–5712
ahmet.ulu@ktu.edu.tr

[3] Karadeniz Technical University, Engineering Faculty, Department of Computer Engineering, Trabzon, Turkey
ORCID ID 0000–0003–3656–9592
ulduz@ktu.edu.tr

* Corresponding Author
Received: 13/07/2018 Accepted: 25/08/2018

ABSTRACT
Internet of Things (IoT) is a new and advanced network technology that incorporates inter-object communication and sensor technology that connects almost every controllable electronic device to be used in daily life with a different Internet Protocol (IP) address in a network environment. In a such large-scale network, data transmission, process monitoring, data processing and network traffic are also required to be addressed. Today's Internet architecture uses the TCP / IP protocol stack for communication and is insufficient to meet the needs of the large-scale IoT network. Therefore, it will be a big advantage to reduce the data traffic in an IoT network where large amounts of data will be generated. In this study, a new method for reducing the data traffic in a designed IoT network is proposed and the data traffic on the network is reduced by preventing the transfer of useless / repetitive data in the network environment. A four layered (sensing layer, internet/network layer, transport layer and application layer) IoT architecture has been proposed by Çavdar and Öztürk in 2018. In the sensing layer, it is aimed to prevent unnecessary and repeated data from being transferred in the network environment by analyzing and eliminating the data. In addition, preventing the transmission of unnecessary and repetitive data to the network environment will bring many advantages such as storage, data traffic speed and storage cost.

Keywords: *Internet of Things, Big Data, Sensor Technology, Data Transmission*

1. INTRODUCTION

The Internet has begun to be used to share limited data packets in the 1980s, and there has been an increase in the number of devices connected to the internet Quentin Stafford-Fraser, Paul Jardetzky and their colleagues connected a camera to the coffee machine shown in Figure 1 to observe the amount of coffee in the coffee machine in the unit named Trojan Room in Cambridge University and transfer it to a common network, pulling the pictures of the coffee machine at certain time intervals, e.g. a snapshot every 30 seconds. This developed system is regarded as the Internet application of the first objects (Stafford-Fraser, 2001).

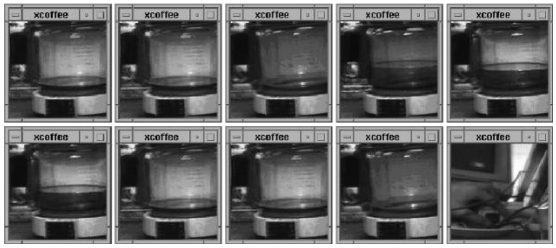

Fig. 1. Trojan Room coffee machine

In later years, an idea was born that each object could be numbered with a different IP number and actively used in the internet environment. Followingly, a toaster machine was invented by John Romkey in early 1990s, which can be opened and closed over the internet (Romkey, 2017). IoT, which has taken its place in everyday life as a practical application on a very small scale, was conceptually used in 1999 by Kevin Ashton in a presentation for a company.

Along with the developing technological infrastructure, a large number of different objects that can be connected to smart devices, mobile phones and internet environment have been produced and continues to be produced. In IoT, the concept of an object is defined as any device that can be connected to the internet and send / receive data (Çavdar and Öztürk, 2018). Companies such as Intel, IBM, and Cisco, which have a large share of information technology in the marketplace, are also continuing to develop various products under IoT (Bozdoğan, 2015). Innovation and progress in the field of information and communication technologies, which have become a part of our developing and everyday life, keeps up evolving, especially in the last thirty years.

As the use of the Internet began to spread, the sharing of information was accelerated, and the technical progresses have taken a long way. Electricity, which is regarded as the greatest invention of the 19th century, nowadays has left its place to the internet and information technologies. Especially, in the past quarter century we have made great progress in science through the developments in the information technologies. In other word, the world has taken its path in science and technology for centuries in the past quarter century (Öztürk *et al*., 2017). In the years when information technology and the internet are actively used, development rate differs by one to seven when compared to the years when information technology is not available. More developments are observed than in the seven years that they have never been used in information technology and the active use of the internet (Stafford-Fraser, 2001).

There are many definitions in the literature for IoT. For example; A. Al-Fuqaha and others have preferred the following definition for IoT: The physical objects of IoT are the systems that control or organize viewing, perception, thinking, decision-making, data sharing and communication with each other (Al-Fuqaha *et al*., 2015). The International Communication Union (ITU)'s definition as follow "Any time any object / device can be connected to any technology." (ITU, 2012). Çavdar and Oztürk have formulated in a different manner; "It is the whole of the global systems that allow objects (smart mobile devices, televisions, cars, etc.) to be addressed and used anytime and anywhere." (Çavdar and Öztürk, 2018).

2. SUGGESTED METHOD

As in all disciplines, a specific road map is created at first step for any project and depending on this road map the work is started. This is similar in Information Technologies (IT). In the IT era, the structure (that can be considered as a road map) and a set of rules constitute the reference model. For this reason, when an application or a project is developed in IOT, with a reference architectural model the system efficiency will be increased and total cost will be reduced.

With the increasing number of things connected to the IoT network, the protocols and architectures that are used today are inadequate and will have difficulties for future needs. There are tens of proposed architectural models existing in the literature due to the lack of a well-defined architectural model. In order to solve this problem, a new four-layered (sensing, internet/network, transport and application layers) architectural model has been proposed by Çavdar and Öztürk, which addressed as a reference architectural model for IoT. It has been thought that it could be useful to select and eliminate the repetitive / useless data in the sensing layer of this proposed model. In the data analysis phase, the detection and the elimination of the redundant data reduce the storage costs. It will also be a good step in terms of minimizing the transaction complexity.

In Figure 2, the 4-layered IoT architectural model proposed by Çavdar and Öztürk in 2018 (Çavdar and Öztürk, 2018), unlike the architectural models in the literature, the data evaluation phase is performed at the detection layer, which can be characterized as physical layer. The transmission of this data in the network environment only for emergency cases will help both in processing large data and avoiding data garbage. The data collected from the sensors should be analyzed to prevent the data from being continuously sent to the network environment if there is no abnormal situation. Thus, data transmission rate can be reduced, the rules defined by the users can be accommodated and the further data transmission can also take place in emergency cases. In addition, if a request is made directly by the client or by the application layer for remote control and inspection, the decision sublayer sends the required data to the upper layer and does not require a separate emergency signal to be transmitted in the network environment.

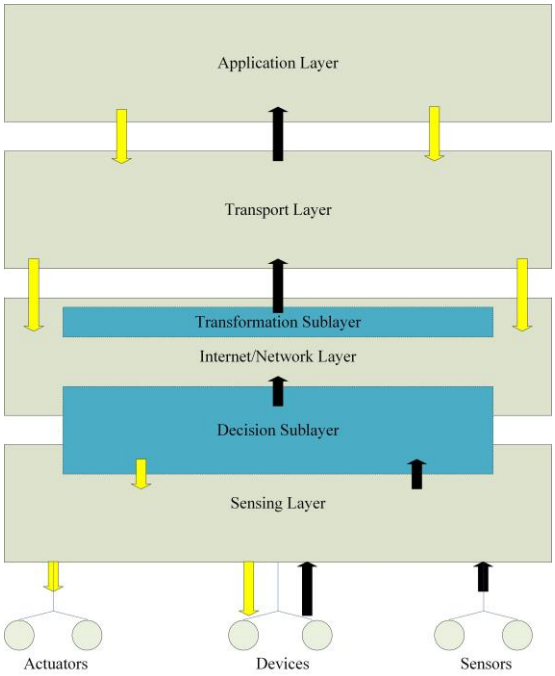

Fig. 2. 4 layered IoT architectural model proposed by Çavdar and Öztürk. (Çavdar and Öztürk, 2018)

In Fig. 3, the flow chart of the data detection, evaluation and routing stages of the decision sublayer are shown. The data coming from the detectors are first compared entirely with the help of the rules defined for the decision sublayer.

The mentioned rules are contained in a modem and central unit are reachable through an interface where the sensors and actuators are connected. The comparisons are performed in this interface, through which the comparison result is sent to the upper layer if it is necessary for different objects and applications, or if the data is requested by the client. Otherwise, the operation is continued by the running connection with the agents and the unnecessary data is terminated. The rules in the decision-making layer, which is the underlying framework to which the sensors are attached for physical conditions such as heat, temperature, humidity, smoke, vibration, etc., bear the conditions that must be under daily and normal conditions. In the simulations, those conditions are chosen as the values closer to normal values. But, in real applications, meteorological data can be sampled in advance and compared with the perceived data during the day to perform more realistic evaluations.

Thus, the system will become more useful and more efficient, and the delays to be experienced due to differences in the sensing and data transmission capacities of detection technologies will be partially overcome (Öztürk, 2018).

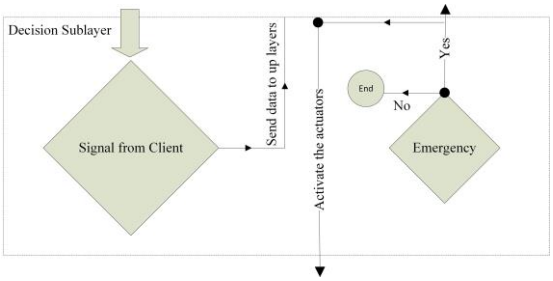

Fig. 3. The internal structure and functioning of the decision sublayer

In the decision sublayer, at the time of unit data transmission the number of data packets (network traffic in an IoT network) can be mathematically formulated as follows in case of a normal network condition:

$$\text{Total Number Of Packages} = \sum \frac{[(S+N)*P]}{T} \quad (1)$$

In a network where the proposed model is used, the number of packets at the time of data transmission in unit time;

$$\text{Total Number Of Packages} = \sum \frac{[((S-G)+N)*P]}{T} \quad (2)$$

S: Number of sensors
N: Number of complex things (PCs, Phones, etc.)
P: Average number of incoming packets
T: Time
G: Data forwarded to actuator without being transmitted to the network environment.

As given in the equations (1) and (2), the increase in the number of sensors leads to an increase in unnecessary data in the network environment. With the help of the proposed method, this data can be eliminated, and the network environment can be used more efficiently. It is more probable that data traffic will diminish considerably when a large number of sensors is considered. Also, mathematically expressed, The decision sublayer and the defined functionalities for large scale IoT networks including large data sets associated with the detection phase and the evaluation process of the traditional and innovative techniques hosted by IoT increase the efficiency of the system. (Öztürk, 2018).

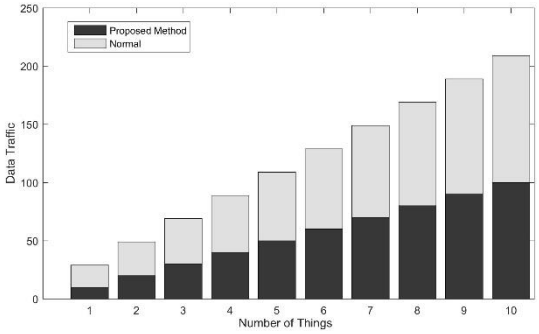

Fig. 4. Comparison of the network data densities in the normal and proposed method.

In accordance with the simulations conducted in Matlab environment, Fig. 4 shows the data density of the network, in which a normal network architecture and the proposed architecture are used. Accordingly, a significant reduction in the number of packets opened on the internet and the number of packets opened on the network and in the data traffic on the network was observed before the Internet (taken from the sensors) from the objects / devices and from some of the data received from the sensors. Here, the reduction in the number of data packets does not cause any packet loss. On the contrary, the data packets excluding the emergency signals coming from the sensors are routed to the actuators.

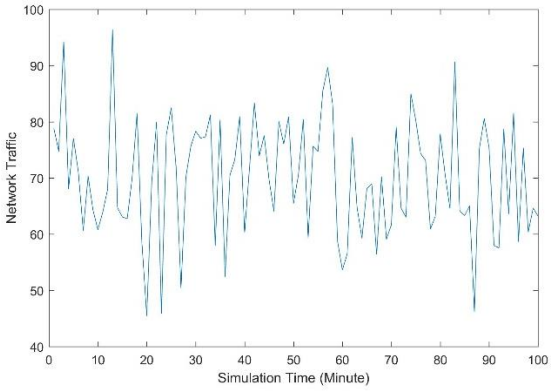

Fig. 5. Observation of network data traffic.

The data is transmitted to the internet environment after analyzing the data coming from the client and the detectors in the decision sublayer. The other remaining packets are forwarded to the agents without being transferred to the internet environment and the expected action is performed at that moment. According to the simulation results depicted in Fig. 5, the data traffic in the network decreases over time through the employment of the proposed method.

3. CONCLUSION

In this study, general information about IoT is given at first. Then, with respect to the detection layer of the previously proposed architectural model, data analysis and elimination of repetitive / useless data are explained and the results are examined. Since there are no simulation studies about the subject, comparison of the proposed method with any other technique could not be performed.

Through this work a new method has been developed to point out the importance of the usage of proposed paradigm, to meet the needs of different applications, to provide meaningful information transfer and to make resources quick and easy to use, since the IoT envisages a world in which billions of devices connect and communicate with each other through wired and wireless networks. Also, from a technical point of view, in a heterogeneous system, extensibility among objects, scalability, functionality, reliability, privacy/security and interoperability are all dependent on the data traffic of the network. In conclusion, this study provides general information about IoT and proposes a new method to reduce data traffic by preventing redundant data communication and transfer of useless data to the network environment in multi object links. The proposed method is explained theoretically, the data flowchart is given , the developed technique is evaluated throughout various simulations, the results are examined and interpreted.

REFERENCES

Al-Fuqaha, A., Guizani, M., Mohammadi, M., Aledhari M., and Ayyash, M. (2015). “Internet of Things: A Survey on Enabling Technologies, Protocols, and Applications,” *IEEE Communications Surveys & Tutorials*, Vol. 17, No. 4, pp. 2347-2376.

Bozdoğan, Z . (2015) “Nesnelerin İnterneti için Mimari Tasarımı”, MSc Thesis, University of Düzce, Düzce, Turkey.

Çavdar, T. and Öztürk, E. (2018). “A Novel Architecture Design for Internet of Things,” *Sakarya University Journal of Science*, Vol 22, No. 1, pp. 39-48.
https://oss.adm.ntu.edu.sg/ctan046/the-trojan-room-coffee-pot/. [Accessed: 9th November 2017].

International Telecommunication Union (ITU), 2012. “Global Information Infrastructure, Internet Protocol Aspects and Next-Generation Networks,”

Öztürk, E., Kakız, M. T., and Çavdar, T. (2017) “The Economical Importance and Contribution of Information Technologies to Rural and Regional Development: An Empirical Analysis,” *Proc., In 4th International Regional Development Conference*, IRDC, Tunceli, Turkey, pp. 684-690.

Öztürk, E. (2018). Proposing A Novel General Purposed Architectural Model For The Internet Of Things, MSc Thesis, Karadeniz Technical University, Trabzon, Turkey.

Romkey, J. (2017) “Toast of the IoT: The 1990 Interop Internet Toaster,” *IEEE Consumer Electronics Magazine*, Vol. 6, No. 1, pp. 116-119.

Stafford-Fraser, Q. (2001) “On site: The life and times of the first Web Cam.” *Communications of the ACM*, Vol 44, No. 7, pp. 25-26.

Turkish Journal of Engineering

Turkish Journal of Engineering (TUJE)
Vol. 3, Issue 1, pp. 43-50, January 2019
ISSN 2587-1366, Turkey
DOI: 10.31127/tuje.452865
Research Article

COMPARISON OF EFFECT OF NICKEL CONCENTRATION ON CRYSTALLOGRAPHIC STRUCTURE AND MORPHOLOGY OF ZINC OXIDE NANOPOWDERS

Saadet Yıldırımcan [1] and Selma Erat *[2,3]

[1] Toros University, Faculty of Engineering, Department of Electrical-Electronics Engineering, Mersin, Turkey
ORCID ID 0000 – 0002 – 9044 – 6908
saadetyildirimcan@gmail.com

[2] Mersin University, Vocational School of Technical Sciences, Department of Medical Services and Techniques, Program of Opticianry, Mersin, Turkey
[3] Advanced Technology, Research and Application Center, Mersin University, Mersin, Turkey
ORCID ID 0000 – 0001 – 7187 – 7668
selmaerat33@gmail.com

* Corresponding Author
Received: 10/08/2018 Accepted: 11/09/2018

ABSTRACT
In this study, we work on the effect of Ni doping on the crystallographic structure, morphology, and optical properties of ZnO nanoparticles. ZnO and Ni doped ZnO nanopowders were synthesized by sol-gel technique with different Ni concentration (5%, 10%, and 15%). The crystallographic structure was characterized by conventional X-ray Diffraction (XRD) technique. The results confirm that Ni doping does not change the single hexagonal phase existing in pure ZnO whereas in high Ni doping concentration (10% and 15%) causes to grow a secondary phase due to presence of NiO. FE-SEM, EDX, FTIR techniques are used for morphology, elemental, and chemical analyses of the samples. Optical properties of the samples are investigated by using UV-VIS spectrophotometer.

Keywords: *ZnO, Nickel, Crystallographic Structure, Morphology, Optical Properties*

1. INTRODUCTION

Recently, zinc oxide (ZnO) being a member of II-VI group has attracted much attention due to its potential applications in diverse fields (Vijayaprasath *et al.*, 2016; Kittilstved *et al.*, 2006). For instance, ZnO with a direct wide-band gap (in bulk form, 3.37 eV at 300 K), large exciton binding energy (60 meV), remarkable piezoelectric, electro-optic properties, and great chemical stability, (Bappaditya *et al.*, 2015; Dietl, 2007; Pearton *et al.*, 2005) has received eminent attention for its electronic and photonic applications (Yildirimcan *et al.*, 2016) such as photodetectors (Kind *et al.*, 2002), photodiodes (Lee *et al.*, 2002), light emitting diodes (Saito *et al.*, 2002), surface acoustic wave filters (Emanetoglu *et al.*, 1999), photonic crystals (Chen *et al.*, 2000), optical modulator waveguides (Koch *et al.*, 1995), room-temperature ultraviolent (UV) lasers (Huang *et al.*, 2001), gas sensors (Mitra *et al.*, 1998; Godavarti *et al.*, 2017), and solar cells and flat panel displayers (Law *et al.*, 2005; Martinson *et al.*, 2007; Shoushtari *et al.*, 2017; El-Hilo *et al.*, 2009; Ellmer *et al.*, 2008).

It is known that the physical properties of nanosized materials are greatly affected by their size and shape (Romeiro *et al.*, 2015). There are several methods to synthesize nanoparticles. Some of the methods to prepare ZnO nanoparticles are in following: microwave-assisted synthesis (Schneider *et al.*, 2010), wet chemical (Toloman *et al.*, 2013), hydrothermal synthesis (Li *et al.*, 2001), aerosol spray analysis (Motaung *et al.*, 2014), hydrolysis condensation (Cohn *et al.*, 2012), and sol-gel processing (Bahnemann *et al.*, 1987). Doping ZnO with transition metal (TM) such as Cr, Fe, Co, Mn, or Ni results in some important changes in microstructure and further in physical properties such as optical, electrical, and magnetic properties. It is expected that Ni^{2+} ion thanks to its smaller ionic radius (0.55 Å) compared to Zn^{2+} (0.60 Å) (Bappaditya *et al.*, 2015) have a larger solubility in ZnO, which is mostly crystallized in hexagonal wurtzite structure (mainly with 110 preferred orientation) with tetrahedrally coordinated O^{2-} and Zn^{2+} ions (Samanta *et al.*, 2018). It was reported that the chemical stability on Ni^{2+} ion upon occupying Zn^{2+} sites, makes it unique and identifies it as one of the most efficient doping element because it enhances ZnO with optical and electrical properties (Fabbiyola *et al.*, 2017; Raja *et al.*, 2014).

There are also some other studies about Ni doped ZnO using sol-gel method (Srinet *et al.*, 2013; Liu *et al.*, 2014), low temperature hydrothermal method (Xu *et al.*, 2016), low temperature wet chemical method (Rana *et al.*, 2016) and about shape controlled magnetic nanoplatelets of Ni doped ZnO (Jadhav *et al.*, 2016). The crystallographic structure and morphology of Ni doped ZnO, and further physical properties, are affected by preparation technique and external conditions such as concentration of Ni, reaction temperature, reaction time, annealing temperature, pH value, starting precursors, solution concentration, and etc.

In this study, ZnO nanopowders doped with different Ni concentration were synthesized by sol-gel technique using zinc nitrate hexahydrate ($Zn(NO_3)_2.6H_2O$) and nickel nitrate hexahydrate ($Ni(NO_3)_2.6H_2O$) at pH value of 10. The samples were annealed at 500°C for 2h. The crystallographic structure of the samples was investigated by conventional x-ray diffraction (XRD) technique and morphology of the samples was investigated by field emission-scanning electron microscopy (FE-SEM) along with elemental analysis by energy dispersive x-ray (EDX). Besides, Fourier transform infrared spectroscopy (FTIR) technique is used to analyse the chemical bonding and constituting elements of the samples. Further, the optical properties of Ni doped ZnO nanopowders were investigated by using UV-VIS spectrometer and the results were presented in detail.

2. EXPERIMENTAL PROCESS

ZnO and Ni doped ZnO nanopowders were prepared by using sol-gel technique. The zinc nitrate hexahydrate ($Zn(NO_3)_2.6H_2O$, Acros Organics), nickel nitrate hexahydrate ($Ni(NO_3)_2.6H_2O$, Sigma Aldrich, for Ni doped ZnO), polyethylene glycol (PEG300, Aldrich Chemistry) and ammonia (NH_3, Analar Normapur) were used as precursors. As a first step, 2.97 g of $Zn(NO_3)_2.6H_2O$ was dissolved in 100 mL of distilled water (Yildirimcan *et al.*, 2016). As a second step, 3.36 g PEG300 was added into the existing solution. The pH of the solution was adjusted to 10 by using ammonia (NH_3). The resulting solution was mixed overnight at 80°C using a magnetic stirrer to get a homogeneous solution in which precipitates were visible. Then, the water in the final solution was evaporated at 100°C. Finally, the precipitate was annealed at 500°C for 2 h. The similar procedure was followed in order to produce Ni doped ZnO nanopowders. $Ni(NO_3)_2.6H_2O$ was dissolved in distilled water at certain ratios. The prepared Ni solution was added into the pure ZnO precursor solution at stoichiometric ratios, 5%, 10% and 15%. Also, Ni doped ZnO nanopowders were produced at pH=10 and annealed at 500°C for 2 h.

The crystallographic structure of the samples were investigated by using x-ray diffraction (XRD) (Bruker D8 Advanced Series powder diffractometer) (40 kV, 40 mA, Cu$K\alpha$ λ=1.5405 Å) in steps of 0.02° in the rage of $20° \leq 2\theta \leq 85°$. Field emission-scanning electron microscopy (FE-SEM) (Zeiss/Supra 55 FE-SEM) was used in order to determine the morphology of the samples. The Zeiss/Supra 55 FE-SEM was equipped with an energy dispersive x-ray spectrometer, which was used to record the EDX diffractogram for elemental analysis. Fourier transform infrared (FTIR) spectra were recorded by using Perkin Elmer spectrometer with ATR unit in order to analyse the chemical bonding and constituting elements of the samples.

3. RESULTS AND DISCUSSIONS

Structural, elemental and morphological analyzes along with determination of optical properties were made in detail and results were presented in the individual parts in following. The results were compared with literature and discussed.

3.1. Structural Analysis of the ZnO and ZnO:Ni Nanoparticles

It is known that the possible growth mechanism of the nanomaterials can be described on basis of chemical

reactions and nucleation process (Rana *et al.*, 2016). The possible chemical reactions, which are responsible for the growth on Ni doped ZnO nanostructure were already given in (Rana *et al.*, 2016). The XRD diffraction patterns of the pure ZnO and Ni doped ZnO nanopowders synthesized by sol-gel technique are shown in Fig. 1(a), enlarged in Fig. 1(b), respectively.

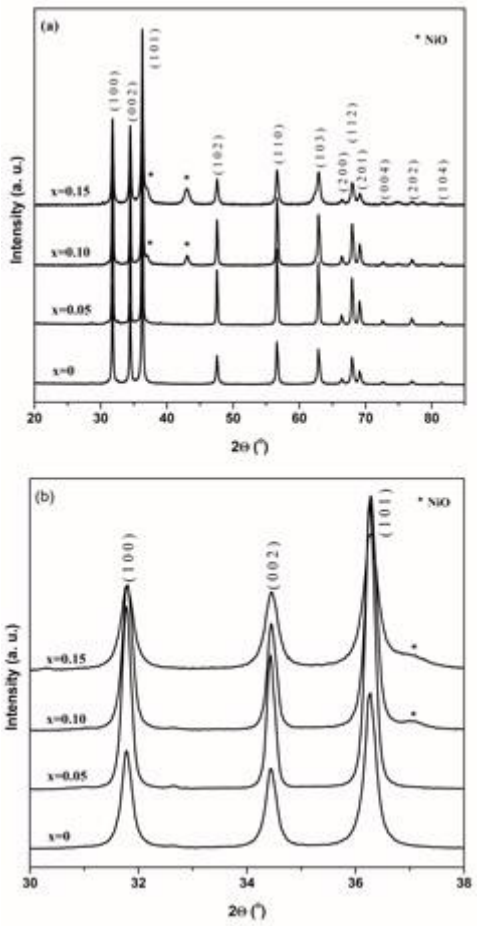

Fig. 1. (a) X-ray diffraction patterns for Ni doped ZnO nanocrystals depending on Ni concentration; (b) expanded view of (100), (002) and (101) peaks in all of the samples

The sharp peaks in Fig. 1 are evidence that pure and Ni doped ZnO nanoparticles are well crystallized. Pure ZnO exhibits a hexagonal phase of wurtzite type with (101) preferred growth direction and it is phase pure, which means no extra peaks, are observed. In other word, all the major diffraction peaks for the sample x=0 can be perfectly indexed with pure ZnO (phase: hexagonal, lattice: primitive, JCPDS 036-1451). Doping ZnO with different Ni concentration does not change the hexagonal phase. However, for the samples with x=0.10 and x=0.15 a secondary phase is observed. The diffraction peaks occurred at 2θ=37.01° and 2θ=43.09° are attributed to presence of NiO (JCPDS 004-0835). This is in agreement with the literature (Srinet *et al.*, 2013) in which a secondary phase is observed for Ni concentration of 6%. Our sample with x=0.05 prepared with sol-gel technique is phase pure whereas it was observed in literature that the sample with x=0.05 prepared with ball milling technique existed a secondary phase due to NiO/Ni (Bappaditya *et al.*, 2015). The lattice parameters (*a*, *c*) of pure and Ni doped ZnO nanopowders were calculated using the XRD data with the help of Bragg Law

$$2dsin\theta = n\lambda \quad (1)$$

(*n*=1; λ is the wavelength of incident X-ray used) and following formula, which is defined for hexagonal phase:

$$\frac{1}{d^2} = \frac{4}{3}\left[\frac{h^2+hk+k^2}{a^2}\right] + \frac{l^2}{c^2} \quad (2)$$

where *d* is the distance between two different planes and (*hkl*) are the Miller indexes (Yildirimcan *et al.*, 2016). The calculation of *a*, *c* and *d* were made with respect to (100), (002), (101) diffraction peaks and then average values were calculated and the values were given in Table 1.

Table 1. Lattice parameters of *a*, *c*, and *d* of the pure ZnO and Ni doped ZnO

Sample	*a* (Å)	*c* (Å)	*d* (Å)
x=0	3.2235	5.2640	2.6299
x=0.05	3.2238	5.2645	2.6302
x=0.10	3.2228	5.2628	2.6293
x=0.15	3.2232	5.2634	2.6296

Note: x is mol of Ni concentration.

The average crystallite sizes of pure and Ni doped ZnO nanopowders are calculated by applying Debye-Scherrer formula:

$$D_{hkl} = \frac{K\lambda}{\beta\cos\theta} \quad (3)$$

where *D* is the average crystallite size, β is the full width half maximum (FWHM) of the 2θ peak (100), *K* is the shape factor of the particles (used as 0.9), θ is the Bragg angle, λ is the wavelength of incident X-ray used.

The calculated crystallite size, dislocation density, and strain of pure ZnO and Ni doped ZnO nanopwders are listed in Table 2. The FWHM (β $x10^{-3}$)(rad) values are 3.799, 3.473, 3.850, and 4.616 for the samples with x=0, x=0.05, x=0.10, and x=0.15, respectively.

Table 2. Crystallite size, dislocation density, strain of pure ZnO and Ni doped ZnO nanopowders

Sample	Crystallite size (nm)	Dislocation density ($x10^{-4}$ lines/nm^2)	Strain ($x10^{-4}$)
x=0	37.93	6.950	9.135
x=0.05	41.50	5.808	8.351
x=0.10	37.43	7.138	9.257
x=0.15	31.20	10.262	11.10

Note: Calculations were made with respect to (100) peak of XRD. x is mol of Ni concentration.

The crystallite size is increased from 37.93 nm to 41.50 nm with 5% Ni doping into ZnO, which is also

confirmed by (Vignesh *et al.*, 2014). However, for higher Ni doping causes a decrease in the crystallite size for example it is 37.43 nm for the sample with x=0.10 and 31.20 nm for x=0.15. There is no linear correlation between concentration of Ni and crystallite size of the samples. This situation was concluded in the literature (Rana *et al.*, 2016) that the reason might be dissimilar conditions for different doping concentration as well as a lot of distortions in the host ZnO lattice that turns out lattice relaxation or compression in the host lattice because of the vacancy and/or interstitial defect already existing in the host lattice. The sample with x=0.05 having the highest crystallite size showing the smallest dislocation density and the smallest strain.

3.2. Elemental Analysis of the ZnO and Ni:ZnO Nanoparticles

The EDX diffractogram of pure ZnO and Ni doped ZnO are shown in Fig. 2. The diffractogram confirm the presence of the elements Zn, Ni, and O, and no other impurities in the samples. The peaks labeled as platinum (Pt), and palladium (Pd) are due to surface coating materials. The weight and atomic ratio of the samples obtained by EDX are given in Table 3.

Table 3. EDX elemental analysis of ZnO and Ni doped ZnO nanopowders

Sample	Element	Weight (%)	Atomic (%)
x=0	Zn	67.52	50.37
	Ni	-	-
	O	14.51	44.23
x=0.05	Zn	75.38	52.81
	Ni	0.50	0.39
	O	15.52	44.45
x=0.10	Zn	62.41	43.00
	Ni	5.00	3.84
	O	17.38	48.95
x=0.15	Zn	50.46	34.58
	Ni	12.79	9.76
	O	17.31	48.48

Note: x is mol of Ni concentration.

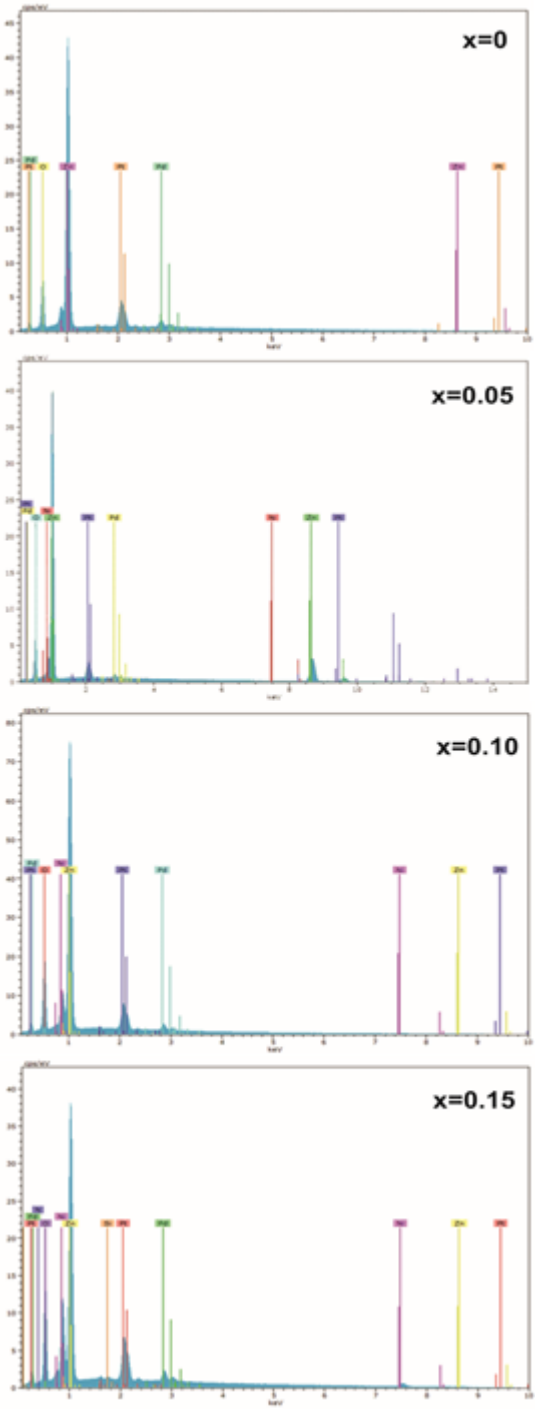

Fig. 2. EDX diffractogram of pure ZnO and Ni doped ZnO. x is mol of Ni concentration.

3.3. FT-IR Analysis of the ZnO and Ni:ZnO Nanoparticles

The chemical bonding of the nanopowders can be analyzed by using FTIR spectroscopy. Thus, FTIR spectra of pure ZnO and Ni doped ZnO were recorded in order to study the composition and chemical structure of the samples in the wave number range of 400-4000 cm^{-1} at room temperature. Fig. 3 shows the comparison of the transmittance of the samples.

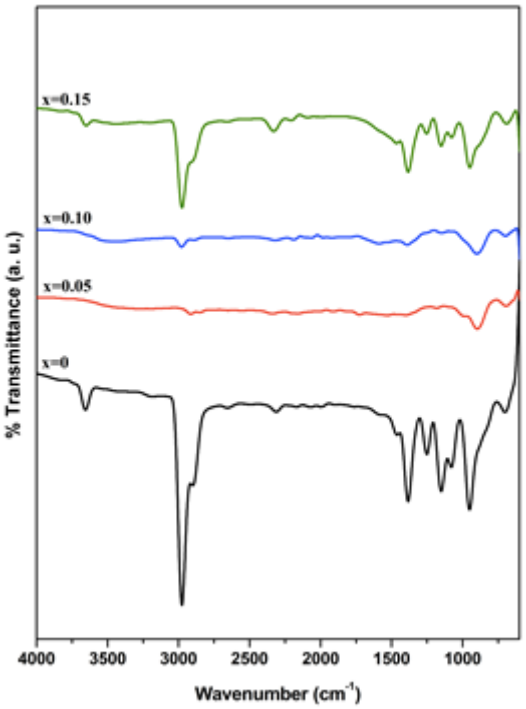

Fig. 3. FTIR spectra of pure ZnO and Ni doped ZnO. x is mol of Ni concentration.

The observed band at 3656 cm^{-1} which is quite dominant for the sample x=0 compared to the others is corresponded to stretching vibration of H_2O. It was already mentioned that the FTIR peaks at 3500-3800 cm^{-1} (both) were corresponded to stretching vibration of H_2O (Yildirimcan *et al.*, 2016). The observed bands at 2982 cm^{-1} and 2889 cm^{-1} are due to the symmetric and asymmetric $–CH_2$ stretching modes. The vibration bands between 2300 cm^{-1} and 2400 cm^{-1}, which are at 2316 cm^{-1} in the present study, were assigned to the CO_2 mode in air (Yildirimcan *et al.*, 2016). The peak at 1382 cm^{-1} is corresponded to the symmetric C=O stretching vibration modes (Samanta *et al.*, 2018). The peak at 1075 cm^{-1} is ascribed to bending vibrations of –OH groups and the peak at 946 cm^{-1} is attributed to symmetric stretching vibrations of NO_3^{-1} ions.

3.4. Microstructure Analysis of ZnO and Ni:ZnO Nanoparticles

The surface morphologies of ZnO and Ni doped ZnO nano particles are investigated by FE-SEM (see Fig. 4). It is observed that pure ZnO is composed of closely packed spherical nanoparticles. Once ZnO is doped with 5% Ni, nanorods start to exist along with spherical nanoparticles. These nanorods are not homogenous in another word, the sample with x=0.05 includes nanorods having the length ranging from nanometer to micrometer. The nanorod structure becomes more like nanoneedle once the Ni concentration is increased upto x=0.10. Besides, agglomerated nanoparticles still exist in the sample. On the other hand, nanorods mostly disappeared agglomerated spherical nanoparticles becomes dominant. The agglomeration of Ni doped ZnO was also observed in the literature (Vignesh *et al.*, 2014).

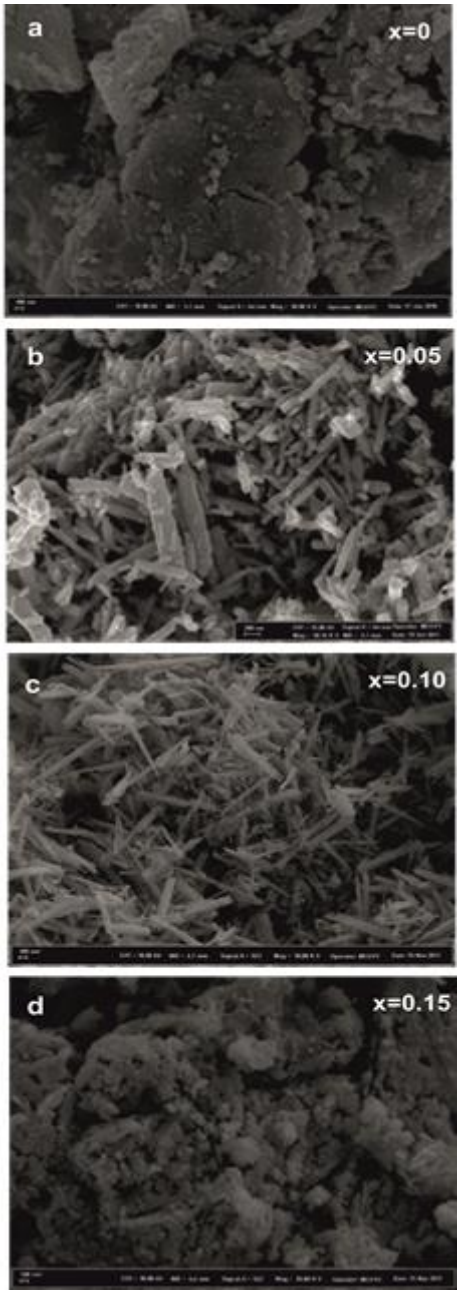

Fig. 4. SEM pictures of a) pure ZnO, b) x=0.05, c) x=0.10, d) x=0.15, x is mol of Ni concentration

3.5. Optical properties of ZnO and Ni:ZnO Nanoparticles

Fig. 5 shows the absorbance spectra of pure and Ni-doped ZnO nanoparticles. The sample doped 5% Ni shows the highest intensity.

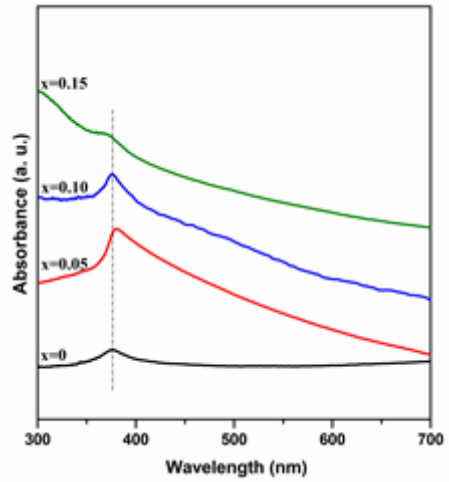

Fig. 5. Absorbance spectra of pure ZnO and Ni doped ZnO. x is mol of Ni concentration

The absorbance peaks appear in the range of 350- 400 nm. While the absorbance peak increases as doping 5% Ni^{2+}, it decreases as doping 10% and 15% Ni^{2+}, respectively. The absorption peak (known as excitonic absorption peak) of pure ZnO and Ni doped ZnO (5%, 10% and 15%) nanoparticles were observed in the wavelength around 376 nm, 380 nm, 375 nm and 370 nm, respectively. The absorption peak of pure ZnO is shifted to higher wavelength once ZnO is doped with 5% Ni similar to (Jadhav *et al.*, 2016). It is also mentioned in the literature (Guruvammal *et al.*, 2016) that one reason for red shift could be the sp-d exchange interactions between the band electrons and the localized d-electrons of the Ni^{2+} ions. However, blue shift is observed for higher Ni doping concentrations (10% and 15%). The absorption blue shift is explained by Burstein-Moss effect (Samanta *et al.*, 2018; Fabbiyola *et al.*, 2017; Rajakarthikeyan *et al.*, 2017)

4. CONCLUSIONS

The effects of Ni doping concentration on the physical properties such as structural, morphological, and optical properties of ZnO nanoparticles prepared by sol-gel technique have been investigated. Because of its smaller ionic radius compared to Zn^{2+}, the Ni^{2+} have a larger solubility in ZnO. However, there is a solubility limit: the sample with x=0.05 shows pure hexagonal phase whereas x=0.10 and x=0.15 show a secondary phase due to existing of NiO. The elemental and chemical analysis have been done by EDX and FTIR and given in parts of 3.2 and 3.3, respectively. The sample with x=0.05 has the highest crystallite size (41.50 nm) and the smallest dislocation density and following the smallest strain. The sample includes both spherical nanoparticles and nanorods ranging the length from nanometer to micrometer whereas pure ZnO includes only agglomerated spherical nanoparticles. The nanorods change into the form of nanoneedles which are deteriorated for the sample x=0.10. Nanorods or nanoneedles are mostly disappeared in the sample with x=0.15. Optical properties of the samples have been studied and the absorbance peaks are found to be at 376 nm, 380 nm, 375 nm, and 370 nm for the sample with x=0, x=0.05, x=0.10, and x=0.15, respectively.

REFERENCES

Bahnemann, D. W., Kormann, C. and Hoffmann M. R. (1987). "Preparation and characterization of quantum size zinc oxide: a detailed spectroscopic study." *J. Phys. Chem*., Vol. 91, No. 14, pp. 3789-3798.

Bappaditya P., Sarkar, D. and Giri, P. K. (2015). "Structural, optical, and magnetic properties of Ni doped ZnO nanoparticles: Correlation of magnetic moment with defect density." *Applied Surface Science*, Vol. 356, pp. 804-811.

Chen, Y. F., Bagnall, D. and Yao, T. F. (2000). "ZnO as a novel material for the UV region." *Mater. Sci. Eng. B*, Vol. 75, pp. 190-198.

Cohn, A.W., Kittilstved, K. R. and Gamelin, D. R. (2012). "Tuning the Potentials of "Extra" Electrons in Colloidal n-Type ZnO Nanocrystals via Mg^{2+} Substitution." *J. Am. Chem. Soc*., Vol. 134, No. 18, pp. 7937-7943.

Dietl, T., (2007). "Origin of ferromagnetic response in diluted magnetic semiconductors and oxides." *J. Phys.: Condens. Matter*, Vol. 19 No. 16, pp. 165204.

El-Hilo, M., Dakhel, A. A. and Ali-Mohamed, A.Y. (2009). "Room temperature ferromagnetism in nanocrystalline Ni-doped ZnO synthesized by co-precipitation." *J. Magn. and Magn. Mater*., Vol. 321 No. 14, pp. 2279-2283.

Ellmer, K., Klein, A. and Rech, B. (2008). *Transparent conductive zinc oxide – Basics and applications in thin film solar cells*, Springer Series in Materials Science, Germany.

Emanetoglu, N. W., Gorla, C., Liu, Y., Liang, S. and Lu, Y. (1999). "Epitaxial ZnO piezoelectric thin films for saw filters." *Mater. Sci. Semicond. Process*., Vol. 2, No. 3, pp. 247–252.

Fabbiyola, S., Sailaja, V., John Kennedy, L., Bououdina, M. and Judith Vijaya, J. (2017). "Optical and magnetic properties of Ni-doped ZnO nanoparticles." *Journal of Alloys and Compounds*, Vol. 694, pp. 522-531.

Godavarti, U., Mote, V. D. and Dasari, M. (2017). "Precipitated nickel doped ZnO nanoparticles with enhanced low temperature ethanol sensing properties." *Modern Electronic Materials*, Vol. 3, pp. 179-185.

Guruvammal, D., Selvaraj, S. and Meenakshi Sundar, S. (2016). "Effect of Ni-doping on the structural, optical and magnetic properties of ZnO nanoparticles by solvothermal method." *Journal of Alloys and Compounds*, Vol. 682, pp. 850-855.

Huang, M. H., Mao, S., Feick, H., Yan, H. Q., Wu, Y. Y., Kind, H., Weber, E., Russo, R. and Yang, P. D. (2001). "Room-temperature ultraviolet nanowire nanolasers." *Science*, Vol. 292, pp. 1897-1899.

Jadhav, J. and Biswas, S. (2016). "Shape-controlled

magnetic nanoplatelets of Ni-doped ZnO synthesized via a chemical precursor." *Journal of Alloys and Compounds*, Vol. 664, pp. 71-82.

Kind, H., Yan, H. Q., Messer, B., Law, M. and Yang, P. D. (2002). "Nanowire Ultraviolet Photodetectors and Optical Switches." *Adv. Mater*., Vol. 14, pp.158.

Kittilstved, K. R., Liu, W. K. and Gamelin, D. R. (2006). "Electronic structure, origins of polarity-dependent high-TC ferromagnetism in oxide-diluted magnetic semiconductors." *Nat. Mater*., Vol. 5, pp. 291-297.

Koch, M. H., Timbrell, P. Y. and Lamb, R. N. (1995). "The influence of film crystallinity on the coupling efficiency of ZnO optical modulator waveguides." Semicond. Sci. Technol., Vol. 10, pp. 1523-1527.

Law, M., Greene, L. E., Johnson, J. C., Saykally, R. and Yang, P. D. (2005). "Nanowire dye-sensitized solar cells." *Nat. Mater*., Vol. 4, pp. 455-459.

Lee, J. Y., Choi, Y. S., Kim, J. H., Park M. O., Im, S. (2002). "Optimizing n-ZnO/p-Si heterojunctions for photodiode applications." *Thin Solid Films*, Vol. 403, pp. 553-557.

Li, W. J., Shi, E. W., Zheng, Y. Q. and Yin, Z. W. (2001). "Hydrothermal preparation of nanometer ZnO nanopowders." *J. Mater. Sci. Lett*., Vol. 20, pp. 1381-1383.

Liu, Y., Liu, H., Chen, Z., Kadasala, N., Mao, C., Wang, Y., Zhang, Y., Liu, H., Liu, Y., Yang, J. and Yan, Y. (2014). "Effects of Ni concentration on structural, magnetic and optical properties of Ni-doped ZnO nanoparticles." *Journal of Alloys and Compounds*, Vol. 604, pp. 281-285.

Martinson, A. B. F., Elam, J. W., Hupp, J. T. and Pellin, M. J. (2007). "ZnO Nanotube Based Dye-Sensitized Solar Cells." *Nano Lett*., Vol. 7, No. 8, pp. 2183–2187.

Mitra, P., Chatterjee, A. P. and Maiti, H. S. (1998). "ZnO thin film sensor." *Mater. Lett*., Vol. 35, pp. 33-38.

Motaung, D. E., Kortidis, I., Papadaki, D., Nkosi, S. S., Mhlongo, G. H., Wesley-Smith, J., Malgas, G. F., Mwakikunga, B. W., Coetsee, E., Swart, H. C., Kiriakidis, G. and Ray, S. S. (2014). "Defect-induced magnetism in un-doped and Mn-doped wide band gap Zinc oxide grown by aerosol spray pyrolysis." *Appl. Surf. Sci*., Vol. 311, pp. 14-26.

Pearton, S. J., Norton, D. P., Ip, K., Heo, Y. W., Steiner, T. (2005). "Recent progress in processing and properties of ZnO." *Prog. Mater. Sci*., Vol. 50, No. 3, pp. 293–340.

Raja, K., Ramesh, P. S. and Geetha, D. (2014). "Synthesis, structural and optical properties of ZnO and Ni-doped ZnO hexagonal nanorods by Co-precipitation method." *Spectrochimica Acta Part A: Molecular and Biomolecular Spectroscopy*, Vol. 120, pp. 19-24.

Rajakarthikeyan, R. K., and Muthukumaran, S. (2017). "Investigation of microstructure, electrical and photoluminescence behaviour of Ni-doped $Zn_{0.96}Mn_{0.04}O$ nanoparticles: Effect of Ni concentration." *Opt. Mater*., Vol. 69, pp. 382-391.

Rana, A. K., Bankar, P., Kumar, Y., More, M. A., Late, D. J., Shirage, P. M. (2016). "Synthesis of Ni-doped ZnO nanostructures by low-temperature wet chemical method and their enhanced field emission properties." *RSC Adv*., Vol. 6, pp. 104318-104324.

Romeiro, F. C., Marinho, J. Z., Lemos, S. C. S., de Moura, A. P., Freire, P. G., da Silva, L. F., Longo, E., Munoz, R. A. A. and Lima, R. C. (2015). "Rapid synthesis of Co, Ni co-doped ZnO nanoparticles: Optical and electrochemical properties." *Journal of Solid State Chemistry*, Vol. 230, pp. 343-349.

Saito, N., Haneda, H., Sekiguchi, T., Ohashi, N., Sakaguchi, I. and Koumoto, K. (2002). "Low-Temperature Fabrication of Light-Emitting Zinc Oxide Micropatterns Using Self-Assembled Monolayers." *Adv. Mater*., Vol. 14, No. 6, pp. 418-421.

Samanta, A., Goswami, M. N. and Mahapatra, P. K. (2018). "Magnetic and electric properties of Ni-doped ZnO nanoparticles exhibit diluted magnetic semiconductor in nature." *Journal of Alloys and Compounds*, Vol. 730, pp. 399-407.

Schneider, J. J., Hoffmann, R. C., Engstler, J., Klyszcz, A., Erdem, E., Jakes, P., Eichel, R. A., Pitta-Bauermann L. and Bill, J. (2010). "Synthesis, characterization, defect chemistry, and FET properties of microwave-derived nanoscaled zinc oxide." *Chem. Mater*., Vol. 22, No. 2203-2212.

Shoushtari, M. Z., Poormoghadam, A. and Farbod, M. (2017). "The size dependence of the magnetic properties of ZnO and $Zn_{1-x}Ni_xO$ nanoparticles." *Materials Research Bulletin*, Vol. 88, pp. 315-319.

Srinet, G., Kumar, R. and Sajal, V. (2013). "Structural, optical, vibrational, and magnetic properties of sol-gel derived Ni doped ZnO nanoparticles." *Journal of Applied Physics*, Vol. 114, pp. 033912.

Toloman, D., Mesaros, A., Popa, A., Raita, O., Silipas, T. D. B., Vasile, S., Pana, O. and Giurgiu, L. M. (2013). "Evidence by EPR of ferromagnetic phase in Mn-doped ZnO nanoparticles annealed at different temperatures." *Journal of Alloys and Compounds*, Vol. 551, pp. 502-507.

Vignesh, K., Rajarajan, M. and Suganthi, A. (2014). "Visible light assisted photocatalytic performance of Ni and Th co-doped ZnO nanoparticles for the degradation of methylene blue dye." *J. Ind. Eng. Chem*., Vol. 20, No. 5, pp. 3826-3833.

Vijayaprasath, G., Murugan, R., Asaithambi, S., Sakthivel, P., Mahalingam, T., Hayakawa, Y. and Ravi G. (2016). "Structural and magnetic behavior of Ni/Mn co-doped ZnO nanoparticles prepared by co-precipitation method." *Ceramics International*, Vol. 42, pp. 2836-2845.

Xu, K., Liu, C., Chen, R., Fang, X., Wu, X. and Liu, J.

(2016). "Structural and room temperature ferromagnetic properties of Ni doped ZnO nanoparticles via low-temperature hydrothermal method." *Physica B*, Vol. 502, pp. 155-159.

Yildirimcan, S., Ocakoglu, K., Erat, S., Emen, F. M., Repp, S. and Erdem, E. (2016). "The effect of growing time and Mn concentration on the defect structure of ZnO nanocrystals: X-ray diffraction, infrared and EPR spectroscopy." *RSC Adv.*, Vol. *6*, No. 45, pp. 39511–39521.

CONTENTS

ISSN 2587-1366

TURKISH JOURNAL OF ENGINEERING

VOLUME 3 ISSUE 1 JANUARY 2019